ABSTRACT

Title of Dissertation : RAPID ASSESSMENT OF BGA FATIGUE LIFE UNDER VIBRATION LOADING

Mei-Ling Wu, Doctor of Philosophy, 2006

Dissertation Directed By: Professor Donald Barker
Department of Mechanical Engineering

Ball Grid Array (BGA) packages are a relatively new package type and have rapidly become the package style of choice. Much high density, high I/O count semiconductor devices are now only offered in this package style. Designers are naturally concerned about the robustness of BGA packages in a vibration environment when their experience base is with products using more traditional compliant gull or J leaded surface mount packages. Because designers simply do not have the experience, tools are needed to assess the vibration fatigue life of BGA packages during early design stages and not have to wait for product qualification testing, or field returns, to determine if a problem exists.

This dissertation emphasizes a rapid assessment methodology to determine fatigue life of BGA components. If time and money were not an issue, clearly one would use a general-purpose finite element program to determine the dynamic response of the printed wiring board in the vibration environment. Once the response of the board was determined, one would determine the location and value of the critical stress in the component of interest. Knowing the critical stress, one would estimate the fatigue life from a damage model. The time required building the FEA model, conducting the analysis, and post-process the results would take at least a few days to weeks. This is too time-consuming, except in the most critical applications. It is not a process that can be used in everyday design and what-if simulations. The rapid assessment approach proposed in this research focuses on a physics of failure type approach to damage analysis and involves global and local modeling to determine the critical stress in the component of interest. A fatigue damage model then estimates the life. Once implemented in software, i.e. the new version of *CALCE_PWA,* the entire fatigue life assessment is anticipated to be executed by an average engineer in real time and take only minutes to generate accurate results.

RAPID ASSESSMENT of BGA FATIGUE LIFE under VIBRATION LOADING

By

Mei-Ling Wu

Dissertation submitted to the Faculty of the Graduate School of the
University of Maryland, College Park, in partial fulfillment
of the requirements for the degree of
Doctor of Philosophy
2006

Advisory Committee:
Professor Donald Barker, Chair/Advisor
Professor Abhijit Dasgupta
Professor Bilal Ayyub
Professor Peter Sandborn
Professor Patrick McCluskey

© Copyright by
Mei-Ling Wu
2006

Dedication

To my parents, my grandparents, and my two younger brothers

Acknowledgements

Thanks to my advisor, Dr. Donald Barker, who provided thoughtful guidance and encouragement through what seemed to be a never-ending process. He provided direction to my research and timely help that enabled me to complete my program of study. I have learned substantially from his uncompromising emphasis on quality and meaningful research, and the significance of written and oral communication in research. I would also like to thank my committee members, Dr. Abhijit Dasgupta, Dr. Bilal Ayyub, Dr. Peter Sandborn and Dr. Patrick McCluskey, for their critical suggestions and advice.

My final, and most heartfelt, acknowledgment must go to my parents, my grandparents, and my two younger brothers. I could not have finished my research without their support and encouragement during my doctoral study.

Finally, the following friends have helped in various ways: Morrigan Johnson, James Watkins, Aaron Johnson, Patrice Gregory, Alan Yu, Gil Sharon, and Saifa Hasin.

Table of Contents

ABSTRACT 1
Dedication ii
Acknowledgements iii
Table of Contents iv
List of Tables vi
List of Figures viii
Chapter 1: Introduction 1
1.1 Objective 1
1.2 Motivation 3
1.3 Problem Statement and Research Scope 5
1.4 Summary 6
Chapter 2: Literature Review 10
2.1 Empirical Base Model Paper 13
2.2 Analytical Model Approach Papers 18
2.3 Finite Element Analysis Model Approach papers 28
2.4 Experimental Approach Papers 36
2.5 Bending and Twisting Analysis Approach Papers 44
2.6 Summary of Literature Review 47
2.7 Observations of the Literature Review Survey 48
2.8 Overall conclusion: 51
Chapter 3: Technical Approach 52
3.1 Random Vibration Environment 52
3.2 Probability and Statistics 57
3.2.1 G_{rms} 57
3.2.2 Assuming an Normal Probability Distribution 59
3.2.3 Linear Damage Superposition with a Normal Probability Distribution 59
3.3 General Physical Description of BGA Damage under Random Vibration 64
3.4 Review of PBGA, CBGA, and CSP Package Structures 69
3.4.1 Structure of PBGA 70
3.4.2 Structure of CSP 72
3.4.3 Structure of CBGA 73
3.5 Structure of Global and Local Model 75
3.5.1 Global Model 76
3.5.2 Local Model 76
3.6 Summary 77
Chapter 4: Global Model 79
4.1 Global Model Approach 83
4.1.1 Fundamental Mode is the Primary Mode of Interest 88
4.1.2 2D and 3D Comparison 89
4.1.3 Single Packages Type and Mixed Packages Types 94
4.2 DOE and ANOVA for Global Model 98
4.2.1 DOE and ANOVA Analysis for Model Development 101
4.2.2 CALCE_PWA for K_{CALCE_PWA} 118

4.2.3 Calculation of Moment through Curvature 120
4.3 Uncertainty Issue 122
4.3.1 Global Life UncertaintyIssue Analysis 122
4.4 Summary 132
Chapter 5: Local Model 134
5.1 Local Model Approach 138
5.1.1 Solder Joint Shape 139
5.1.2 Mesh Problem 142
5.2 DOE and ANOV Approach for Local Model 146
5.2.1 DOE and ANOVA Analysis for Model Development 148
5.3 Local Life Uncertainty Issue Analysis 162
5.4 Summary 166
Chapter 6: Damage Model 168
6.1 Basquin High Cycle Fatigue Power Law Model 169
6.2 Accumulation of Fatigue Damage 171
6.2.1 Critical Fatigue Damage Ratio 173
6.3 Summary 175
Chapter 7: Case Study 176
7.1 Case Study 1: EMMA Project 177
7.1.1 Case Study 1: EMMA—Global Model 178
7.1.2 Case Study 1: EMMA Project Calculation of Bending Moment 184
7.1.3 Case study 1: EMMA—Damage Model 185
7.2 Case Study 2: JGPP Project 191
7.2.1 Case Study 2: JGPP—Global Model 192
7.2.2 Case Study 2: JGPP—Local Model 194
7.2.3 Case study 2: JGPP—Damage Model 195
7.3 Uncertainty Issue Analysis in the Lifetime distribution 200
7.3.1 Uncertainty Analysis in the Measured (Experimented) Life 201
7.3.2 Uncertainty Analysis in the Predicted (Calculated) Life 204
7.3.3 Uncertainty Analysis Combined the Predicted Life and Measure Life .. 211
Chapter 8: Conclusion and Future work 212
Appendices A: Design of Experimental Methodology (RSM and ANOVA) 220
Appendices B: Additional Figures and Tables in Chapter 4-Chapter7 231
Appendices C: Matlab Global Model Failure Analysis Codes 248
Appendices D: Matlab Local Model Failure Analysis Codes 251
Appendices E: Matlab Global-Local Model Failure Analysis Codes 253
Bibliography 256

List of Tables

Table2.1: Quad Flat Packages and BGA Yield Comparisons (Source: IBM)................ 10

Table3.1: Summation for width= β 64
Table3.2: PBGA Specifications 71
Table3.3: PBGA Dimensions in (mm) 71
Table3.4: PBGA Material Properties 71
Table3.5: CSP Specifications 72
Table3.6: CSP Dimensions in (mm) 72
Table3.7: CSP Material Properties 73
Table3.8: CBGA Specifications 74
Table3.9: CBGA Dimensions in (mm) 74
Table3.10: CBGA Material Properties 74

Table4.1: Comparison of 2D and 3D FEA Results 94
Table4.2: Example for PBGA 2D and 3D Comparison with Different Variables........... 94
Table4.3: Global Model Comparison of Single Packages and Mix Packages................ 98
Table4.4: Possible Critical Factors identify 105
Table4.5: D_{ratio} Value for PBGA Package 108
Table4.6: $\frac{ball\ span\ length}{Neighboring\ component\ and\ location}$ Value for PBGA Package 109
Table4.7: Functional relationship, Correction Factor: C for the PBGA...................... 115
Table4.8: Functional relationship, Correction Factor: C for the CBGA...................... 115
Table4.9: Functional relationship, Correction Factor: C for the CSP 116
Table4.10: Functional relationship, Correction Factor: C for the PBGA..................... 116
Table4.11: Functional relationship, Correction Factor: C for the CBGA 117
Table4.12: Functional relationship, Correction Factor: C for the CSP 117
Table4.13: *CALCE_PWA* Components Spreadsheet 120
Table4.14: Actual Curvature and Moment's Relationship for PBGA.......................... 121
Table4.15: Actual Curvature and Moment's Relationship for CBGA 121
Table4.16: Actual Curvature and Moment's Relationship for CSP 121
Table4.17: Critical Factors 123
Table4.18: Nominal Values for PBGA Packaging in Uncertainty Issue 124
Table4.19: The Correction Factor C in the Particular Parameter Value 128
Table4.20: Comparison of the particular nominal value and 95% of data Range with Monte Carlo simulation random variables for the correction factor C 128
Table4.21: The of data 95% Range in the correction factor C 129
Table4.22: The 80% of data Range in the correction factor C 129
Table4.23: The 95% of data Range in the Correction Factor C and Final Life Cycle for the ***Young's Modulus' Standard Deviation 1% of Mean Value*** 130
Table4.24: The 95% of data Range in the Correction Factor C and Final Life Cycle for the ***Young's Modulus' Standard Deviation 5% of Mean Value*** 130
Table4.25: *CALCE_PWA* Curvature as a Function of PWB Young's Modulus 131

Table5.1: Comparison of 2-D Rectangular and Ball Shapes in solder joint 141
Table5.2: CACLE_FEN&ANSYS' Mesh Density and Von Mises Stress Results 144
Table5.3: Possible Critical Factors Identified by Using Plot Trend in Local Model 151
Table5.4: Possible Critical Factors Identify by 2-level factorial DOE in Local Model 153
Table5.5: D_{ratio} Value for PBGA Package in Local Model 155
Table5.6: Ball Diameter Value for PBGA Package in Local Model 155
Table5.7: Functional Relationship in Critical Solder Joint S for the PBGA 161
Table5.8: Functional Relationship in Critical Solder Joint S for the CBGA 161
Table5.9: Functional Relationship in Critical Solder Joint S for the CSP 161
Table5.10: Nominal Values (PBGA) for Uncertainty Issue in Local Model 163
Table5.11: Comparison the particular nominal value and Monte Carlo simulation random variables for the critical solder joint stress S 165
Table5.12: The 80% and 95% of data Range in the Local Solder Joint Stress, S 165
Table5.13: 1% of Material Properties of the Standard deviation in the Local Model Solder Joint Stress S 166
Table5.14: 5% of Material Properties of the Standard deviation in the Local Model Solder Joint Stress S 166

Table7.1: PBGA 580 Geometry and Material Properties 179
Table7.2: CBGA 256 Geometry and Material Properties... 179
Table7.3: CSP BGA64 Geometry and Material Properties 180
Table7.4: Functional Relationship in Correction Factor: C for the CBGA 180
Table7.5: Functional Relationship in Correction Factor: C for the PBGA 180
Table7.6: Functional Relationship in Correction Factor: C for the CSP...................... 181
Table7.7: Functional Relationship in Critical Solder Joint S for the PBGA 182
Table7.8: Functional Relationship in Critical Solder Joint S for the CBGA 182
Table7.9: Functional Relationship in Critical Solder Joint S for the CSP 183
Table7.10: Functional relationship C for PBGA 183
Table7.11: Functional relationship C for CBGA... 184
Table7.12: Functional relationship C for CSP... 184
Table7.13: Critical Solder Joint Stress for PBGA in Functional Relationship S 184
Table7.14: Critical Solder Joint Stress for CBGA in functional relationship S 185
Table7.15: Critical Solder Joint Stress for CSP in functional relationship S 185
Table7.16: PBGA 225 Material Properties and Geometry in JGPP 193
Table7.17: JGPP Correction Parameter ***C*** for Global Model 194
Table7.18: Critical Solder Joint Stress for PBGA in *CALCE_FEA* 195
Table7.19: Damage Ratio for Time to Failure in JGPP.. 196
Table7.20: Combine Global and Local model Critical Solder Joint Stress in ***1%*** of Material Properties of the Standard Deviation for the PBGA package 208
Table7.21: Combine Global and Local Model's Final Critical Solder Joint Stress in ***5%*** of Material Properties of the Standard Deviation for the PBGA package 209

List of Figures

Figure2.1: A Vibration Spring-Mass System 14
Figure2.2: Schematic Model of a Hybrid Integrated Circuits/PWB Assembly 20

Figure3.1: Time Domain 54
Figure3.2: Frequency Domain 54
Figure3.3: Standard Normal Distribution 61
Figure3.4: PWB Deformation Expressed in Terms of the Radii of Curvatures 66
Figure3.5: Two Dimensional View of a Populated PWB 67
Figure3.6: Plate for Bending Moment and Curvature Relationship 68
Figure3.7: Perspective View of a PBGA 70
Figure3.8: Components of a PBGA Device 71
Figure3.9: Component of a CSP Device 72
Figure3.10: Components of a CBGA Device 73
Figure3.11: Basic Building Blocks for BGA Simulations 74
Figure3.12: Global Model 76
Figure3.13: Local Model 77

Figure4.1: Complete Global and Local model Approach 83
Figure4.2: A Typical Meshed PWB from *CALCE_PWA* 85
Figure4.3: A Much Finer Meshed 2D Analysis of a PWB with simple models of BGA components from *ANSYS* 86
Figure4.4: Comparison of 2D and 3D FEA % Difference 91
Figure4.5: Comparison of 2D and 3D FEA % Difference 91
Figure4.6: Comparison of 2D and 3D FEA % Difference 92
Figure4.7: Model Structure with Some Location Gap Size but Varying Component Length 93
Figure4.8: Global Model for PBGA Components Mounted on the PWB Vs. PWB with No Components Mounted 96
Figure4.9: Global Model for CSP Components Mounted on the PWB vs. PWB with No Components Mounted 96
Figure4.10: Global Model Approach Output 100
Figure4.11: Global Model's Flowchart of DOE 101
Figure4.12: Global Model Using by ANSYS 103
Figure4.13: PWB's Thickness Vs. Correction Factor C (Left); 104
Figure4.14: Overmold Thickness vs. Correction Factor C (Left); 106
Figure4.15: $\frac{\text{ball span length}}{\text{Neighboring component and location}}$ Vs. Correction Factor, C 107
Figure4.16: CBGA Correction Factor for Global Model: Predicted Vs. Actual 110
Figure4.17: Verification of Correction Factor C for PBGA 112
Figure4.18: Verification of Correction Factor C for CBGA 112
Figure4.19: Verification of Correction Factor C for CSP 113
Figure4.20: Global Model form *CALCE_PWA* 118
Figure4.21: *CALCE_PWA* FEA Mesh 119

Figure4.22: *CALCE_PWA's* Random Curvature 119
Figure4.23: Histogram of Monte Carlo Simulation for Correction Factor C 126
Figure4.24: Histogram of Monte Carlo Simulation for Correction Factor C Using Central 95% of Data 127

Figure5.1: Complete Local Model Approach 137
Figure5.2: Local FEA Model of Solder Joint 140
Figure5.3: Left: *CALCE_FEA* and Right: *ANSYS* 142
Figure5.4: Mesh Comparison, Left: *CALCE_FEA* (simple mesh); 143
Figure5.5: Local Model for *CALCE_FEA* 145
Figure5.6: Local model Approach 147
Figure5.7: PBGA Slice Model 256 I/O Full Array 149
Figure5.8: Local Model Solder Joint Von Mises Stress 149
Figure5.9: Left: Number of Solder Joints vs. Von Mises Stress; Right: Ball Diameter Vs. Von Mises Stress 152
Figure5.10: CBGA Functional Relationship Factor for Local Model: 156
Figure5.11: Verification of Functional Relationship Factors: Critical Solder Joint S for CBGA 159
Figure5.12: Verification of Functional Relationship Factors: Critical Solder Joint S for PBGA 159
Figure5.13: Verification of Functional Relationship Factors: Critical Solder Joint S for CSP 160
Figure5.14: Histogram of Monte Carlo Simulation for the Critical Solder Joint Stress S 164
Figure5.15: Histogram of Monte Carlo Simulation for Critical Solder Joint Stress S using central 95% of Data 164

Figure6.1: $S-N$ Curves 171

Figure7.1: EMMA test Board 178
Figure7.2: EMMA Report: Rapid Assessment Model for Experiment Life 187
Figure7.3: EMMA Report: *CALCE_PWA* Model for Experiment Life Vs. Calculated Life 187
Figure7.4: EMMA Report: Rapid Assessment Model for Experiment Life 190
Figure7.5: EMMA Report: *CALCE_PWA* Model for Experiment Life 190
Figure7.6: JGPP Assembly Vibration Completed Test Vehicle 192
Figure7.7: JGPP Project's Rapid Assessment Methodology for Experimented Life Vs. Calculated Life 197
Figure7.8: JGPP Project's *CALCE_PWA* Model for Experiment Life Vs. Calculated Life 197
Figure7.9: JGPP's Rapid Assessment Model for Experiment Life Vs. Calculated Life 199
Figure7.10: JGPP Project's *CALCE_PWA* Model for Experiment Life vs. Calculated Life 199
Figure7.11: Measured (Experimented) Life- Life Cycle in the Uncertainties Issue for 5%, 50% and 95% survive 203
Figure7.12: Uncertainties Issue for 5%, 50% and 95% survive 204

Figure7.13: Uncertainty Issue for the Combine Global and Local Model's functions for PBGA Package.. 206
Figure7.14: Log-Log S-N Curve.. 206
Figure7.15: Uncertainty in the Calculated (Predicted) Life.. 210
Figure7.16: Uncertainties Issue for 90% of data 210
Figure7.17: Calculated and Measured Life: Life Cycle Uncertainty Issue 211

Chapter 1: Introduction

1.1 Objective

The objective of this research is to develop a rapid assessment methodology that can determine the solder joint fatigue life of Ball Grid Array (BGA) packages under vibration loading. BGA packages are a relatively new package type and are not only becoming the package style of choice, but also becoming the only package style offered by the parts suppliers, for high density, high I/O counts semiconductor devices. Designers are naturally worried about the robustness of BGA packages in a vibration environment. This concern is understandable in that they have experience fielding products using more traditional packages such as insertion mount or peripheral leaded surface mount packages, which employ compliant gull or J leads. They simply do not have the experience base of using BGA type packages in a vibration environment. Without this experience base, designers need tools to assess the vibration fatigue life of these packages during the early design stages and not have to wait for product qualification testing, or field returns, to determine if a problem exists. There are many types of BGA packages. In this dissertation we will focus on the more common types of BGAs, which have been used extensively in telecommunications, military, and aircraft electronics as well as commercial personal portable electronics. In this dissertation, it must be pointed out that a “rapid” assessment methodology to determine fatigue life is emphasized. If time and money were not an issue, one would use a general-purpose finite element analysis (FEA) to determine the dynamic response of the printed wiring board (PWB) in the vibration

environment. The value of the critical stress in the critical solder ball, in the critical BGA component would then be determined. Knowing the critical stress, one could then estimate the fatigue life of the solder ball using a fatigue damage model.

There are several problems with using a general-purpose finite element analysis approach. First, it would require an experienced modeler to conduct the analysis. Second, meshing the PWB would involve tens of thousands of elements in order to obtain the required resolution to find the critical stress location(s) and value(s). In reality, it would require a global-local type modeling approach. A coarse model of the entire PWB, with particular attention to the boundary conditions, would need to be built to determine the response of the PWB to the vibration environment. This is the global model. The next step would be to construct a detailed model of the particular component of interest, using boundary condition inputs from the global model. This would be the local model. This local model of a particular component would have enough resolution to determine the critical location and value of the stresses and strains in the solder joints. The stress and strain values would then be input into a fatigue damage model to determine fatigue life. The time to build the model(s), conduct the analyses, and post-process the results would take days. This would be very time-consuming, and expensive. It could also preclude the possibility of running various "what-if's" or parametric studies simply due to time constraints. The rapid assessment approach that is being proposed in this research, once implemented in software as a new version of the current PWB analysis program *CALCE_PWA* is anticipated to be executed by an average engineer in real time and take only minutes to obtain accurate results.

1.2 Motivation

Since the first large scale adoption of surface mount packaging in the 80's, extensive research has been conducted in the area of solder joint fatigue, but it has primarily been aimed at low cycle solder joint fatigue under thermal cycling. However, many modern electronic products have to endure severe environments that involve not only thermal but also dynamic loading conditions that result in high cycle fatigue. Vibration loading has become very important in the reliability assessment of modern electronic systems. It has always been difficult to obtain an estimate of field failures in terms of how many solder joint fatigue failures are caused by thermal cycling and how many are caused by vibration. One of the more quoted values dates back to Steinberg [1988] where it was estimated that 80% are caused by thermal issues and 20% caused by some form of vibration or shock. Regardless, modern engineers recognize that electronic products are now being used in more and more severe environments and their environmental limits will be continually tested in new applications.

One only needs to think of commercial personal portable electronic products such as cell phones, personal data assistants, and entertainment devices (as exemplified by the I-pod) to realize that electronic products are no longer exclusively used in a relatively benign office environment. Recent events in the Middle East have brought to the forefront the new military battlefield electronic applications. Electronics are becoming more complex while being subjected to a more strenuous environment that requires ruggedness under drop, shock, and vibration and combined loads that involve humidity, dirt, and thermal cycling. Moving beyond personal devices, all transportation vehicles (cars, planes, trains,

busses, cars, etc.) are being controlled by electronics. We are now living in a drive-by-wire condition, where throttles, brakes, and even steering are now being controlled by electronics and not mechanical linkages. Any electronics in a vehicle must be able to survive in a vibration environment.

All electronics must be able to handle the various loads seen in manufacturing, screening, as well as shipping, even if their entire life is spent sitting in a relatively benign office environment. One of the major reliability issues for today's electronics is solder interconnects failure due to thermal and vibration fatigue. An extensive amount of research has focused on thermal fatigue and most designers are relatively comfortable designing for this environment. Lau's books [Lau, 1997] provide a good review of the thermal fatigue problem and various fatigue life assessment approaches.

Vibration loading has become much more important in the reliability assessment of modern electronic systems. The current challenge is how to execute the vibration fatigue life analysis rapidly and accurately. There are two basic approaches to determine the vibration fatigue life: either through experiment or through some type of modeling or simulation. Measuring the fatigue life of the actual product in an experiment is obviously the most accurate, but often the answer is needed before the product is built. Experiments are also very expensive to conduct, both in terms of the time expended as well as the equipment and personnel needed to run the tests. Modeling or simulation can be cheaper and more efficient, but accuracy of the results is always a concern.

Previous work analyzing the fatigue life of electronic products in a vibration environment has included experiments, and various modeling approaches. The most common modeling approach has been with the use of the finite element technique. There are advantages and disadvantages to each approach. Chapter 2 will review the previous work in the area of determining the fatigue life of an electronic product in a vibration environment. This dissertation is concerned with a rapid assessment technique that can be conducted by an engineer in almost real time. The goals are to have an efficient and better accurate approach that uses as a basic framework the *CALCE_* software. The details of the approach are presented in Chapters 4, 5 and 6.

1.3 Problem Statement and Research Scope

The currently available *CALCE* software [*CALCE _PWA*, Version 4.1] for evaluating PWB and their solder attaches uses a vibration fatigue life model which is basically an empirical model. The model has been demonstrated in the past to do an acceptable fatigue life assessment for most components.

The problem with the model, since it is empirical, is that it must be calibrated for new component styles and new materials as they become available from the various component makers. Such calibration efforts are time consuming and require expensive experiments. The research presented in this dissertation attempts to move in a direction to improve the current *CALCE* model. The major improvement is due to breaking up the current empirical model into a separate stress analysis model and a separate fatigue damage model. The current *CALCE* empirical model does not calculate a stress, but

rather a fictitious damage parameter that is only loosely related to stress. The calculation of this fictitious damage parameter only considers the overall package size and considers no other material or geometric parameters of the particular package. The approach taken in this dissertation calculates an actual stress in the critical solder joint and considers all package geometry and material details. This new approach conducts a true stress analysis, where the previous approach only considers package size and style. By breaking up the analysis model into a true stress analysis followed by a damage analysis, one should be able to directly investigate and predict the influence of new component families (geometries) and new materials. The previous model required the new calibration factors to be developed after experimental data became available.

The approach in this dissertation will involve global (entire PWB) and local (particular component of interest) modeling approaches. In the global model approach, the vibration response of the PWB will be determined. This global model will give us the response of the PWB at specific component locations of interest. This response is then fed into a local stress analysis for accurate assessment of the critical stresses in the solder joints of interest. The stresses are then fed into a fatigue damage model to predict the life.

1.4 Summary

The remainder of the dissertation is broken into eight chapters. The content of these chapters is summarized below:

Chapter 2: Literature Review

Chapter 2 will briefly review what has been done in the reliability of BGA under vibrations in the four major categories: empirical base equation, analytical model, finite element analysis model and experiment model. There are many types of BGA packages. In this dissertation, only plastic ball grid array (PBGA), ceramic ball grid array (CBGA) and chip scale packaging (CSP) will be focused on and the history for each component packaging will be indicated. The vibration fatigue analysis of PWB and components has been performed mainly with various analytic and empirically derived models, traditional finite element analysis using general-purpose finite element analysis software, and by conducting experimental tests with actual hardware.

Chapter 3: Technical Approach

This chapter explains the technical approach used in solving the problem. The general approach is based upon understanding and using the underlying physics of the problem. The underlying physics allows one to identify the critical failure mechanism and ultimately the critical loads and damage model that are necessary to arrive at a final life model for the BGA device in question. This approach has become known as the Physics of Failure (PoF) approach in the electronics packaging community. There are two approaches to describe the random vibration environment. The most obvious approach is to work in the time domain by simply recording a time history of some parameters that describes the motions. The other approach is to work within the frequency domain, which can be thought of as a Fourier transform of the time domain recording. Both

approaches have their advantages and their disadvantages, and will be discussed in more detail in this chapter.

Chapter 4: Global Model Approach

The purpose of the global model is to determine the overall or global response of the PWB. The global model contains the geometric and material details of the PWB and its boundary conditions. The global model does not contain enough detail to accurately determine the stresses in the various component attaches. The global model is intended to only provide boundary condition information for a more detailed local model that will model a particular component of interest.

Chapter 5: Local Model Approach

The global model should give us the accurate curvature, which in turn can easily be converted into the accurate bending moment executed at specific locations of interest. This accurate moment is then fed into a local stress analysis, which has enough resolution to determine the critical stress in the various component attaches.

Chapter 6: Damage Model Approach

Once the critical solder ball stress has been determined, a damage model or law is required to calculate the fatigue life. The fatigue failure will be in the region known as high cycle fatigue. High cycle fatigue damage life is driven by elastic stresses, and plastic stresses are negligible to non-existent. A simple high cycle fatigue damage model will be used to calculate solder joint life.

Chapter 7: Case Study

Chapter 7 will demonstrate the new rapid assessment for two cases. In both cases, we will focus on the BGA type components including PBGA, CBGA and CSP components. Predicted life will be compared to experimental results. The goal in this chapter will be to demonstrate that the rapid assessment methodology developed in this research is easy to use, rapid, and accurate for assessing the fatigue life of BGA solder joint under vibration loading.

Chapter 8: Conclusions and Future Work

The work in this dissertation developed the rapid assessment methodology of BGA packaging fatigue life under vibration loading. These parts included global and local model approaches. This chapter will present conclusions based upon the research presented in this dissertation and offers recommendations for the further work.

Chapter 2: Literature Review

The major trend today is to make electronic products lighter, smaller, thinner, and faster, while at the same time more reliable, more powerful and cheaper. Ball grid array (BGA) and chip scale packages (CSP) are becoming the dominate package styles. Thus the solder joint reliability of these package styles is an important aspect of the electronic product's reliability.

BGA packages have a distinct advantage over more traditional perimeter leaded packages such as quad flat packs (QFP). Primarily due to the larger pitches of BGA packages and the lack of delicate leads that can be bent, BGAs have been shown to have a much higher yield in board assembly as shown in Table2.1. BGA uses solder balls on the underside for the substrate to PWB interconnects, thus eliminating delicate leads, and makes the BGA a more robust package than a QFP. It also has the advantage of making the BGA self-centering during re-flow. This allows relaxed placement accuracy and is a distinct advantage that BGA has over high I/O QFP devices. Because the BGA is also physically smaller it usually has better electrical characteristics than flat pack devices.

Table2.1: Quad Flat Packages and BGA Yield Comparisons (Source: IBM)

	QFP		BGA
Pitch size (mm)	0.5	0.4	1.27
Industry (ppm/lead)	200	6000	0.5-3
IBM (ppm/lead)	75	600	0.5-3

There are many types of BGA packages. For example: Plastic ball Grid Array (PBGA), Ceramic Ball Grid Array (CBGA), Chip Scale Packaging (CSP), Ceramic Column Grid Array (CCGA), Tape Automated Bonded Ball Grid Array (TBGA), Micro Ball Grid Array (μBGA), Mini Ball Grid Array (mini BGA), and so on. In this dissertation, the focus is only on the basic or generic BGA styles; i.e. plastic ball grid array (PBGA), ceramic ball grid array (CBGA) and chip scale packaging (CSP). The PBGA package style has evolved from the original Motorola over-molded-pad-array-carrier (OMPAC). This package is basically an epoxy laminate substrate with solder balls on one side and a die mounted and wire bonded to the other side of the substrate. The die and wire bonds are protected with a plastic over mold. The CBGA has evolved from the original IBM controlled-collapse-chip-connection (C4) package and is simply a ceramic package body with a ball array on the bottom and a die typically flip chip mounted on the other side of the ceramic substrate. The die may or may not be hermetically sealed with a lid. In the simplest of concepts a CSP is simple a PBGA where the entire package body plan view dimensions are on-the-order-of, or less than 120% of the die size.

Extensive research and much has been published in the area of BGA solder joint reliability under thermal cycling. However, much less research has been done in the area of BGA reliability under vibration loading. In fact, there is only a limited amount of published research on solder joint reliability under vibration for any component or package style. Thus the literature review presented in this chapter will include the major papers on solder joint reliability under vibration, regardless of the package style.

When one views the papers on the fatigue analysis of PWB and components, the papers fall into 4 general categories or primary analysis methodologies. First there are the papers which develop or use empirically based formulas or equations. These are formulas that have evolved based upon experience or from a fit to experimental data. The formulas have little or no correlation to the underlying physics or dynamics of the problem. The second sets of papers develop or use analytic models which are based on the physics and dynamics of the problem, but generally involve simplifying assumptions. The distinction between the first and second set of papers is somewhat arbitrary. The third sets of papers are those papers which rely upon finite element modeling. The fourth sets of papers are those papers which rely upon only experimental results. Most of the papers at least refer to some experimental validation or confirmation, but the papers in this last group are primarily driven by the experiments. The papers in each of these four categories will be reviewed and discussed in:

1) Empirically based equation in Chapter 2.1
2) Analytical models in Chapter 2.2
3) Finite element analysis models in Chapter 2.3
4) Experimental analysis models in Chapter 2.4

In addition, the reliability of BGA packages under bending, twisting and impact, will be briefly reviewed in Chapter 2.5 since many of the failures observed in this type of loading are similar to those seen under vibration.

2.1 Empirical Base Model Paper

- An empirical model or equation is based on design experience or test experience and is generally not based completely on the physics of the problem. Probably the best known empirical model to estimate component life under vibration is Steinberg's model [Steinberg, 1973, 1988, and 2001]. Steinberg first published his of referenced book, *Vibration Analysis for Electronic Equipment*, in 1973. He revised this book twice, in 1988 and in 2001. His approach was based on his testing and experience, and not on any kind of stress analysis. His earliest model was simply:

$$d = 0.003 \cdot b \quad \text{Equation2.1}$$

where the maximum board displacement, d, as modeled by a simple single degree of freedom system was to be kept below $0.003 \cdot b$, where b is the short side dimension of a rectangular PWB. His later model was a little more sophisticated in that the critical displacement accounted for the style, size, and location of the component on the PWB. But the model suffered from the draw back that it cannot be used outside the range and configuration of the assembly used in the derivation of the model. It cannot be used to evaluate new products or emerging technologies with any confidence.

Steinberg's critical PWB displacement is an empirically determined value. In addition, Figure2.1 shows that the calculated displacement of the PWB displacement is not the actual PWB displacement, but a fictitious value correlated as if the PWB were a simple spring mass system. Steinberg in addition assumed the PWB was simply supported along

all four edges. Thus the maximum PWB displacement and maximum PWB curvature occurs at the center of the PWB and this is where Steinberg assumed the most fatigue damage occurred. For components mounted at other positions on the PWB, a position factor is used to scale the damage. Steinberg's empirical equation resulted in a simple and easy to use method for evaluating the fatigue life in random vibration. The latest model also accounts for different package styles. For example, in Equation2.2 the constant, c for a standard dual inline package will be 1; but for the BGA the constant will be 2.25. This factor, c adjusts the life for packages that are not as robust as the standard dual inline package.

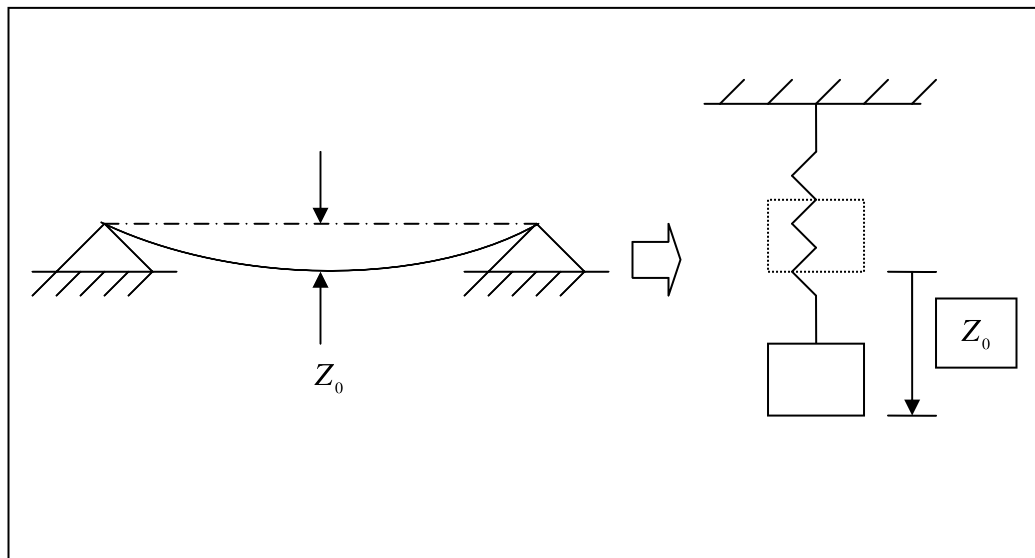

Figure2.1: A Vibration Spring-Mass System

$$Z_0 = \frac{0.00022B}{chr\sqrt{L}} \qquad \text{Equation2.2}$$

Z_0 :Maximum or critical PWB displacement (in)

B : Length of PWB edge parallel to component (in)

L : Length of electronic component (in)

h : height or thickness of PWB (in)

r : relative position factor for component on printed wring board

c : constant for different types of electronic components

$$N_0 \cdot Z_0^{\,b} = N_1 \cdot Z_1^{\,b} \qquad \text{Equation2.3}$$

N_0 : time to failure at critical maximum deflection Z_0

: 10^7 cycle under harmonic loading

: $2 \cdot 10^7$ cycle under random loading

N_1 : time to failure at displacement Z_1

b : fatigue exponent=6.4

Once the maximum or critical PWB displacement is calculated based on board and package style and dimensions, one calculates the actual PWB displacement under the particular vibration environment. Steinberg continually recommends estimating the actual PWB displacement with a fictitious displacement calculated as if the PWB were a simple single degree of freedom system. With a single degree of freedom system the displacement can be calculated from the natural frequency and results in the equation

$$Z = \frac{9.8 G_{in} Q}{f_n} \qquad \text{Equation2.4}$$

Were Z is the displacement in inches, G_{in} is the input acceleration in units of g, f_n is the natural frequency in units of cycles/second, and Q is the transmissibility of the system (approximated as the square root of the natural frequency f_n). One can calculate the actual fatigue life by using the Basquin high cycle fatigue relation as shown in Equation2.3. Steinberg rates his critical displacement as being good for 10 million stress reversals under harmonic vibration (sinusoidal) and about 20 million stress reversals under random vibration. Steinberg recommends using a fatigue exponent of $b = 6.4$. Steinberg only presents a heuristic argument for this value even in his earliest publications, but over time this value of the fatigue exponent has seemed to work quite well. Some of the most recent research at *CALCE* is demonstrating that this fatigue exponent is a good estimate of the high cycle fatigue exponent for near eutectic solder.

Since Steinberg's empirical model is based on his experience, it can only be applied to PWB constructed in exactly the same manner from which the origin failure data was obtained. It cannot be used to evaluate new components or emerging technologies. Even though the Steinberg's empirical model has some disadvantages, it is easy to use and can be used to make rough estimates about the fatigue life of the components.

- Marstein [1987] followed Steinberg's empirical model quite closely and illustrated how it could be used to design an electronic system to survive a high vibration and shock

environment. Marstein discussed how most modern electronic systems are composed of two major mechanical elements: an equipment chassis and a plug in printed circuit board (PCB) assembly. He concluded that the fatigue life of different components, component leads and solder joints, were based on the dynamic displacement of the PCB which in tern was a function of the natural frequency of the PCB. Marstein basically just recast Steinberg's equations to calculate the critical natural frequency of the PCB as shown in the following equation:

$$f_n = \left[\frac{29.4tc\sqrt{\frac{\pi}{2}pL}}{0.00022B} \right]^{0.8} \qquad \text{Equation2.5}$$

p : Power Spectral Density (PSD) input at f_n, (g^2/Hz)

L : Length of electronic component (in)

t : Height or thickness of PWB (in)

c : Constant for different types of electronic components

Marstein's approach to design was to insure the natural frequency of the PCB was higher than the critical value as calculated in Equation2.5.

2.2 *Analytical Model Approach Papers*

An analytical model is generally based upon the physics that are driving the problem, but almost always involve simplifying assumptions to reduce the mathematical complexity. The analytic model can help to quickly identify critical parameters and is generally less computationally intensive than numerical models. A few of the available analytical models are described below:

- Sloan [1985] in his book "Design and Packaging of Electronic Equipment" presented a relative comprehensive review of the calculations needed for the design of electronic equipment to survive various environments, including shock and vibration. His design calculations were typically discussed in terms of simple dynamics and strength of materials concepts. He basically pointed out various practical methods to calculate the critical stresses. As such, he really never developed what could be considered a model that could be applied to a generic PWB. It was a design approach that needed to be applied to each unique piece of electronic equipment. Thus his book is a good review reference, but doesn't give the user a final model to use to evaluate the fatigue life of components on a PWB.

From Sloan's design view point, failures due to vibration occur because the accumulated stress reversals exceed the endurance strength of the materials involved. Steady state excitation at equipment resonance contributes dramatically to the cumulative process. The nature of response amplitudes is dependent upon the characteristics of the design and input excitation. Vibration can be either translation or rotational, or a combination of

both, the result of a cyclic variation of force, displacement, strain or pressure. By the limitation of displacement, component stresses will be reduced correspondingly, increasing the vibration lifetime of the equipment. Although fatigue is indicative of many stress reversals, the time to failure may be short due to the frequencies involved. Based on his Chapters 6 through 8, we can get and review a lot of concepts, and learn about the design and packaging of electronic equipment such as force systems in electronic equipment, displacements stresses in equipment, and dynamic characteristics of electronic equipment. Chapter 8, dynamic characteristics of electronic equipments, is especially useful, as it illustrates the relationships that determine the static displacements, and that stresses in an assembly also form the basis of predicting its dynamic behavior. The motions an assembly can ascribe are also dependent upon damping and inertia forces within the configuration and the nature of the disturbance. The response may be developed in either the frequency or time domains. Overall, he described a more detailed design and packaging of electronic package in this book, and it serves as a good reference.

- Suhir [1988] created one of the most frequently cited analytic models in a technical note he wrote in 1988. Suhir was concerned with an anomaly he encountered in testing large multichip modules in that some of the smaller modules failed before larger modules. Something that he thought was counter-intuitive. Suhir treated the component –board assembly, part-board assembly, as a series of long, narrow rectangular plates connected by a continuous elastic attachment as shown Figure2.2. Suhir assumed the part's compliant leads transmitted only axial forces and the number of leads was

sufficiently large to be replaced by continuous elastic medium. Suhir was interested in calculating the maximum attach stress and the distribution along the part length.

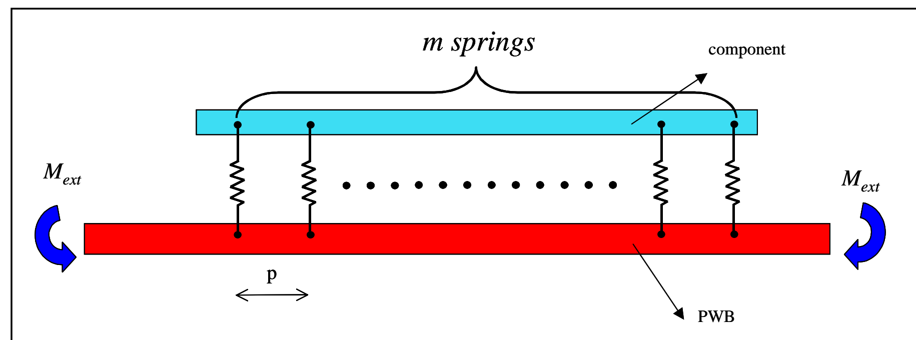

Figure2.2: Schematic Model of a Hybrid Integrated Circuits/PWB Assembly

Starting with two beams, with elastic attach between them, Suhir derived the complete equations for the deformations of the beams using classical beam theory. One beam was loaded by a bending moment at the ends and represented the PWB. The other beam represented the component. Having solved for the complete deformations of the two beams, Suhir had also solved for the attach stress, since it was simply related to the difference in displacement between the two beams. Suhir pointed out that somewhat surprising maximum attach stresses can be generated based upon the stiffness of the PWB, component, and attach. He demonstrated why some of the smaller components he tested under bending failed before some of the larger components.

Even thought Suhir's model was limited due to the continuous elastic attach assumption, several individuals (Ling's PhD dissertation, 1997) have attempted to use his underlying

equations to estimate attach stresses in various components subjected to bending. In the early part of this researcher's PhD studies, attempts were made to use Suhir's model. It was rapidly recognized the most parts and particularly BGAs have a fewer number of leads and the continuous attach assumption becomes questionable. To overcome this assumption, attempts were made to create a model of two beams separated with discrete attaches. The model was continually refined making it more and more general. The individual attaches were continually made more general, first supporting only tension, then supporting tension and shear, and finally supporting tension, shear, and bending. Only when the individual attaches supported tension, shear, and bending did the model results start to agree with more detailed finite element calculations. It rapidly became evident that this "simple model" was starting to become more and more complex and it suffered from the short comings of working with only full array type packages with a constant pitch. It became apparent that there was not an "easy" way to fix the short comings of the original Suhir model.

- Barker, et al. [1992, 1993], proposed some analytical methods to estimate the vibration fatigue life of leaded surface mount components. They discussed the assumptions and details of the fatigue life calculations required to predict the fatigue life of quad leaded surface mount components operating in a vibration environment and also presented that it does not require complex finite element modeling, nor does it reduce the problem to a simple empirical equation. There are three steps in their approach to calculation the vibration fatigue life of components mounted on a PWB: First, the modal analysis of the PWB to determine the boards' natural frequency. Second, a dynamics

analysis of the PWB to determine the boards response, and third, a stress analysis of the individual component attaches. Their approach is concerned primarily with the third step and is based on a stress analysis of the leads and the solder joints; it is formulated on fundamental geometry and material properties, and not on a specific manufacturing technology a specific component design. Their final critical attach stress used in a high cycle fatigue relationship is easily calculated by dividing the attach force with the nominal cross-sectional area. Final fatigue life is calculated using a Miner's superposition of the damage due to the lower order vibration modes.

- Barker et al. [1993] proposed the analytical method to estimating the vibration fatigue life of quad leaded surface mount components. They addressed how the difference in displacement can be calculated between the two end points of the corner lead attaching the component to the PWB. This difference in displacements at the two ends of the lead forms the displacement boundary condition, which is necessary for a stress analysis of the lead. Their approach can be broken down into three distinct steps as discussed previously. Their methodology gives a better understanding and better prediction of vibration fatigue failures than Suhir' analytical method but this method is only valid for relatively compliant leads and where the rigid assumption of the component with respect to the PWB is valid, is not able to handle stiffer leads, cannot compute the out-of-plane deflection of the corner lead in a local component mounted on the PWB assembly, and the high cycle fatigue property data is lacking for common lead materials.

- Sidharth and Barker [1996] extended Suhir's solution to include the rotational stiffness of the leads. They addressed the determination of the out-of-plane displacements of the corner leads of peripheral leaded components when the local peripheral leaded component/board assembly is subjected to bending moments in two directions (along x and y directions). Their solution is achieved by using a combination of finite element analysis (FEA), design of experiments (DOE and analytical techniques. The out-of-plane displacement can then be applied as a boundary condition on a local lead model to determine the stresses, which in turn can be used to estimate the fatigue life. Their model uses the functional form, which captures the basic physics of the problem and also reviews the different preliminary analyses. After that, a full factorial DOE matrix is setup to identify finite element simulations to be conducted. They help in reducing expensive prototyping when developing or evaluating new products by lending themselves to parametric/sensitivity studies.

- Sidharth and Barker [1996] address the determination of the out-of-plane displacement of the corner leads of peripheral leaded components when the local peripheral leaded component/ board assembly is subjected to bending moments in two directions (along x and y direction). The problem with this analytical model can be stated as follows:

First, this analysis is limited to square shaped components, which is a practical assumption, as most of the peripheral leaded components are square.

Second, all analyses are linear elastic.

Third, only the small deflection theory for thin plates is applied.

Fourth, they only use two level five factors full factorial matrix for the corner lead model, which is a very rough estimate of the problem.

Although their methodology is only a rough estimate of the problem, it still gives us a very helpful reference for the DOE approaches. They proposed more detail and how to set up the critical factors in their studies; even through we use three-levels and only two factors in our approaches. In comparison with our rapid assessment model, we use a finite element code to determine the dynamic response of the PWB in question. The proposed analysis uses a PoF type approach to damage analysis and involves global and local model approaches. It is the curvature of the PWB in the region of the component of interest that is driving the components solders joint damage. In other words, damage in the component attach is driven by the curvature at PCB in the region of the component. Once the response of the PWB was determined, one would determine the location and value of the critical stress in the component of interest. Knowing the critical stress, one could estimate the fatigue life from a damage model. A combination of FEA runs, DOE, and analytical approaches shall be used to quantify the out-of-plane curvature of the solder joints.

- Engel [1990] analyzed the flexibility of circuit card systems by subjecting them to bending, taking both x and y directions into account. He found that the maximum lead forces arose in the corner leads of the module and depended on the bending mounts and the stiffness of the system, including lead stiffness. His study of stiffness and lead forces

was based on primarily axial loading of the leads, an action recognized as crucial on the basis of his earlier work [1986] determining both experimental failure mechanisms and fatigue lives of J-leads. Later, Engel, et al. further investigated the stiffness of such surface mounted assemblies. They found the stiffness of circuit cards and modules can be determined by three-points bending tests. In this paper, two kinds of leads were studied: J-leads, and gullwings. In those models, the leads were considered a continuous elastic foundation connecting the module to the board. Engel and Ling [1993] extended the study to cover torsion. Engel summarized the analysis for the local assembly of compliant leaded systems. Mechanics assumptions and simplified materials, geometry, boundary conditions, and loadings limit the use of an analytical model.

The stiffness properties of the two most prevalent lead types during the time of the paper, the J-lead and gulling were obtained, in three perpendicular directions (x, y, and z). In addition, experimental measurements of subassemblies of module/card sandwiches were made, including various popular design configurations, such as double-sided and stacked module arrangements. In Engel, 1991, they only concentrated on modules having two rows of leads (two-lead row), such as Small Outline J-leaded (SOJ) package, small outline transistor packaging (SOT), and small outline IC's (SOIC). Comparing the experimental stiffness measurements of five distinct configurations with corresponding analytical results, the elastic solder attachment of the leads was found to render a condition half-way between free and hinged.

Engel's general conclusion was that the highest stresses were caused by the stiffest leads and in the stiffest directions. This conclusion, though somewhat intuitive, is born out in this dissertation where the stiff CBGA component typically fails before the more compliant PBGA component even though they may have the same dimension balls and bodies.

- Singal and Gorman [1992] developed a general analytical solution for the free vibration of rectangular plates resting on fixed supports and with attached masses. Their comprehensive analytical procedure based on the superposition method is described for establishing the free vibration frequencies and model shapes of thin plates resting on rigid point supports and with attached masses. Their analysis is obtained by superimposing several forced vibration solutions associated with the plate and constraining coefficients appearing in the forcing functions so as to satisfy all prescribed boundary conditions. In their analytical procedure they described the analyst with a powerful tool for predicting the natural frequencies of rigid point supported thin rectangular plates with or without attached masses. Their solution being analytical in nature possesses numerous advantages over possible numerical solutions such as those obtained by the finite element method. They demonstrated how the effects of added masses, including their rotary inertia, could be taken into account in predicting free vibration frequencies and mode shapes of thin plates resting on rigid point supports. The problem with this work, as with most analytic solutions, is that if the final solution is not simple to use or easy to understand, rarely is it used. This paper falls into the category of a solution that is not easy to neither implement nor understand.

- Darbha and Dasgupta [1997] presented an analytical methodology to analyze stresses in surface mount solder joints subjected to vibration loading using a generalized multi-domain Rayleigh-Ritz approach. The advantage of their approach is in its computational efficiency, compared to general-purpose finite element methods. Their technique is modified and adapted for analyzing stresses caused by out-of-plane flexural dynamic modes of the PWB. Their approach is two-step procedures where the local PWB curvatures are first estimated and the resulting deformations in the solder interconnect are then determined from the local PWB curvatures. The deformations, stresses, and strains in the solder joint are predicted using a modified version of the multinomial Rayleigh-Ritz (MDRR) approach. They also pointed out that the vibration of solder interconnects in an electronic package can be categorized into two critical modes: first, low frequency out-of-plane board vibration and second, high frequency in-plane component vibration. They used a simple two-dimensional example of elastic field analysis due to vibration loading condition for J-leaded surface mount solder joints. The input boundary conditions for the first step are the bending moments in the PWB due to random vibration, and then the stiffness of the interconnect assembly is predicted using an energy method and curved-beam analysis. In this analytical method, the surface mount component and PWB are assumed as flat substrates and lead/solder joint assembly is assumed to transmit axial force only. Stiffness of the lead/solder joint assembly and the bending moments induced in the PWB due to random vibration are two of the main inputs to Suhir's model to compute the curvature.

From Darbha and Dasgupta's final results, an enhanced Rayleigh-Ritx scheme has been presented, based on selective localized colonies of nested sub-domains, to systematically analyze the stress and strain fields in solder joint in a cost-effective manner. Again this is not another example of a solution that is not easy to implement nor is it easy to convince others that it is implemented correctly. For the same amount of effort one could use a more well established and understood method such as finite element analysis. Darbha and Dasgupta [1997] used the finite element method to calculate the stiffness matrices of various "J" and gull leads. Their method is to predict the stress, strain, and energy density distributions in the solder domain under combined cyclic thermal and vibration loading conditions with adequate accuracy for fatigue damage predictions, yet they use only a fraction of the degrees of freedom typically required in a full scale finite element analysis. Their proposed analysis uses two-step procedures where the local PWB curvatures are first estimated and the resulting deformations in the solder interconnect are then determined from the local printed wiring curvatures. The description of their approach is a good reference for the stress analysis of surface mounted interconnections due to vibration loading. The only limitation is one must use a modified version of the multi-domain Rayleigh-Ritz technique. As mentioned previously, this technique is complicated and not easy to implement by the average user.

2.3 Finite Element Analysis Model Approach papers

A finite element analysis model is capable of representing the geometry, the material behavior, and the boundary conditions easier and thus more accurately than empirical or analytic approaches. However, finite element analysis models are computationally

expensive and simplifying assumptions are needed to reduce the modeling and computational time. Several authors have presented various finite element analysis based approaches to predict solder joint fatigue life.

- Roberts and Stillo [1991] used a finite element model to analyze the vibration fatigue in ceramic capacitor leads under random vibration. In their analysis, however, only a specific PWB and an assumed dynamic random excitation were considered; therefore, their final results are only applicable to this specific PWB and this random excitation. Their investigation was to perform a random vibration finite element analysis (FEA) of a PWB (PWB) assembly with the ceramic capacitor and other components attached and to compare the results with an experimental random vibration test of the same PWB assembly in its chassis. The mode shapes, natural frequencies, and accelerations from the test would be compared with those from the finite element model. The finite element results would also be used to help explain any failure that might occur in the capacitor leads during the test and to help predict future fatigue failures. After comparing the FEA analysis results with the experimental results they concluded in general they agreed, but indicated the FEA model needed additional refinement and more detail added in the area of the lead/PWB interface. They also recognized that their FEA board boundary conditions were not well modeled due to the use of wedge lock card guides in the experiment.

- Pitarresi et al. [1991] have done experimental and FEA modeling work to characterize the natural frequencies, mode shape, transmissibility, and damping at the

board level. Later, Pitarresi [1992] uses the simple plate vibration models, various material/geometric property smearing approaches, as well as detailed finite element modeling. Smearing techniques derive their name from the fact that the material and geometric properties are smeared in an effort to reduce the complexity of the model. In a smeared representation, the focus is on determining the effective homogenized properties of the leads, component and PWB, rather than their individual properties. Variations of the smearing technique include global and local smearing. For the globally smeared model, the mass and stiffness are determined for the entire card and then these modified values are used in lieu of the actual properties. A locally smeared model is simply a refinement of the global smear in which sub-regions of smeared properties are defined. Although the finite element method provides a relatively efficient means for implementing the smearing approach, analytical methods may also be employed. A detail finite element model is one in which key components on the card are directly modeled.

- Pitarresi and Akanda [1993] estimated the response of surface mount solder joint subject to random excitation using the sub-modeling approach in finite element analysis and compare it to the experimental results. They also considered the forced response in the leads and solder joints of a surface mounted component under random vibration. They presented a development of the theoretical basis for random base excitation of circuit cards to model, via the finite element method, this phenomenon, and finally to verify the approach by means of experimental measurements. The analysis begins with the assumption that mode shapes and natural frequencies of the populated circuit card are

available. The sub-modeling approach was found to be an effective means of simplifying the construction of a finite element model of a card/module/lead configuration. Although not as simple as a smearing technique, the advantage was that information about the leads was readily accessible. The mode superposition post-processor provided an efficient means for computing the output power spectral density (PSD) using the mode superposition methodology described in their approach, and experimental measurements of the random vibration response of a surface mounted lead were possible through the use of a laser vibrometer. Predicted absolute PSD of the lead were in good agreement with those measured.

- In Jih and Jung's [1998] approach, the detailed three-dimensional local models of solder joint and lead frame with various lengths of interfacial crack were first built as the equivalent beam element in the global model to determine the effective stiffness and mass matrix of the equivalent beam element. The global model then consisted of the PWB and component connected by the equivalent beams with the effective properties of the local model previously determined. The natural frequencies and mode shapes of this global model can be determined by the eigenvalue and eigenvector calculation form finite element analysis. Furthermore, a mode superposition technique was employed in FEA to determine the absolute displacement PSD at any points on the global model, which was subjected to random base excitation at the supports of the PWB. Finally, the absolute displacements PSD on the top and bottom of the critical corner pin were statically applied to the local model for calculating the J-integral, which represents the crack growth driving force. In this model, Jih and Jung use a general-purpose program, ABAQUS.

The plastic body of the 160 pin gull wing lead QFP was also modeled as shell element. In their approach, an advanced global/local finite element modeling technique combined with the fracture mechanics approach has been demonstrated in their study as effective method to study the effect of vibration fatigue on the reliability of solder joint with a thermal cycling induced interfacial crack.

- Jung [1998] used finite element modeling to study the crack propagating in surface mount solder joints under vibration loading. In his work, the use of multi-domain method (MDM) as a direct stress analysis method to extract the effective local stiffness of BGA assemblies for determining high-cycle fatigue life has been extended. This method simulates a three-point bend test for flexural stiffness calculation. It demonstrates that the force-deflection relationship at the center of the system can be accurately achieved with proper constraints at the ends. The flexural stiffness is then calculated on the basis of beam theory. This calculation produces numerical results for various part-board connections, both with and without underfill. The accuracy of the formulation is examined for layered assembly. The results for long-layered beam theory agree with those based on layered beam theory. Their method is based on the MDM vibration principle with superposition of displacements at high-gradient stress regions, and this method requires less computational time than the finite element method while preserving the accuracy of the region of interest. They presented the two-dimensional modeling capability of the MDM approach. Two methods, finite element methodology (FEM) and MDM, are used with favorable results. They believe that MDM is an efficient method

for this type of analysis; it saves half the computation time but retains accuracy, when compared with FEM.

- Wong et al. [1999] developed a vibration fatigue life prediction model for BGA solder joint. In this study, three-dimensional global/local finite element models were first constructed with MSC/PATRAN code. For the global model including BGA package soldered onto the PWB, linear finite element dynamic analyses with the excitation normal to the PWB was conducted using MSC/NASTRAN code to determine the dynamic responses at the two ends of BGA solder joint. In these analyses, a single-degree-of-freedom system was assumed. A steady-state harmonic response provides phase angle values while a random response furnishes the power spectral densities as well as their root mean square values. For the local model having a refined mesh to simulate the local region in detail, a linear finite element static analysis was conducted by applying the derived RMS values with their corresponding phase angles to this model in order to determine the solder effective stress/strain RMS. This model, combined with a three-band technique and the derived solder effective strain, was then used to predict the BGA solder joint survivability. To estimate the solder joint fatigue life, an empirically derived formula of universal slopes based on high-cycle fatigue test data (Manson, 1965) was used in this work. More comments on this paper will be presented in section 2.5 when we review the experimental papers.

- Li [2001] considered a detailed modeling approach for random vibration analysis of electronic components. He presented a general methodology of failure analysis and

fatigue prediction of these electronic components under automotive vibration environments. Mechanical performance of these packages is studied through finite element modeling approach for given vibration environments in automotive application. In dealing with the solder joint fatigue life prediction, Li first employed an approach of system level modeling that contains all the involved components. Beams and pipes with effective material properties represent the component leads and solder balls. Global/local finite element analysis modeling is then used for correlation and solution of the stresses on solder fillets. Stresses of the leads are directly obtained from the global model, and the results are correlated with those obtained from detailed local mode. Using the dynamic responses of the leads from the system level mode as inputs, the solder/ lead joint detail model as gull wing lead detailed joint model is then used to solve for local stress in solder fillets. Three-dimensional local model is subjected to displacement loads that were obtained from the system level model. Cumulative damages of the copper leads and solders are further analyzed at various excitation levels using the correlated global/local finite element analysis model.

- Perkins [2004] discusses vibration experiments and modeling for specific components (CCGA) and developed procedures to predict the failure location and behavior of the filed solder joint using the sub-modeling approach. In particular, Perkins discusses the out-of-plane sinusoidal vibration experiments at 1G, 3G, 5G, and 10G, the analytical modeling, and the numerical modeling. Finite element models were developed to predict the failure location and behavior of the failed solder joints. In his work he has developed a finite-element model of electronic packages for vibration and thermo-mechanical

environments that avoids a local-global or sub-modeling approach. In order to capture all mode shapes, to account for inertial forces, and to account for possible plasticity in the solder joint, a full three-dimensional model is necessary. A hybrid three-dimensional model that consists of three-dimensional solid elements for solder joint of interest and equivalent beam elements for other solder joints was developed. The board and the ceramic substrate were represented using solid element. After the analytical and the finite element model are discussed, the solder joint fatigue life can be predicted using a stress based high cycle fatigue approach.

From a review of the above papers using finite element modeling to attempt to determine the vibration fatigue life of components attached to a PWB, some general observations or conclusions can be drawn: Numerical models (FEA models) are expensive both in terms of the modeling effort (meshing the model), solving the equations (computation time), and reducing the data. To overcome this expense, certain simplifying assumptions are needed. Typical circuit card assemblies contain many components, each with multiple solder joints. It is impractical to mesh the PWB good enough to get accurate answers in a single step. The use of finite element analysis to predict stresses in critical component leads would save time and money over conventional experimental testing. Due to the many parts to be analyzed in a typical PWB, various simplifying assumptions are required and a methodology that breaks the problem up into segments so that each component can be looked at rapidly.

2.4 Experimental Approach Papers

The various experimental papers on the fatigue life of components mounted to PWB s involved modal analysis and qualification type testing where the cycles to failure were measured. The key papers, and particularly those dealing with BGA components, will be reviewed. Some papers only reported on the experimental data. Other papers compared the experimental data to a failure prediction model, where finite element analysis was the dominate prediction tool. In this section, we will primarily review their approaches. Comments on the relevance of the work will be addressed in section 2.7 where summary conclusions will be drawn.

- Lau, et al. [1990] studied solder joint reliability under shock and vibration. They also conducted in-plane random vibration testing, in-plane shock testing, out-of-plane shock testing, and out-of-plane vibration testing. Their testing was limited to determining the failure status after certain cycles of dynamic loading. Lau, et al. [1993, 1996] conducted vibration reliability testing of Surface Mount connectors and solder bumped flip chip. The most commonly observed failures modes were overload and fatigue. Examples of fatigue failure include the vibration of a PWB with surface mount connectors soldered to its surfaces, and the temperature cycling of surface mount connectors. They experimentally studied the solder joint reliability of five different surface mount connectors such as Single Inline Memory Module socket (SIMM), and Zero Insertion Force flex circuit connector (ZIF) and eleven different test methods, for example: thermal cycling, in-plane vibration, out-of-plane vibration, mechanical overload by bending, twisting, pulling, and pushing.

According to Lau [1995] the effects of shipping and functional environmental stress factors on the vibration responses of the solder joints have been determined by out-of-plane vibration experiments and a mathematical analysis. The reliability of solder bumped flip chips on organic coated copper printed circuit board has been studied by shock and vibration test and a mathematical analysis. The natural frequencies, excitation frequencies, excitation magnitude, velocity, and acceleration of the solder bumped flip chip vibration system have been systematically and carefully determined in this work, and it also mentions that the shock and vibration test results of the solder bumped flip chip assemblies are much better than that other surface mount technology assemblies, for example, plastic QFP and plastic leaded chip carrier, and surface mount technology connectors. Lau, et al. [1993, 1996, 1997) conducted vibration reliability testing of surface mount connectors, PBGA assemblies and flip chip assemblies using sweep sinusoidal excitation. They reported that the failure in a PBGA solder joint was caused by the crack near the interface between the solder joint and the copper pad on the bottom surface of the PBGA component. Their testing was limited to determine the failure status after certain cycles of dynamic loading, and limited to the solder joint failure occur at the solder joint at the package corner under vibration testing, meaning the high stress region is imperfect condition.

- Lee and Ham [1996] developed a fatigue-testing system to study the integrity of electronic packaging subjected to mechanical vibration. A data acquisition system was developed for the fatigue test of the electronic board. The fixture for the specimen was designed to be suitable for measuring the fatigue life of a typical module/lead/PWB

electronic system subjected to vibration. With this automated fatigue-testing machine, the mechanical integrity of surface mount component with the spider gullwing leads was studied by a mechanical flexural fatigue test. An experimental method was developed to measure the changes in electrical resistance in the lead, which is used to indicate a fatigue. A relationship between the loading force and the fatigue life of the high-cycle region was discussed for the lead of spider gullwing type surface mount components. In this paper, fatigue tests were performed in a similar loading configuration at the frequency of 40 Hz to obtain the high-cycle fatigue data within 104~107 cycle range, and the reliability of a 132 spider gullwing leaded ceramic flat-pack has been studied by high-cycle fatigue testing. The onset of failure was measured by monitoring changes in resistance of daisy chained circuits. Ham and Lee noted that failures always occurs in the leads rather than in the solder joint for the spider gullwing type lead under vibration loading, and high-cycle fatigue curve corresponding to the 104~107 cycles.

- Wong, et al [1999, 2000, 2002, and 2004] reported on a series of experiments to model the dynamic response of a PWB under out-of-plane vibration and also investigates the random response of a BGA component. His final model evolved from an empirical formula of universal slopes, which is derived from high-cycle fatigue test data using a curve fitting technique over twenty-nine different materials of metals. Wong, et al compared the experimental data to three-dimensional finite element models. Test vehicles with, 304 pin CBGA, 600 PBGA, 352 PBGA, and 313 pins PBGA were used to calibrate the proposed life prediction model. Based on the measurement results, a destructive physical analysis was then conducted to further verify the failure locations

and crack paths of the solder joints. One of the primary purposes of these papers was to confirm the failure locations of the solder joints during the vibration test. The results show the three points: First, solder cracks occur at the solder/package interface for the 313 pins PBGA. Second, the solder joints of the 304 pins CBGA have longer fatigue lives. Third, the first solder joint failure location for the 304 pins CBGA is at the lower-right corner solder joint ball. The first conclusion from this paper is generally inconsistent with others' observations and is probably due to detailed construction details of the particular PBGA used. Wong also concludes in the papers that further improvements in his methodology, and FEA is needed. He privately has also indicated that the experiment suffered from small sample sizes and small variations in package sizes.

- In order to understand the high-cycle reliability of plastic BGA interconnections subjected to external vibration loading, constant-amplitude vibration testing of a PBGA assembly was conducted by Yang, et al [1999]. Usually, a modal test can be conducted in three different ways: normal modal testing, impact hammer testing, and vibration shaker testing. In Yang's experimental test, since the PBGA and PWB assembly is a simple and small structure, impact hammer and vibration shakers methods were considered. In order to verify the material mechanical properties and boundary condition used in finite element modeling, modal tests of the assembly with two-side clamped, one-side clamped and free boundary condition were conducted. Tests could separate the influence of material properties and boundary condition to the finite element model. Some factors that could influence the accuracy of modal testing, such as measuring

location, mass influence of transducers and pre-stressed phenomena were also discussed in this paper. In Yang [2002], he continued his original work and conducted vibration testing of plastic BGA assemblies and found that the dynamics response of the assembly under out-of-plane sinusoidal vibration excitations was highly nonlinear. The test vehicle is an assembly with four 256 I/O PBGA modules mounted on the FR-4 PWB. In this test, the assembly was clamped at two opposite sides on a fixture, which was bolted to a vibration shaker. During the test, the resistances of PBGA modules were continuously monitored, so that any fatigue failure could be detected, and the vibration cycle to failure of the PBGA modules measure.

Yang concluded the failed PBGA solder joints were located at the corners of PBGA components. Most failures were due to cracks near the copper pad on the PWB side. The first-time-to-failure (FTTF) in this result is very close to the test results reported by Lau et al [1996], but the failure location is different. Lau reported that the failure in a PBGA solder joint was caused by the crack near the interface between the solder joint and the copper pad on the bottom surface of the PBGA component. Lau and Yang's results are closer, with only the location different; this is because in the high stress region, if the perfect conditions such as geometry solder joint configurations, and vibration profiles, the BGA solder joint failure most likely occurred at the solder joints at the PWB corners during the FEA model. Otherwise, under imperfect conditions, the solder joint failure may be caused by the crack near the interface between the solder joint and the copper pad on the bottom surface of the component or on the upper surface of the component.

- Liguore and Followell [1995] reported a test program to obtain structural fatigue data for surface mount technology solder joints exposed to an out-of-plane random vibration environment. A total of eight printed circuit board specimens with nine surface mounted components were fabricated and tested such as 68 pin J-lead, 32 pin LLCC (leadless chip carrier), and 84 pin LLCC. The purpose of their study was to collect vibration fatigue data of solder joints for LLCC and J-leads in realistic service environments. Specially, the test objectives included determining the effect of component location on solder fatigue life; the effect of ambient temperature on fatigue life; the effect of component size and the number of pins on fatigue life; and the relative durability of J-leaded components and leadless chip carriers of the same size. Time to failure data for individual solder joints was recorded. Their approach assumes that the failure free operating period of fatigue life can be quantified as a function of the imposed environment and the structural and material properties of the component. Liguor and Followell [1995] demonstrated that the vibration fatigue life of leadless chip carrier solder joints could be one to two orders of magnitude less than that of J-lead solder joints due to a lack of a lead wire to absorb the vibration loads. According to Liguor and Followell [1995] the same methodology would be used in the BGA solder joints since no compliance leads or solder joints are available to reduce the stresses and strains in these solder joints. Thus, the BGA solder vibration fatigue damage becomes one of the major concerns in electronic package design.

- Basaran and Zhao [2001] presented the results of a series of laboratory tests dedicated to the investigation of dynamic behavior of 63Sn/37Sb eutectic solder joints in a new

generation high performance CPU chip with BGA configuration. Their purpose is to study the nonlinear inelastic response of the solder joints under harmonic vibration at a certain temperature, and the role of dynamic loading to the fatigue life of the solder joints. Their approach is based on two relatively independent parts in the entire testing procedure; one is the loading part and the other is the optical measurement part. For the first part, an environmental thermal chamber and an electro-dynamic shaker are used simultaneously. For the second part a laser Moiré interferometry device was designed and manufactured for deformation measurement at the resolution of half of the light wavelength. From this paper, one was performed to study inelastic behavior of solder joint of BGA packages and was found that at elevated temperature, vibration and shock can cause the accumulation of inelastic strains and damage in solder joint. Testing is performed on real life electronic packages that provide true perspective of reliability and failure analysis of BGA solder joints. In harmonic vibration test, sine-wave vibration were conducted at 20o and 10o C. The plastic deformation in each solder joint after each vibration test was measured by laser Moiré interferometry.

In this paper, contrary to the popular belief that all vibration-induced strains are elastic, it is shown that vibration can cause significant inelastic strain. It is noteworthy that Basaran and Zhao observed that at higher temperature solder material softens, and the yield point is much lower than that at room temperature. With the same frequency, solder material responds plastically at high temperature while it responds elastically at lower temperature. Therefore, vibration at high homologous temperature is very harmful to solder joint fatigue life. Essentially the solder behaves elastically for higher

frequencies and inelastically for lower frequencies. This is due to the fact that at lower frequencies the period of the loading is higher. The time dependent inelastic deformations are directly related to the period of the load. When the load has a longer period the material has more time to creep. Consequently for vibrations with small frequencies creep dominates the response.

- The Electronic Miniaturization for Missile Applications (EMMA) project and associated final report [Wilcoxon, 2001] has been widely referenced by researchers and engineers in the field. This report documents vibration testing of circuit cards populated daisy chain leaded, BGA (BGA), Chip Scale Package (CSP), and Direct Chip Attach (DCA) components. The testing matrix was originally set up to try and determine variations in fatigue life as a function of component type, board construction and manufacturing processes, and vibration level. Unfortunately too many variables were explored in too few test replications and resulted in data that was somewhat inconclusive. Ferdie [2000] attempted to use these results to estimate coefficients for accepted empirical correlations to predicting component fatigue life. He also attempted to provide general design guidelines for the use of area array packages in high vibration environments. The EMMA test results are used later in Chapter 7.

- The JGPP report [Joint Group on Pollution Prevention, Woodrow, 2005] is another large experimental test program with various BGA components. This test program was originally set up to compare the performance of various solders under various types of thermal and vibration loading. The JGPP experiment will be discussed further in Chapter

7 where the vibration test data on eutectic solder is used to compare with the predictions from the BGA fatigue life model developed in this dissertation.

2.5 Bending and Twisting Analysis Approach Papers

Several investigators have proposed solder joint reliability under PWB twisting and bending. Bending tests have been conducted on various component board assemblies and the results are somewhat relevant to this dissertation in that the deformation of the PWB is similar to what occurs under vibration. Other researchers have tested surface mount component assemblies by twisting to verify the structural integrity or robustness of electronic packaging assemblies. During torsional flexing, the leads are substantially stressed, and their solder joints are subjected to appreciable mechanical loading. The geometry of the torsional flexing is relatively simple, and structural analysis benefits from symmetries. Bending and torsional deformations arise in various dynamic modes of the PWB and occur in the various stages of product life, such as in handling and shipping.

➢ Bradley's [1995] is the earliest evaluation that used a simple static test where boards were bent in a single stroke until the joints or components failed. In more recent evaluations, cyclic bending is being used to test solder joint reliability. A variety of environmental stress factors such as shock, vibration, temperature, and humidity may lead to solder joint failure. Bradley pointed out that the one of primary issues in considering the reliability of the resulting solder joints is the PWB finish. While the paper deals with fatigue and creep failures of the solder itself, there is limited quantitative or predictive information on the influence of the termination interfaces on solder joint

integrity. Bend testing was conducted on soldered assemblies in a three-point bend mode under a positive bending configuration. The failure of the solder joints during the bend tests was observed by physically removing the partially adhering chip carrier from the PWB. The majority of solder joint failures were due to issues with the termination metallurgy. In order to consider the relative integrity of solders joint reliability as a function of the termination interface, it is necessary to test under conditions of high-imposed strain rates.

- Lau, et al. reported [1995] bending and twisting experiments and determined the effects of overload environmental stress factors on the mechanical responses of the solder joints and studied mechanical and vibration responses of PBGA assemblies due to overload environmental stress factors. The most commonly observed failure modes were overload and fatigue. Overload failure occurred whenever the stress in the solder joint brought about by the imposed stress factors is greater than strength of the solder alloy. An example would be extensive bending and twisting of a PWB with PBGA soldered to its surface. On the other hand, fatigue failure takes place via the initiation and slow propagation of a crack until it becomes unstable. The stress factors that typically cause failure by fatigue are far below the overload failure levels. Examples of fatigue failure include the vibration of a PWB with plastic BGA soldered to its surface and the power cycling of a PBGA, which is soldered to the surface of a PWB. They conducted bending and twisting experiments to stimulate the effects of overload environmental stress factors and out-of-plane board vibration on solder joint reliability.

- The reliability of area array solder joints in bending was investigated by both testing and analytical methods [Darveaux, 2002]. Darveaux pointed out the PWB bending failure can occur in at least three different regimes. Creep rupture can be caused by localized bending of a board, possibly due to a screw that secures a board to housing. A component near the hold down screw can fail over time because the joints creep under tensile loading, and they eventually rupture. Creep rupture can occur days or even years after product assembly in a factory. A second board bending failure mode occurs due to key press action. A third board bending failure mode occurs when portable products are dropped. With the advent of fine pitch BGA and CSP, it has become clear that PWB bending is a critical factor in portable product reliability. In his approach, he used both three-point and four-point configurations to characterize the reliability of CSP assemblies under cyclic loading. Four different failure modes were observed in the bend testing. Similar to the solder joint fatigue life under vibration loading, the solder joint failure occurs at the solder joint at near on the PWB side.

- Tu [2000] pointed out that the bending in particular is the main form of mechanical stress that assembled PCB carrying BGA components bears in practice; additionally the failure modes of the BGA assemblies have been analyzed and compared with the mechanical failure modes of PBGA and CBGA assemblies. In their study they have covered work on the mechanical reliability of BGA assemblies evaluated through low cyclic bending, vibration and impact for different reflow temperature profiles and ambient to optimize the reflow parameters; they also focused on the reliability of BGA assemblies evaluated through cyclic bending. Based on the results the optimal heating

profile is given. Additionally the failure modes of the BGA assemblies have been analyzed and compared with the mechanical failure modes of PBGA, and CBGA assemblies.

2.6 Summary of Literature Review

In reviewing the literatures that arrives a final failure model, it was observed that there were two basic types of models developed. There was the class of models that resulted in a final single equation. This equation was typically an empirical equation and not derived rigorously from first principles. The second type or class of failure model employed a stress analysis and followed by a damage analysis through the use of a high cycle fatigue relation.

Empirical model:

In the empirical model, the key approach is fitting the resulting equation to a series of experimental results that have measured the fatigue life of the component. The accuracy of the experimental results will have a direct impact on the final empirical model. Since the empirical model is derived from the experimental results, the empirical model will only work under the specific condition of underlying experiment, i.e. specific component types, specific board geometries, specific vibration environment other than used in the experiment. It is not possible to extrapolate to other component types or other geometries and loads with any degree of confidence.

$$N_f = f(loading\ and\ Geometries)$$
$$N_f = life\ cycle\ to\ failure\ or\ time\ to\ failure$$
Equation2.6

Stress analysis followed by damage analysis:

The stress analysis is done through analytic or numerical methods to determine the critical stress in the critical component lead. This stress is then used as an input to a high cycle fatigue model to predict life. This approach is more flexible and more general in that the stress analysis can be conducted on any new or different component. It is assumed that the high cycle fatigue model reflects only material property information and should be independent of geometry.

$$\sigma = f(loading, stress\ and\ Geometries)$$
$$\sigma : stress$$
Equation 2.7

Knowing the stress, one would estimate the fatigue life from the damage analysis.

$$N_f = f(\sigma)$$
$$N_f = life\ cycle\ to\ failure\ or\ time\ to\ failure$$
Equation 2.8

2.7 Observations of the Literature Review Survey

The various papers discussing the failure of components mounted on PWB s subjected to a vibration load can be broadly categorized into 4 groups. The groups are those that discussed failure in terms of 1) an empirically developed failure model, 2) an analytically

based failure model, 3) a FEA based model, and 4) experimental observations. There are advantage and disadvantages of each approach.

1. Empirical base model:

Empirical equation is based on experience or the analysis of actual testing data not necessarily calculated from a theoretical basis or on proven theory.

Steinberg's simple empirical equation [1973, 1988, and 2000] is the best known and probably the most often cited model in the area of PWB vibration fatigue. It is very easy to use an offer a very rapid assessment of vibration life as long as the component in question was part of the original data set used to calibrate the model. The primary issue with this model and all empirical models is that they are based upon a fit to experimental data. They cannot be applied to new component package styles, new package sizes, or new solder types without expensive experimental testing and re-calibration.

2. Analytical analysis model:

An analytical model is typically based upon first principles and can help to quickly identify the parameters of interest in vibration analysis and is computationally less intensive than numerical models.

Analytic models are generally a stress analysis based upon first principles followed by a damage analysis. The accuracy of the model is a function of the simplifying assumptions used in the development of the closed form equations. These models are good for

identifying critical parameters and insight into the overall problem, but rarely offer the accuracy needed for an accurate analysis.

3. Finite element analysis model:

Compared to analytical models, numerical models are capable of representing the geometry, the material behavior, and the boundary conditions more accurately, and are capable of capturing the full spectrum of modes. However, some disadvantages still exist.

The FEA method though offering the capability for a very accurate stress analysis, suffers from the expenses associated with meshing, computation time, and data analysis time. To efficiently employ the finite element approach, a global local modeling scheme is required. Overcoming the issues associated with using finite element modeling for the practical assessment of components on PWB have been discussed by many papers and will be also discussed further in this dissertation in a later chapter.

4. Experimental analysis model:

Experimental tests are time-consuming and expensive.

Due to the expense of experimental testing, it is never possible to test all the variables one may wish to explore. This is complicated by the natural stochastic behavior of fatigue failures. Rarely are experiments conducted with enough replicates to confidently understand the failure distributions. This makes life difficult because many times quoted

failure data has inconstancies in it that are most probably explained by limited data and incomplete failure distribution information. In published papers that present experimental data, rarely do the papers contain enough details of the experiment that the results can be used confidently. This dissertation will use and discuss in more detail the experimental data from the EMMA and JGPP reports.

2.8 Overall conclusion:

In general the few vibration life assessment models that do exist are either too cumbersome to efficiently use (such as setup the detail finite element model, required an experience modeler conduct the results and post-process the results), or too empirical to use with new components or new advances in materials and only work in the specific condition or assumptions under which they were developed.

This dissertation will attempt to develop a rapid assessment model for BGA components that has the advantage of being efficient and easy to use. The approach will employ a stress analysis followed by a damage analysis. This research aims to build upon the model within the previously developed CALCE software to yield a very accurate and rapid assessment model for BGA fatigue life under vibration loading.

Chapter 3: Technical Approach

This chapter will start out with a brief review of the vibration environment and how it is typically characterized and end up with a review of BGA devices. The review of BGA devices is important in that there is not a single universal BGA design. Each manufacturer uses a slightly different geometry and combination of materials. The purpose of this final review is to show how BGA devices can be broadly broken into three general classes; PBGA, CBGA, and CSP. Within each of these three classes there are many sub-classes, but for general design considerations one can define a "typical" construction. This "typical" construction is used in the dissertation for the simulation modeling in order to obtain generalized results.

3.1 Random Vibration Environment

Vibration can either be periodic or random. Periodic or harmonic vibration is an oscillatory motion at a particular frequency, and thus the instantaneous position of the object can be predicted at any given time. Random vibration is an oscillatory type motion where the instantaneous position of the object cannot be predicted, but with a thorough understanding of the environment, the position of the object can be probabilistically determined. Electronic systems more commonly encounter random vibration than a simple harmonic type vibration. Typical random vibration environments include most transportation environments, e.g. aircraft turbulence, road undulations, or even the hand transportation of portable electronic products. Harmonic vibration is most

commonly seen very close to rotation machinery, but generally there is a strong harmonic vibration superimposed over a background random vibration.

The response of a system to a random vibration environment is more complicated than to a simple harmonic excitation. But once one understands the analysis for a random vibration environment, the general approach can then be simplified and applied to the special case of harmonic excitation. Therefore, this dissertation concentrates on the response of a BGA component mounted on a PWB in a random vibration environment. A theoretical background of the concepts of random vibration theory and practices can be found in Bendat and Piersol [1986], Wirsching et al. [1995], Shinozuka and Jan [1972], Meirovitch [1967], Elishakoff [1983] and Lin [1973].

There are two approaches to characterizing or describing the random vibration environment. The most obvious approach is to work in the time domain by simply recording a time history of some parameter such as displacement, velocity or acceleration that describes the motion as shown in Figure3.1. The other approach is to work within the frequency domain as shown in Figure3.2, which can be thought of as a Fourier transform of the time domain recording. Both approaches have their advantages and their disadvantages.

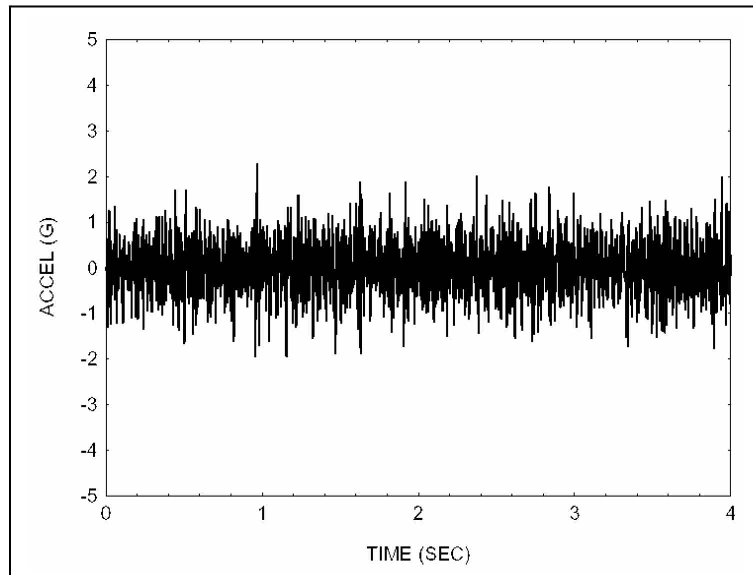

Figure3.1: Time Domain

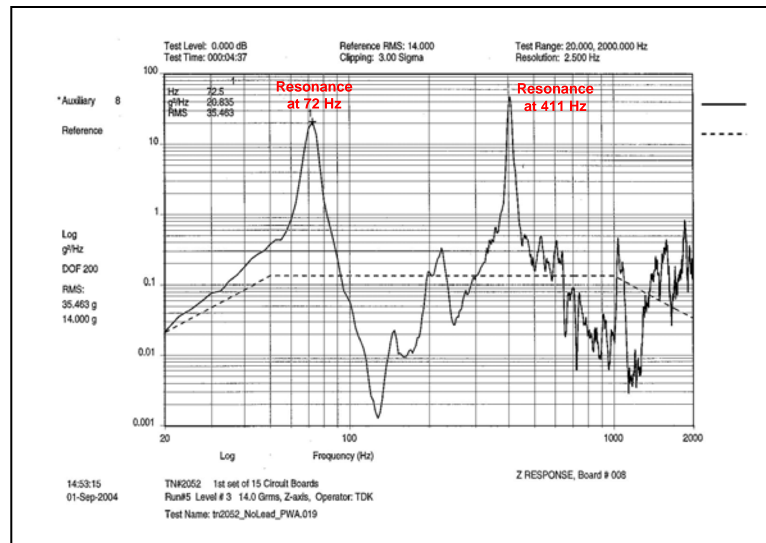

Figure3.2: Frequency Domain

Typically the time domain approach is used when characterizing or measuring an environment. The sampling rate and precision must be chosen so that the events of concern (frequency, ramp rates, and amplitudes) are adequately captured. The primary

problem with the time domain approach is the volume of data generated due to the sampling rate and time duration of the recording. If the random vibration environment can be considered a stationary process such that the mean and variance of the measured parameter do not change over time, the recording duration only need to be long enough to be able to calculate various statistical quantities on the measured parameter. Unfortunately we rarely see a completely stationary process. Typically we must assume that a certain recording duration adequately characterizes the environment or more appropriately the environment phase such as harsh turbulence, mild turbulence, smooth air, etc.

When conducting a fatigue damage estimation and life prediction with a time history various cycle-counting methods are used to reduce the random data into blocks of similar amplitude cycles. A time history or even load blocks from a cycle counting method is difficult to directly use in either vibration testing, vibration simulation with finite element modeling, or even when writing qualification or product specifications [Kumar, and Abhijit, 1999]. Typically in each of these situations it is easier to work within the frequency domain primarily because of the ease of specifying the vibration environment in the frequency domain.

The PSD is the most commonly used function to describe a random vibration environment in the frequency domain. PSD describes how the power (or variance) of a time series is distributed with frequency. If $f(t)$ is a signal, then the spectral density $\Phi(\omega)$ of the signal is the square of the magnitude of the continuous Fourier Transform of

the signal. Similarly, the PSD can be expressed in terms of the discrete Fourier Transform.

Historically product qualification tests were conducted on electro-dynamic shakers using acceleration PSD curves as an input. However, due to the inherent limitations of these shakers, frequencies less than 50 Hz were ignored due to the extremely large shaker head motions and frequencies greater than 2000 Hz were difficult for the shaker to achieve. High frequencies (>2000 Hz) were not considered to be critical because of the associated small motions and the general belief that the electronic assembly acted somewhat like a low pass filter and thus prevented the components from seeing the very high frequencies. Typically random vibration environments were defined for acceptance, qualification, and screening tests in the form of an acceleration PSD curve with a frequency between about 50 and 2000 Hz.

Since most products are designed for a random vibration environment that has been characterized with acceleration PSD curve, the rapid assessment approach developed in this dissertation will use the acceleration PSD curve as an input for analysis purposes. This does not exclude an environment that has been characterized with an acceleration time history, since the time history can always be easily converted into an acceleration PSD curve.

3.2 *Probability and Statistics*

3.2.1 G_{rms}

When the mean (μ) of the random variable (X) is zero, the standard deviation (σ) is equal to the root mean square of the random variable (X_{rms}):

$$\sigma = \sqrt{E(X^2) - \mu^2} = \sqrt{E(X^2)} = X_{rms} \qquad \text{Equation3.1}$$

where $E(X^2)$ is the expected value of the random variable squared. In random vibration environments under a constant velocity condition, the mean acceleration is zero. Thus, the standard deviation of the acceleration G is equal to the root mean square of the acceleration:

$$\sigma_G = G_{rms} \qquad \text{Equation3.2}$$

In the preceding section when talking about the square root of the area under the acceleration PSD curve, the term G_{rms} was used to express the root mean square of the random vibration acceleration in units of g or gravity. The G_{rms} value is a very useful amplitude measurement that indicates the variability of the acceleration. Unfortunately in random vibration, engineers commonly use the term G_{rms} in two distinctly different ways measuring two distinctly different quantities. When talking about the square root of the area under the acceleration PSD curve, the G_{rms} value is a statistic over the entire

vibration spectrum from the lowest measured frequencies up to the highest measured frequencies. Similarly engineers can also talk about the response of a PWB. A structure's response is a function of the vibration level at or near the structure's natural frequencies. Vibrations not near the structures natural frequencies have little influence on the structures dynamic motion. Thus engineers commonly also use the statistic G_{rms}, to describe the random vibration acceleration level at the PWB's natural frequency. One statistic is a measure of the random vibration over the entire frequency spectrum; the other is a measure of the random vibration at a particular frequency. Both are root mean square acceleration amplitude statistics, but they are two completely different measurements. Unfortunately this naturally leads to erroneous interpretations and misunderstandings. As an example one can have a random vibration environment with a very large G_{rms} level when talking about the complete frequency spectrum. A high G_{rms} value can easily occur if the vibration environment has been measured out to and includes some high frequencies. Remember that the G_{rms} measurement over the entire vibration frequency spectrum is the square root of the area under the acceleration PSD curve. The PSD curve is typically plotted in log-log space, so the area under the high frequency portion of the curve contributes more to the G_{rms} than the low frequency region. But the PWB is influenced most by the vibration levels near its natural frequency. If there is very little input near the PWB's natural frequency, the high G_{rms} measurement that represents the entire frequency spectrum is somewhat meaningless and has little correlation to the response of the PWB.

3.2.2 Assuming an Normal Probability Distribution

One needs to be able to determine the probability distribution function of the acceleration level (or any other parameter such as velocity, or displacement) to do any reliability assessment of the BGA component. It was previously explained that in this dissertation, the random vibration environment would be described with an acceleration PSD plot. In this dissertation, we will also assume that the random vibration environment is acceptably modeled with a normal probability distribution of acceleration amplitude. This assumption is generally a good representation of the random vibration environment, and it also simplifies the required calculations.

3.2.3 Linear Damage Superposition with a Normal Probability Distribution

At each particular frequency of interest, the random vibration environment can be considered to be composed of an infinite series of harmonic excitations, of the same frequency, but each having amplitude whose probability of occurring is defined by the normal distribution. The principle of linear damage superposition, or the Miner's rule, simply states:

$$\text{Damage Ratio} = \frac{n_1}{N_1} + \frac{n_2}{N_2} + \frac{n_3}{N_3} + \cdots = \sum_{i=1}^{m} \frac{n_i}{N_i} \qquad \text{Equation3.3}$$

where N_i = number of cycles to failure when subjected only to load amplitude level i

and n_i = number of cycles at the amplitude level i. Note that

$$n_i = t_i \cdot f_n = t \cdot f_n \cdot \alpha_i \qquad \text{Equation3.4}$$

where t_i = time at the amplitude level i in sec; f_n = natural frequency of PWB in cycles/sec; t = total time at a particular amplitude level i; α_i = percentage of time at the amplitude level i. By combining Equations 3.3 and 3.4 the Damage Ratio can be written as:

$$Damage\ Ratio = t \cdot f_n \cdot \left[\frac{\alpha_1}{N_1} + \frac{\alpha_2}{N_2} + \frac{\alpha_3}{N_3} + ... \right] = t \cdot f_n \cdot \sum_{i=1}^{m} \frac{\alpha_i}{N_i} \qquad \text{Equation3.5}$$

Rearrangement of the Basquin power law fatigue damage model gives:

$$N_i = \frac{C}{\sigma_i^{\,b}} \qquad \text{Equation3.6}$$

where N_i is the number of cycles to failure; σ_i is the stress amplitude that the harmonic load applies in the critical region of the component that is being analyzed and ; b and C are material constants. It is reasonable to assume that the resultant stress amplitude in the damage model is directly proportional to the random vibration amplitude at the frequency of interest. Thus if the acceleration amplitude is a normal distribution, then the stress amplitude is also normally distributed.

Figure3.3 is a representation of the normal stress amplitude distribution with mean = 0, and standard deviation $= \sigma_{rms}$.

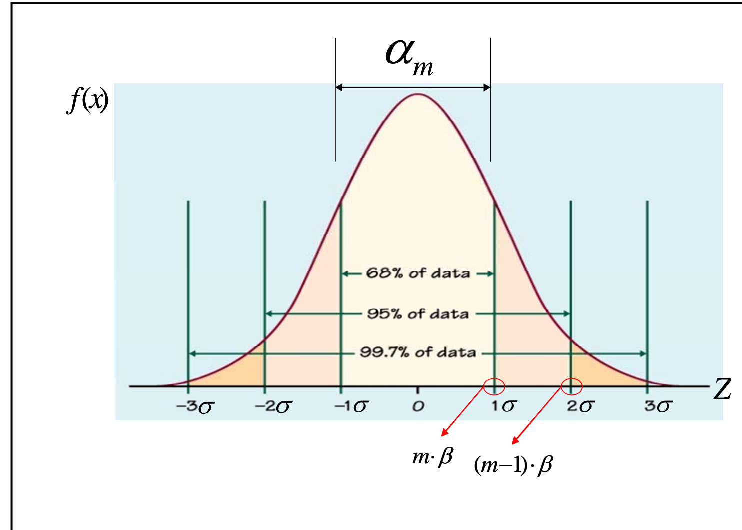

Figure3.3: Standard Normal Distribution

The probability of a particular amplitude (Z) occurring between amplitude $z_1 = (m-1) \cdot \beta$ and $z_2 = m \cdot \beta$ is simply the area under the standard normal curve as shown in Figure3.3 and where m is an integer and β is a width. The width β is introduced because we will be talking about the probability of a particular stress amplitude between $m \cdot \beta$ and $(m-1) \cdot \beta$. This width β will be shrunk in a later numerical calculation. The probability can be expressed as:

$$\Pr[z_1 < Z < z_2] = \Phi(z_2) - \Phi(z_1) = \Phi(m\beta) - \Phi((m-1)\beta) \qquad \text{Equation3.7}$$

where $\Phi(z) = \Pr[Z \le z] = \int_{-\infty}^{z} \frac{1}{2\pi} e^{\frac{-y^2}{2}} dy$. Due to the symmetric nature of the normal distribution the probability can be expressed as:

$$\Pr[z_1 < |Z| < z_2] = 2(\Phi(z_2) - \Phi(z_1)) = 2(\Phi(m\beta) - \Phi((m-1)\beta)) \qquad \text{Equation3.8}$$

The standard normal variable (z_m) is defined by the following equation:

$$z_m = \frac{\sigma_m}{\sigma_{rms}} \qquad \text{Equation3.9}$$

where σ_m is the stress amplitude and σ_{rms} is the root mean square of the stress amplitude (standard deviation). Considering the finite width, β, under the normal distribution curve going from $(m-1)\cdot\beta$ to $m\beta$ results in:

$$z_m = \frac{(m-1)\beta + m\beta}{2} = m\beta - \beta/2 \qquad \text{Equation3.10}$$

where m =1, 2, 3, 4… and for $m >> \beta$

$$z_m = m\beta \qquad \text{Equation3.11}$$

Substituting Equation 3.9 and Equation 3.11 into Equation 3.6 gives:

$$N_m = \frac{C}{(\sigma_m)^b} = \frac{C}{(m\beta)^b (\sigma_{rms})^b} = \frac{N_{rms}}{(m\beta)^b} \qquad \text{Equation3.12}$$

where the term N_{rms} is defined to be

$$N_{rms} = C / (\sigma_{rms})^b \qquad \text{Equation3.13}$$

Substituting Equation 3.12 into the damage ratio equation (Equation 3.5) gives:

$$Damage\ Ratio = t \cdot f_n \sum_{m=1}^{k} \frac{\alpha_m}{N_m} = \frac{t.f_n}{N_{rms}} \sum_{m=1}^{k} \left(\alpha_m (m\beta)^b \right) \qquad \text{Equation3.14}$$

Recognizing that the percentage of time at a particular vibration level, α_m, can be calculated from the normal distribution as pointed out before, and also considering the symmetry of the distribution, the damage ratio becomes:

$$Damage\ \ Ratio = \frac{t.f_n}{N_{rms}} \sum_{m=1}^{k} \left(2\left(\Phi(m\beta) - \Phi((m-1)\beta)\right) \cdot (m\beta)^b \right) \qquad \text{Equation3.15}$$

where the term

$$\sum_{m=1}^{k} \alpha_m (m\beta)^b = \sum_{m=1}^{k} \left(2\left(\Phi(m\beta) - \Phi((m-1)\beta)\right)(m\beta)^b \right) \qquad \text{Equation3.16}$$

Equation3.16 can easily be evaluated using a simple numerical simulation program, where the summation terminates when negligible changes occur at the k level. As shown in Table3.1, the summation rapidly converges to a value of 21.68 for various decreasing

width β. The material constant b has been assumed to be 6.4, which is the typical fatigue exponent assumed in electronic packaging. Later in the dissertation we will address the implications of the uncertainties in the fatigue exponent.

Table3.1: Summation for width= β

1/width=	1	Value=92.7808
1/width=	2	Value=43.5750
1/width=	4	Value=30.3955
1/width=	8	Value=25.5647
1/width=	16	Value=23.4941
1/width=	32	Value=22.5350
1/width=	64	Value=22.0735
1/width=	128	Value=21.8470
1/width=	256	Value=21.7349
1/width=	**512**	**Value=21.68**

3.3 General Physical Description of BGA Damage under Random Vibration

There are two types of motion in random vibration: one motion is the induced curvature or bending in the PWB as the printed wiring assembly moves in a vibratory manner - global motion; the other motion is the component moving with respect to the PWB due to the compliance of the component's attachment – local motion. In this dissertation we will be concentrating only on the curvature or the bending of the PWB for a couple of reasons. The local dynamic motion of a component moving with respect to the PWB is, negligible in general. The natural frequencies of such motion are typically between 10-50 kHz or higher. Such high frequencies imply very small displacement magnitudes. Typical random vibration environments result in very small attachment stresses due to

this local motion. In addition, the electronic equipment racks or housings, and normal PWB acts like low pass filters and prevent most frequencies over 10 kHz from reaching the components.

In this research, the fundamental mode (first mode) of the PWB will be the response of interest. This response represents the largest deflection and curvatures of the PWB and typically accounts for the vast majority of the fatigue damage. Gross vibration fatigue failures such as cracked or broken wires, traces, cases and loose screws are no considered in this dissertation. It is assumed that if the PWB is properly designed to withstand the dynamics environment, this gross failure will not occur. This dissertation is concerned with the failure assessment of the BGA attachments.

In the special case where the first and second modes of vibration occur relatively close together, one may need to use a damage superposition technique to combine the two damages. The approach being developed in this dissertation is not limited to the fundamental mode; a damage superposition methodology could be used to combine any number of critical modes.

This dissertation takes a PoF type approach to damage analysis and models the complete PWB assembly. The model developed is a global–local type. The PWB including its support conditions is typically called the global model. A more detailed model that only deals with a local section of the PWB, including the components of interest, is the local model. Sometimes even a more detailed local model of only the critical BGA attachment

is used. These various levels of modeling are required since it is not possible to realistically model the complete PWB assembly in enough detail to accurately obtain the critical stresses in the BGA attachment.

The curvature induced in the PWB due to the motion of the board under vibration causes damage to the component's attachment. This concept is illustrated in Figure3.4. It is critical to be able to accurately measure or calculate the curvature of the PWB so that we can eventually conduct fatigue damage analysis of the component's attachment.

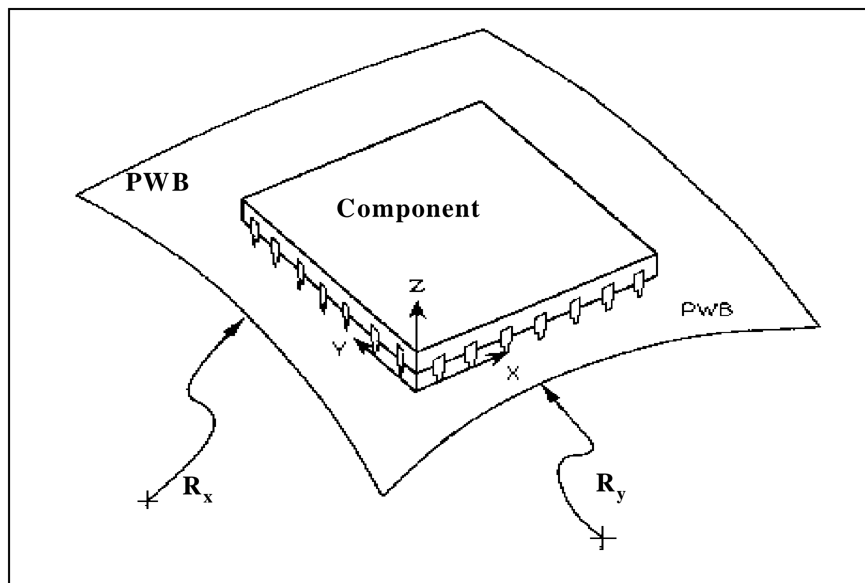

Figure3.4: PWB Deformation Expressed in Terms of the Radii of Curvatures

In reality, every component attached to the PWB stiffens a local section of it. Due to the vibratory type motion or even static bending a deformed PWB does not have smoothly

varying curvature. This fact is illustrated in Figure3.4, which is a 2D finite element simulation of the deformation of a PWB uniformly populated with BGA components. In Figure3.5, the overall view shows what appears to be a smoothly bent or curved PWB. However, the close up image shows the curvature variation in the region between the components. The area of interest is only the PWB and in particular the outer fibers or outside surface of the PWB. The colors in the figure show different levels of stress in the in-plane direction of the PWB. By performing a simple elastic analysis, it can be illustrated that the stress is directly proportional to the in-plane strain of the PWB. From simple plate or beam analysis, it can be shown that the strain in the outer fibers of the board is directly proportional to the board curvature. Thus the color along the top, or bottom, surface of the PWB indicates the curvature of the board.

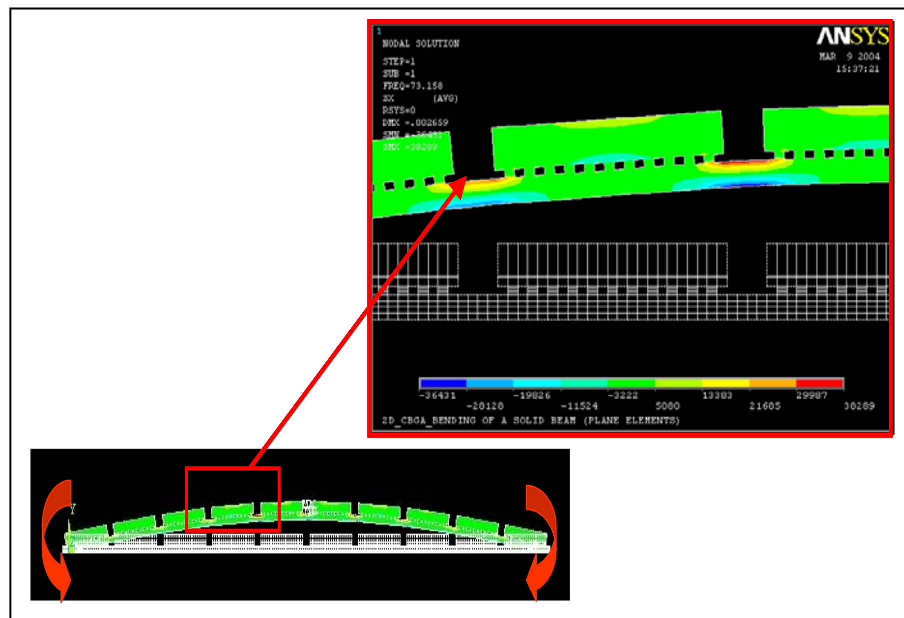

Figure3.5: Two Dimensional View of a Populated PWB

Note that almost all the curvature is concentrated in the region between the components and there is nearly zero curvature under the components. When we know the surface strain in the PWB, we know the curvature. If we know the curvature, we can get the applied bending moment in the PWB from the plate moment-curvature relations as shown in Equation 3.17 and Figure3.6. The bending moment in the PWB is used as a loading condition for the local models that contains only a small section of the PWB and the component of interest.

$$K_{xx} = -\frac{12}{Eh^3}(M_{xx} - \nu M_{yy})$$
$$K_{xx} = \frac{\partial^2 d}{\partial x^2} \cong \frac{1}{\rho}$$
Equation3.17

where K = curvature; M = moment along edge length; E = elastic moment; ν = Poisson's ratio; h = plate thickness; d = the out of plane plate displacement; ρ = radius of curvature.

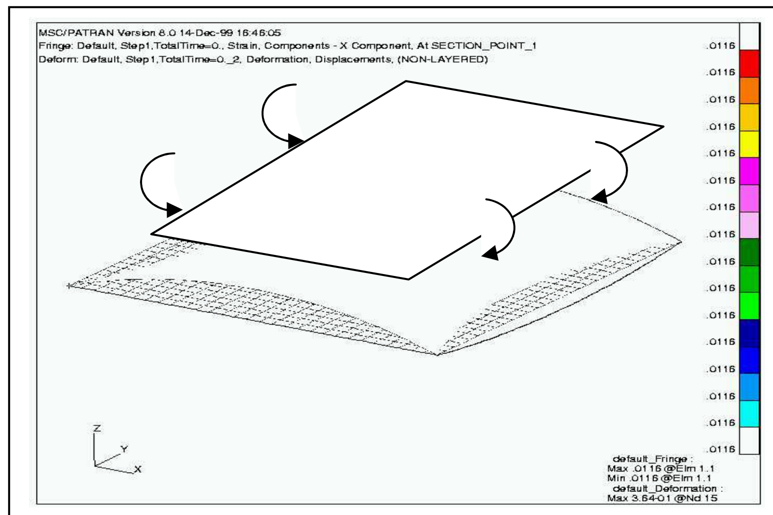

Figure3.6: Plate for Bending Moment and Curvature Relationship

3.4 Review of PBGA, CBGA, and CSP Package Structures

BGA components are becoming the semiconductor package of choice for applications requiring high density and high I/O counts. One of the primary advantages of BGA is that it doesn't require any specialized soldering operations. Any manufacturer used to working with surface mount packages can directly start assembling BGA components. Solder bridging that occurs with fine pitched QFP simply does not occur due to the coarser pitch of most BGA packages. The primary disadvantage of BGA package is that visible inspection of all joints is not possible.

BGA packages have many different names; some names being registered trademarks such as Micro BGA (μBGA) and others being more descriptive of the structure such as ceramic BGA or plastic BGA. The reader is referred to various sources such as Lau [1993], Lau, et al. [1996], Engle [1993], Steinberg [2001], Sloan [1995], and JEDEC (Joint Electron Device Engineering Council) specifications to see the variety of BGA packages. Component package manufactures are continually introducing new packages, but it is possible to generalize BGA packages into three general families: PBGA, CBGA, and CSP. As the names imply, the PBGA package has a plastic body or overmold covering the die. The CBGA package has a ceramic body containing the die. The CSP is a package, which is only slightly larger than the die. A CSP generally has a BGA attachment to the PWB, but many variants exist. In fact each of these three general families has many different sub-classes or variants. This dissertation focuses on the more common and basic types of BGAs that are currently being used extensively in telecommunications, mobile and aircraft electronics.

A representative structure has been chosen for each of the three broad general families. The following is a brief description of these representative structures.

3.4.1 Structure of PBGA

Figure3.7 shows a perspective view of a typical PBGA. Figure3.8 is a cross section view of a PBGA showing the general structure. The package consists of a bismaleimide triazine (BT) substrate, Si (die), plastic overmolding to protect the die, and solder balls to connect the package to the PWB. The detailed metallization of the BT substrate, the die attachment, and the wire bond or flip chip electrical interconnection of the die is not shown in the cross section because in this dissertation these items contribute negligibly to the structural response of the package. Table3.2 summarizes typical details and dimensions of various features. Table3.3and Table3.4 give more detailed dimensions and material properties of the relevant materials.

Figure3.7: Perspective View of a PBGA

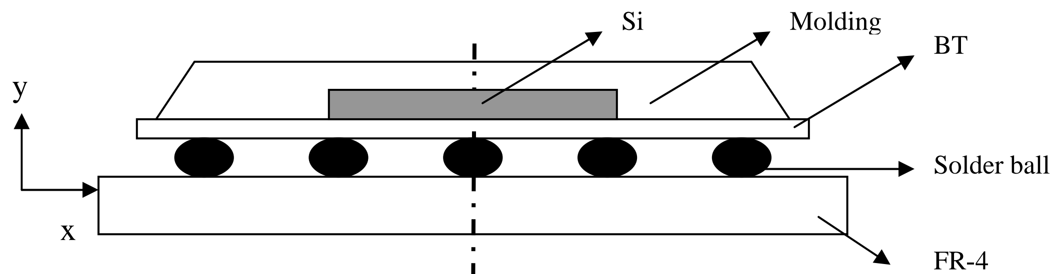

Figure3.8: Components of a PBGA Device

Table3.2: PBGA Specifications

Package size [mm sq.]	15*15
Ball counts [ball]	225
Pitch size [mm sq.]	1.27
Ball Diameter [mm]	0.76
Ball height [mm]	0.46

Table3.3: PBGA Dimensions in (mm)

	BT Substrate	Si (Die)	Molding	Solder ball	FR-4
PBGA	0.36	0.31	0.81	0.76	1.57

Table3.4: PBGA Material Properties

Part	Material	Young's modulus (MPa)	Poisson's ratio
Substrate	BT	19000	0.2
Device	Si (Die)	130000	0.28
Encapsulation	Molding	15500	0.25
Mother board	FR-4	18200	0.19

3.4.2 Structure of CSP

A typical CSP package is similar to the PBGA structure; the primary difference being the package is smaller, being only about 20% larger than the die. A typical cross section is shown in Figure3.9. Table3.5 lists various features; detailed dimensions and material properties are listed in Table3.6 and Table3.7 respectively.

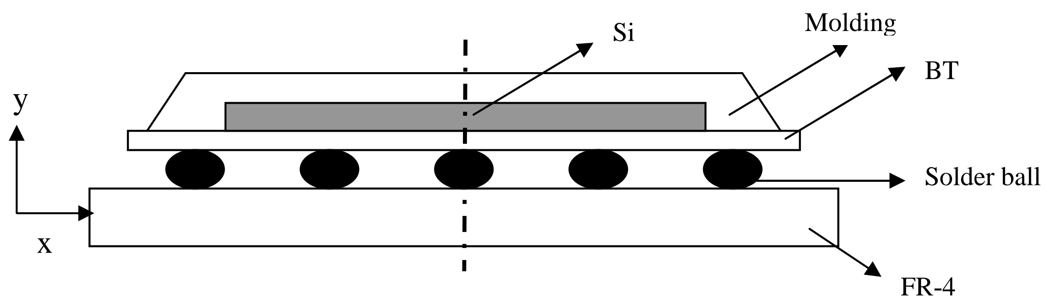

Figure3.9: Component of a CSP Device

Table3.5: CSP Specifications

Package size [mm sq.]	13*13
Ball counts [ball]	196
Pitch size [mm sq.]	0.8
Ball Diameter [mm]	0.435
Ball height [mm]	0.435

Table3.6: CSP Dimensions in (mm)

	BT Substrate	Si (Die)	Molding	Solder ball	FR-4
CSP	0.49	0.29	0.3	0.435	1.57

Table3.7: CSP Material Properties

	Material	Young's modulus (MPa)	Poisson's ratio
Substrate	BT	23500	0.20
Device	Si (Die)	170000	0.28
Encapsulation	Molding	26000	0.30
Mother board	FR-4	18200	0.19

3.4.3 Structure of CBGA

Figure3.10 is a cross section of a typical CBGA package. Structurally the ceramic body is not stiffened or strengthen by the presence of the die, so for simplicity, the package is shown and modeled with a homogenous block of ceramic material representing the package body. Table3.8 summarizes the various features of the CBGA and Table3.9 and Table3.10 show the dimensions and material properties respectively.

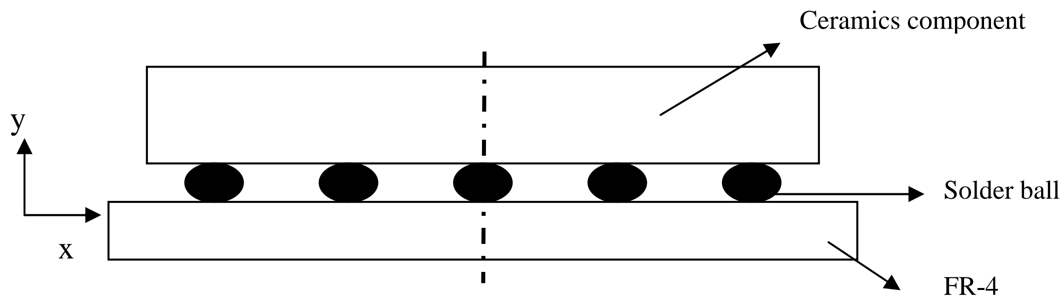

Figure3.10: Components of a CBGA Device

Table3.8: CBGA Specifications

Package size [mm sq.]	19*19
Ball counts [ball]	361
Pitch size [mm sq.]	1.27
Ball Diameter [mm]	0.89
Ball height [mm]	0.62

Table3.9: CBGA Dimensions in (mm)

	BT Substrate	FR-4
CBGA	0.29	1.57

Table3.10: CBGA Material Properties

	Material	Young's modulus (MPa)	Poisson's ratio
Substrate	BT	241000	0.25
Mother board	FR-4	18200	0.19

In this research, two-dimensional (2D) stress plane FEA will be used for much of the simulation. Figure3.11 shows the mesh picture of the three basic package families. These various models were used as building blocks for much of the simulation work.

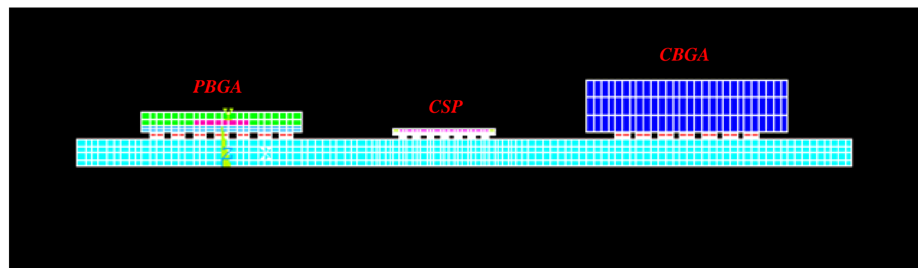

Figure3.11: Basic Building Blocks for BGA Simulations

3.5 Structure of Global and Local Model

Most of the finite element modeling conducted in this dissertation consisted of 2D modeling. 2D modeling was chosen primarily for the speed of implementation, since many different parametric models were going to be run. It was determined early in the research by a direct comparison of 2D models with three-dimensional (3D) models that the 2D models adequately captured the critical response of the PWB. The time penalties and limited computational resources associated with building and running 3D models were avoided with 2D models. Later in the dissertation some selected results from 3D modeling will be discussed showing the favorable comparison to the 2D results.

The 2D models were stress plane models that captured the global interactions of the various substrates and board thickness, pitch of solder joint, and other global parameters that influenced the PWB. The detailed local model was also typically a 2D model that captured the details of the local component-board assembly, such as the solder diameter, solder heights, substrate, die, and package body as well as the PWB.

The finite element stress analysis was performed with the use of general purpose finite element analysis software "ANSYS." The general analysis can be divided into two main steps, namely the global model and local model.

3.5.1 Global Model

Figure3.12 illustrates a FEA of a PWB with a mix component (PBGA-CSP-CBGA-CSP-CSP-PBGA). This particular result was used to identify the locations of critical curvature in the region between two components on the PWB.

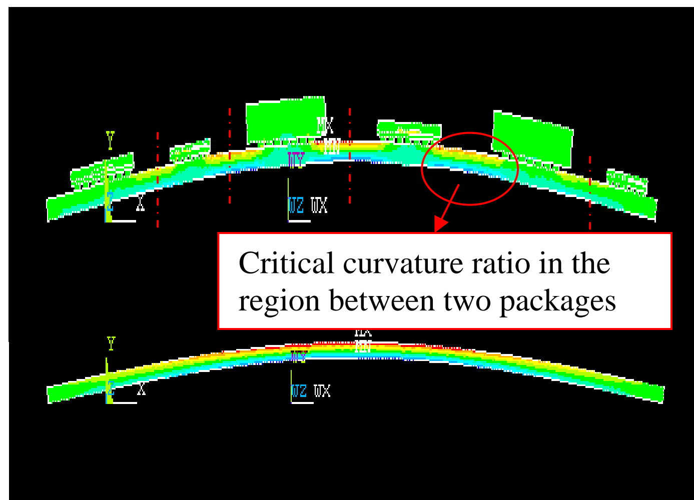

Figure3.12: Global Model

3.5.2 Local Model

A simplified local finite element model is shown in Figure3.13. In the local model the region of interest is the maximum stress in the solder ball. This critical stress is actually the Von Mises stress. The results from the global model are used as a boundary condition to load the local model. The local model boundary condition load is a bending moment applied to the outside edge of the PWB. This bending moment which is calculated knowing the PWB curvature determined in the global model. After

determining the critical stress in the critical solder joint attachment, a power law fatigue damage model is used to calculate the life.

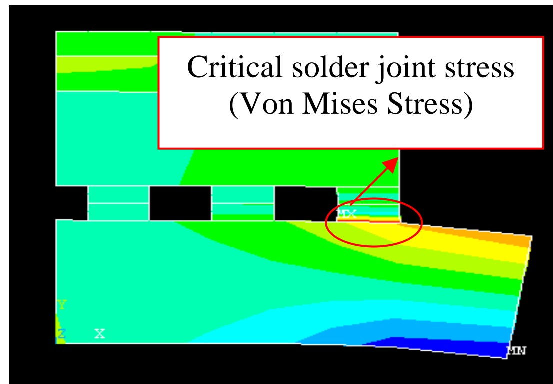

Figure3.13: Local Model

3.6 Summary

This chapter describes the general approach used for determining the fatigue life of a BGA component in a random vibration environment. This approach involves global and local modeling to ultimately determine the critical stress in the critical attachment in a BGA component. Once the critical stress is known, a fatigue damage model is used to estimate life. The stress in the component attachment is driven by the curvature induced in the PWB due to its vibratory motion.

This research only concentrate on the curvature induced damage and ignores any vibratory motion of the component with respect to the PWB. This local component vibratory motion is ignored because the natural frequency of such motion is in the tens of kilohertz region. Such motion is typically not excited.

The approach in this dissertation assumes the fundamental mode causes the most fatigue damage since it represents the largest deflections and curvatures of the PWB. The approach developed in this dissertation can be applied to higher order modes and a damage superposition scheme is used to include potential damage from modes that are close to the natural frequency.

A random vibration environment can be characterized and quantified in either the time domain or the frequency domain. This dissertation has chosen to work within the frequency domain because most qualification, acceptance, and screening specifications are called out in terms of an acceleration PSD plot. The goal of this dissertation is to provide engineers with a rapid vibration assessment approach so that they can easily perform a virtual qualification of their product in the design phase. The choice developing a rapid assessment approach that uses as an input the acceleration PSD curve does not preclude working with vibration environments that have been characterized with an acceleration time history. An acceleration time history can easily be converted into a unique acceleration PSD curve. Primarily for computational ease, though it is a pretty good assumption for most environments anyway, it has been assumed that the random vibration acceleration amplitude is normally distributed.

Chapter 4: Global Model

As introduced in Chapter 3, the rapid life assessment approach for BGA components in a random vibration environment involves a global – local type of analysis. The purpose of the global model is to determine the overall or global response of the PWB. The global model contains the geometric and material details of the PWB and its boundary conditions. The global model does not contain enough detail to accurately determine the stresses in the various component attaches. The global model is intended to only provide boundary condition information for a more detailed local model that will model a particular component of interest. This local model has enough resolution to determine the critical stress in the various component attaches. Once the critical stress is determined, a fatigue damage law is used to calculate life. This chapter discusses the global model; Chapter 5 presents the local model and Chapter 6 will be discusses the damage model.

The global model must be able to give boundary condition loading for a detailed stress analysis in the local component model. This loading needs to be available for any BGA component of interest on the PWB. From the physics of the problem, as discussed in Chapter 3, it is the PWB curvature in the region of the component of interest that needs to be passed on to the local model. The reader is cautioned that potential confusion can result if one does not understand that for a uniform thickness plate such as a PWB, the curvature - K (Greek uppercase letter kappa), ($1/_{radius\ of\ curvature}$) $1/_{\rho}$, bending moment M , and surface strain in the plate - ε , are all directly proportional to each other.

This research will talk of the curvature in the PWB in the region of the component of interest, but for visualization purposes 2D (two-dimensional) finite element plots of in-plane strain are shown in the PWB assemblies to indicate variations in board curvature. The PWB surface strain in these plots is directly proportional to the board curvature. It is the curvature, K , that is used as an input to the local detailed stress analysis model, but for easy implementation purposes in the local model the equivalent loading condition will be accomplished by using a bending moment, M , applied to the edges of the PWB.

PWBs commonly have irregular shapes and they can even have cutouts. PWBs can also have a variety of hold-downs or boundary conditions along their edges or at various internal locations. Their dynamic response is thus not easily modeled using analytic techniques. These responses are much easier to model with finite elements. This research uses two available finite element software packages for calculating the global PWB dynamic response. It was never the intention to develop a custom finite element package, but use available programs that have already had many man-years of refinement. The two programs are *ANSYS*, and *CALCE_PWA*. *ANSYS* is a general-purpose finite element program easily suited for the global or local modeling task. It was chosen over other well known general purpose finite element programs such as *ABAQUS*, *NASTRAN*, *IDEAS*, etc., primarily because it is one of the most popular programs used by industry. *CALCE_PWA* was chosen because it is a finite element based program designed purposefully for assessing the life of PWBs and their components in a various field environment. The goal of this research is to improve upon the current results generated by *CALCE_PWA* and eventually incorporate the improvements into a future

release of *CALCE_PWA (More details on CALCE_PWA can be found CALCE_PWA, Version 4.1 in the Reference).*

The *CALCE_PWA* software already has the capability to assess the life of BGA components, as well as other component styles, in a random vibration environment. The *CALCE* software currently conducts a simple dynamic FEA of the global PWB assembly. From this dynamic response calculation, the curvature of the PWB assembly in the region of the component is input to an empirical life model. The entire life assessment procedure is rapid, and one of the most accurate and easily used vibration life assessment models available to the industry. It has been, and is being used successfully in design and virtual qualifications by aerospace, automotive, and defense industries.

The major shortcoming of the current *CALCE* model is the empirical life model. This model requires tweaking of a calibration constant for component family types, as well as component size. The model is accurate and easily handles different load ranges, once these calibration constants are known. Unfortunately these calibration constants require expensive and time consuming experiments to continually validate and confirm as new component styles and sizes become available. There is nothing fundamentally wrong with an empirical model, as long as it captures the major underlying factors that influence the life. The current model does capture the load influence, but does not capture the component style and size well.

The primary thrust of this research is to develop a better rapid assessment model—a model based more on the underlying physics, which implies a more fundamentally sound stress analysis. Since a rapid assessment is desired, it is recognized that the final model must be simplified along the way. The goal is to retain as much accuracy and physical insight as possible while retaining computation efficiency. Using global modeling, the dynamics response of the PWB will be determined. This global model will give us the accurate curvature, which in turn can easily be converted into the accurate bending moment executed at specific locations of interest. This accurate moment is then fed into a local stress analysis for accurate assessment of fatigue life prediction for particular components. Section 4.1 will go through the global model approach completely. Section 4.2 will illustrate the complete global modeling approach, as shown in Figure4.1 on the left-hand side. Throughout the work, DOE and ANOVA techniques will be used to determine the key parameters and help in the development of a rapid assessment model. In our global modeling approach two major simulation tools are compared, *CALCE_PWA* and *ANSYS*. It is assumed that the *ANSYS* solution is the correct solution and this chapter will explain how the *CALCE* solution can by modified by a correction factor to agree with the *ANSYS* solution. Section 4.3 will briefly present some uncertainty issue concepts. The primary aim of this research is to estimate the error due to structural approximations rather than those due to the finite element technique. Therefore, the focus in section 4.4 is on errors resulting from geometry and material properties representation.

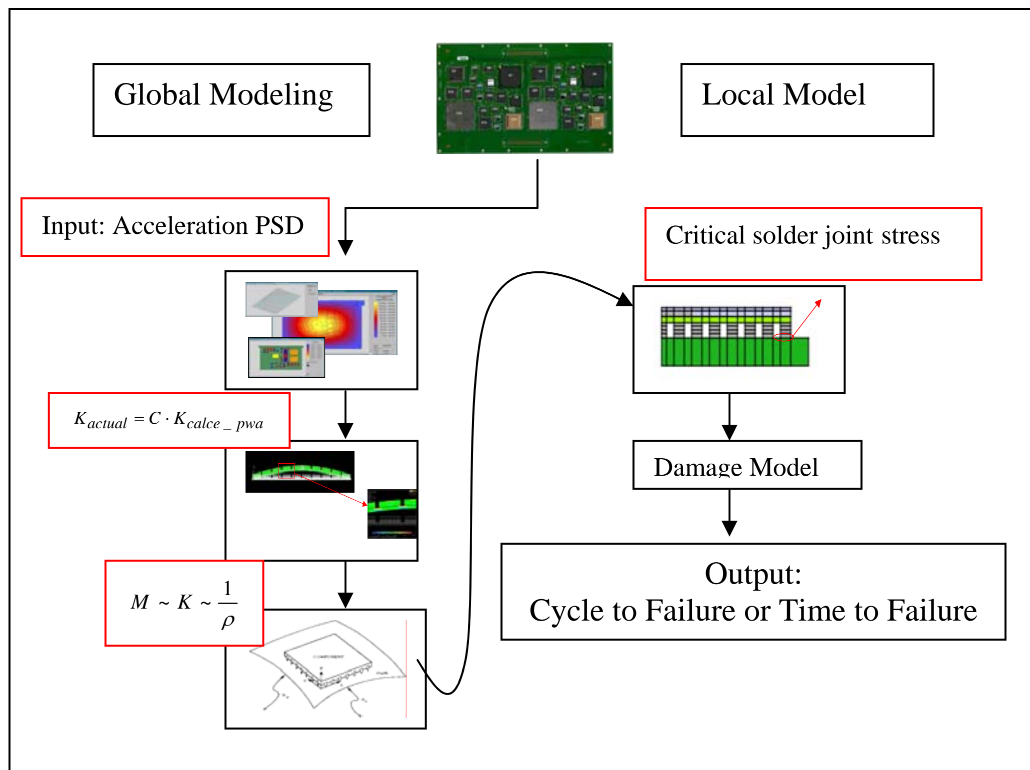

Figure4.1: Complete Global and Local model Approach

The next section will discuss the global modeling approach completely.

4.1 Global Model Approach

One of the objectives of this research is to improve the *CALCE_PWA* software, and in particular the life assessment of BGA components under random vibration loading. Thus it is natural to start with the existing *CALCE_PWA* global model for calculating the response of a PWB assembly. The *CALCE* global model is a finite element analysis model that is used to generate PWB curvature information. This underlying FEA

program uses a relatively coarse grid of plate elements whose properties have been adjusted to include the PWB and the smeared properties of the attached components.

Historically this FEA program was designed only to accurately model the fundamental mode of the PWB. It was formulated to run on PCs with limited memory and computational power. Later it was upgraded to conduct a dynamic analysis to predict the response of a PWB subjected to a random vibration environment specified by an acceleration power spectral density, but the relatively coarse grid of plate elements modeling the board was retained. Past case studies have shown the natural frequency calculation and vibration response portion of *CALCE_PWA* to be quite accurate.

Unfortunately, the FEA mesh in the existing *CALCE_PWA* software is not of sufficient density to capture the detailed curvature information that is needed for an accurate local stress analysis model. The *CALCE_PWA* model captures the curvature trends in the PWB assembly, but does not have the fidelity to capture detailed variations in the curvature. Each component mounted on the PWB locally stiffens or reinforces the board. The board thus “bends” or deforms more in the un-reinforced regions between the components. The *CALCE_PWA* software smears the effect of the components over several elements. These elements are also often of similar size to the components. Rarely are there ever any elements that model only the bare portion of the board between components. It is thus basically impossible for this large mesh to model curvature details. Figure4.2 is a screen capture of a typical meshed PWB from *CALCE_PWA*. The outline of the components and regions of unpopulated board can be seen and compared to

the size of the elements. The plot of the board curvature shows the “smoothed” response. In contrast, Figure4.3 is a plot of a much finer meshed 2D analysis of a PWB uniformly populated with simple models of BGA components done in *ANSYS*. The plot shows the response of the board to a random vibration load. This is a much more detailed FEA with much finer mesh. The colors in the plot represent various levels of board in-plane strain. The strain on the upper and lower surface of the board is directly proportional to the board curvature. Note the board curvature is not uniform. The curvature is a maximum between the components and nearly zero directly under the components. This more detailed curvature response is much different than the smoothed response exhibited in Figure4.2.

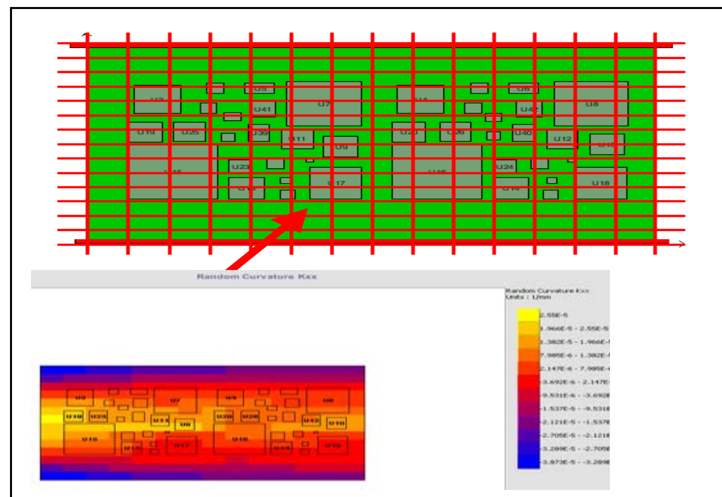

Figure4.2: A Typical Meshed PWB from *CALCE_PWA*

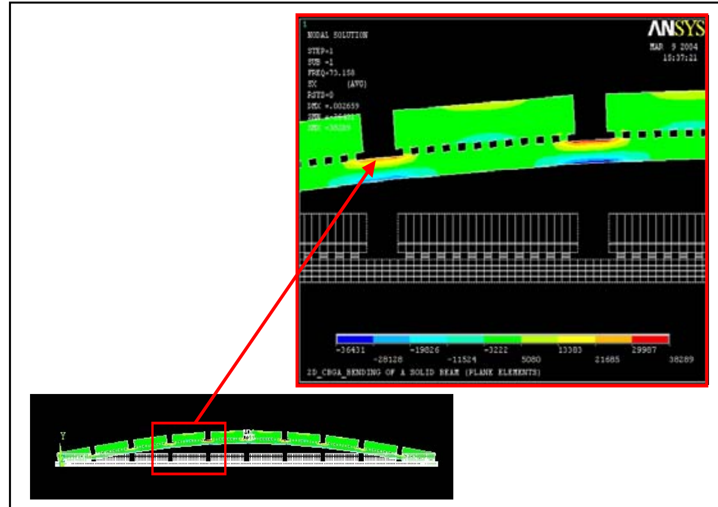

Figure4.3: A Much Finer Meshed 2D Analysis of a PWB with simple models of BGA components from *ANSYS*

By looking at the two figures, one can see that there is two different types of curvature coming into play in the overall response of the PWB. One type of curvature is the gross or smoothed curvature describing the general overall response of the board. The other type of curvature is the detailed or localized curvature due to the reinforcing effect of the components. The *CALCE_PWA* analysis determines the overall or gross curvature response of the board. This response is a function of PWB, geometry, boundary conditions, and smeared weight and stiffness of the attached components. This gross response is also a function of the load or random vibration level and frequency content. The gross curvature response as calculated by the *CALCE_PWA* software will be identified as K_{calce_pwa}.

The detailed curvature response of the PWB is primarily a function of neighboring components, particularly when expressed as a ratio of detailed curvature divided by gross curvature, K_{calce_pwa}. The detailed curvature will be calculated by using a FEA with enough mesh resolution to capture the detailed response. ANSYS will be used for these models and thus the detailed curvature will be called K_{ANSYS}. The intent of this research is to identify and be able to determine the ratio:

$$C = \frac{\mathrm{K}_{ANSYS}}{\mathrm{K}_{CalcePWA}} \qquad \text{Equation4.1}$$

This ratio C is a function of geometry and material properties of the board and components. This research will identify the critical parameters that influence C by using a DOE approach using simulation results from ANSYS and *CALCE_PWA*. The use of DOE and ANOVA to identify the critical parameters and a response surface to generate a functional form for C will be discussed in the next section, section 4.2. Once C is known, it can be used as a correction factor on the output from the *CALCE_PWA* software to calculate the actual curvature, which will be input to a local model.

$$\mathrm{K}_{ACTUAL} = \mathrm{K}_{ANSYS} = C \cdot \mathrm{K}_{CalcePWA} \qquad \text{Equation4.2}$$

Figure4.1 is a simple schematic showing the flow of the life assessment procedure. The procedure starts out with capturing the details of the PWB to be analyzed. Knowing the acceleration PSD of the random vibration, the dynamic response of the PWB is calculated

in the *CALCE_PWA* global model. The *CALCE_PWA* software determines the curvature of the PWB in the region of the component of interest. This *CALCE_PWA* curvature is corrected by a correction factor C that accounts for the detailed component stiffening and interactions with neighbors. The corrected PWB curvature is then used as a boundary condition that is input into a local model for the detailed stress analysis of the component attach. The critical stress is then fed into a fatigue damage model, which outputs life, or cycles to failure.

The next section discusses more detail about the dynamic analysis and response of interest.

4.1.1 Fundamental Mode is the Primary Mode of Interest

As pointed out in Chapter 3, there are two types of motion that could potentially cause fatigue damage to the component attaches (reference Chapter 3, section 3.3). In this research, we will concentrate on the induced curvature or bending in the PWB. In this dissertation, the fundamental mode (first mode) of the PWB will be the response of interest. In the special case where the first and second modes of vibration occur relatively close together, one may need to use a damage superposition technique to combine the two damages. This dissertation is primarily concerned with developing a feasible rapid assessment approach. The approach being developed in this dissertation is not unique for the fundamental mode, and a damage superposition methodology could be used to combine the critical modes, whether it is one, two, three, or more modes.

4.1.2 2D and 3D Comparison

This research will be conducting many finite element simulations in ANSYS to understand the curvature details in the PWB populated with various components. The ultimate goad is to be able to determine the ratio C between the curvatures as calculated in the *CALCE_PWA* and more accurately calculated in ANSYS.

$$C = \frac{K_{ANSYS}}{K_{CalcePWA}} \qquad \text{Equation4.3}$$

It is well understood that the deformation/curvature response of a plate is a 3D problem. It is also recognized that a PWB is populated with components of many different sizes. These components are laid out in a pattern that may be overall rectilinear in nature, but not regular in structure. Due to the different sizes of components the open spaces in the board, or gaps between components, are not in any regular array. This somewhat random layout of components also makes the detailed response of the board a 3D problem. Nonetheless, an argument will be presented that a 2D analysis can be used as a conservative estimate of the actual solution. By conservative it is meant that the 2D curvature will be close to the 3D value, but any errors due to the 2D approximation will predict a greater curvature than exists in the 3D problem. This will be conservative since it will predict a shorter life than may actually occur, thus any error will be on the side of caution.

The reason a 2D simulation is desired is simply for modeling and computation efficiency. ANSYS input procedures that parametrically described the shapes of PBGA, CBGA and

CSP package were developed. For example, in Figure4.4, there are two CBGA components mounted on the PWB; the right-hand side presents the 2D model and the left-hand side presents the 3D model. Each figure compares the curvature between a PWB with components, to a PWB without components. This comparison is expressed as a ratio. The 2Dmodel experienced a 3.1% larger curvature ratio than the 3D model.

To validate the adequacy of 2D FEA with regards to the more complicated 3D analysis, the finite element results obtained through global modeling were directly compared with those from the 3D model. The simulation shows that the curvature ratio values on the global model do not vary significantly between the 2D plane stress and 3D plate models, as can be seen in the Table4.1 (more tables are shown in the appendix B). In the 2D models, the plane stress assumption yields results close to the full 3D predictions. In order to confirm the above with CBGA component package, we build different types of the component package (PBGA, and CSP) mounted on the PWB as shown in Figure4.5, and Figure4.6 to see the 2D and the 3D comparison analysis difference percentage value. The final result values are acceptable as 3.5% difference for PBGA and 3.5% for CSP.

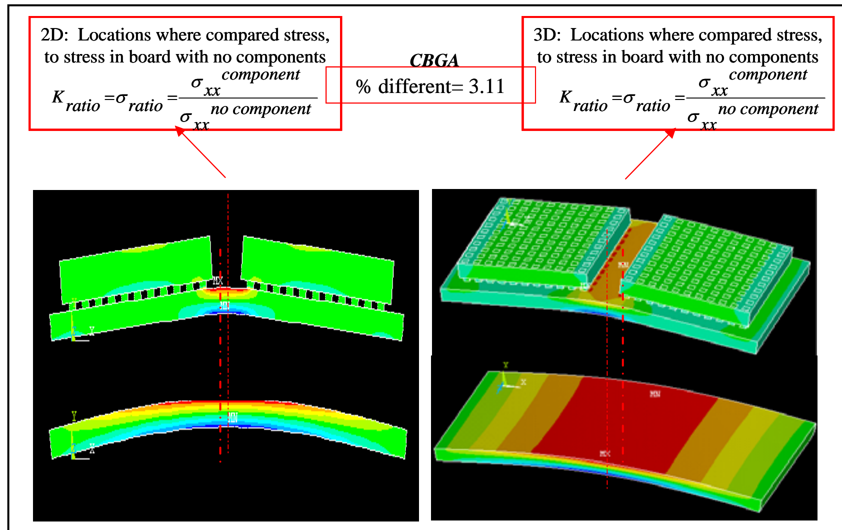

Figure4.4: Comparison of 2D and 3D FEA % Difference
For CBGA 11*11

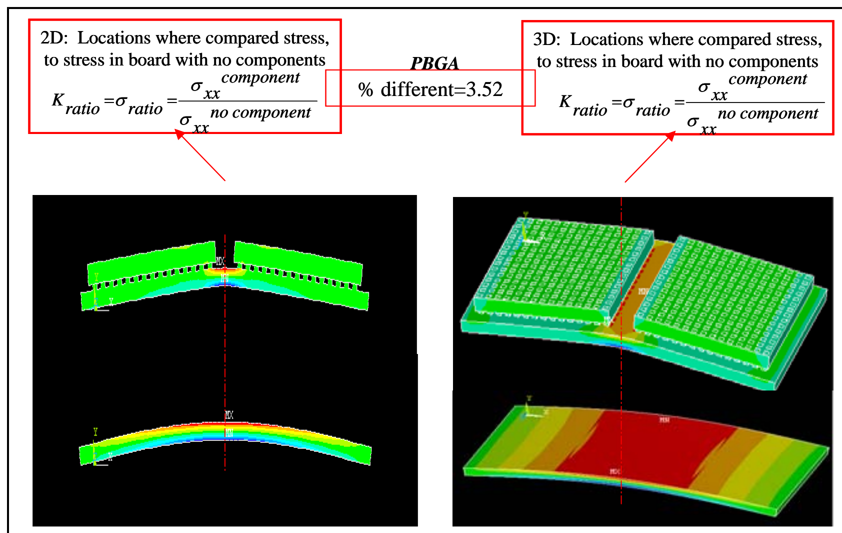

Figure4.5: Comparison of 2D and 3D FEA % Difference
For PBGA 15*15

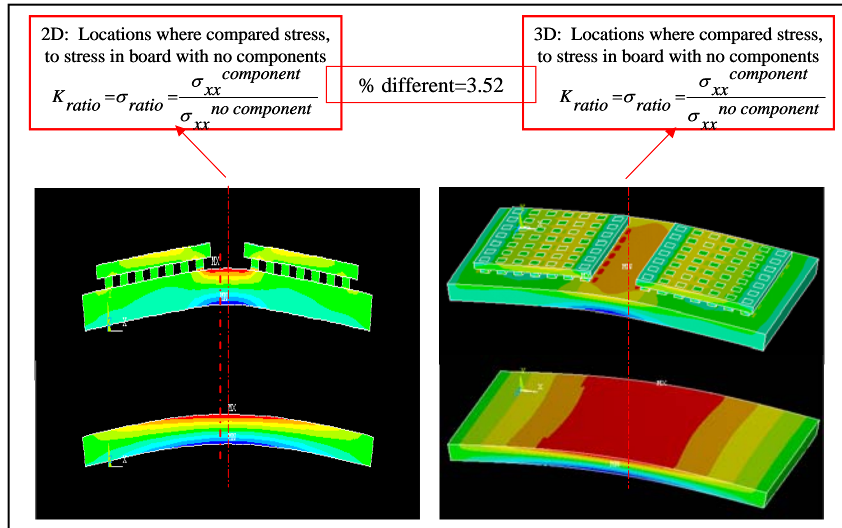

Figure4.6: Comparison of 2D and 3D FEA % Difference
For CSP 7*7

In an attempt to validate the above results, several other FEA studies were conducted to determine the effect of varying any one experimental parameter. For example, the neighboring component and location value were kept the same and the component length was varied, as shown in Figure4.7.

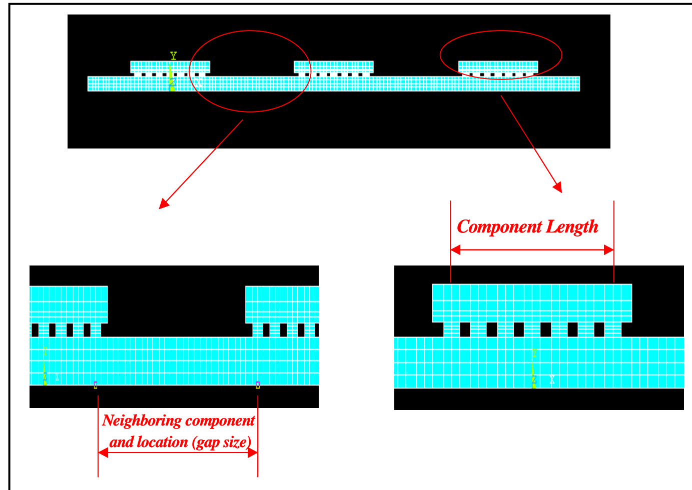

Figure4.7: Model Structure with Some Location Gap Size but Varying Component Length

The component length was also kept the same while varying the values of the neighboring component and location to get the 2D and 3D comparison analysis for different percentage values in PBGA type package. The results seem pretty good for each case. The difference percentage values range between 2 % and 4% as shown in theTable4.2. When the component length is a variable, the 2D and 3D comparison analysis differ from 2.5% to 4.0%. Contrarily when the neighboring component and location value is a variable, the range is from 3.5% to 3.9 %. This tells us that for the 2D and 3D cases component length and the neighboring component and location values do not affect the final results. It also shows agreement between the 2D and 3D models. This model works regardless of the specific component length or the neighboring component and location value. Thus it was concluded that a 2D model was adequate for this research.

Table4.1: Comparison of 2D and 3D FEA Results

CBGA: 11*11 I/O counts	$K_{ratio} = \frac{K_{ANSYS}^{component}}{K_{ANSYS}^{no\ component}}$
2D Finite Element Result	1.51368
3D Finite Element Result	1.46667
% Difference	3.1048

Table4.2: Example for PBGA 2D and 3D Comparison with Different Variables

PBGA: Component length is variables	$K_{ratio} = \frac{K_{ANSYS}^{component}}{K_{ANSYS}^{no\ component}}$ 2D Vs. 3D: % Difference	PBGA: Neighboring component and location is variables	$K_{ratio} = \frac{K_{ANSYS}^{component}}{K_{ANSYS}^{no\ component}}$ 2D Vs. 3D: % Difference
17*17	2.51	2.54	3.51
21*21	3.32	3.81	2.81
35*35	4.03	10.17	3.88

4.1.3 Single Packages Type and Mixed Packages Types

In this research, we used the same type of the components mounted on the PWB to be our 2D model structure in Figure4.8 (more models are shown in the appendix B). For instance, in Figure4.8, there are six PBGA components mounted on the PWB in the top figure, and no components are mounted on the PWB in the bottom figure. We calculated the maximum curvature ratio between no components and components mounted on the PWB as listed:

$$K_{ratio} = \sigma_{ratio} = \frac{\sigma_{xx}^{component}}{\sigma_{xx}^{no\ component}} = \varepsilon_{ratio} = \frac{\varepsilon_{xx}^{component}}{\varepsilon_{xx}^{no\ component}} \qquad \text{Equation4.4}$$

As we discussed in section 4.1.2 the curvature ratio is proportional to the stress ratio. To validate the adequacy of the same type of the components mounted on the PWB with regards to a mix of components (different types of the components) mounted on the PWB analysis, we also built the mix of components as shown in Figure4.9 (more models are shown in the appendix B) to compare them and note the difference. The conclusion for these results (shown in the appendix B) is that we can use the same type of the components to easily run our models because it saves computation time and provides a conservative answer. From Table4.3, the stiffest component (CBGA > PBGA > CSP) causes the maximum curvature (highest stress). In general, we know that the CBGA component is much stiffer than PBGA component and CSP components, and the comparison is shown in Table4.3-the CBGA's curvature ratio value is higher than PBGA and CSP component.

Figure4.9 shows a 2D FEA model with six PBGA components mounted on the PWB, and each component is 15*15 I/O counts. Given the boundary condition, the critical curvature K (or critical stress, σ) is in the center of the PWB, which is marked M_x (maximum). To obtain the K_{ratio}, one needs to evaluate the K or σ on the PWB with no components mounted, and the K or σ on the PWB with components mounted.
The K_{ratio} was estimated using the Equation4.5. The results are presented in the Table4.3. The same was done for the PBGA component and CSP component as shown in the appendix B.

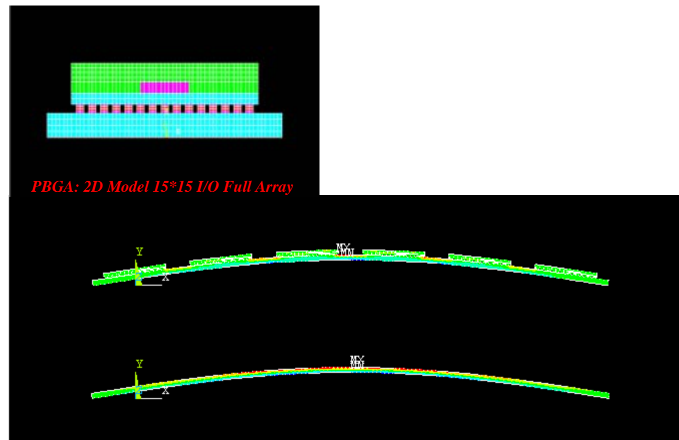

Figure4.8: Global Model for PBGA Components Mounted on the PWB Vs. PWB with No Components Mounted

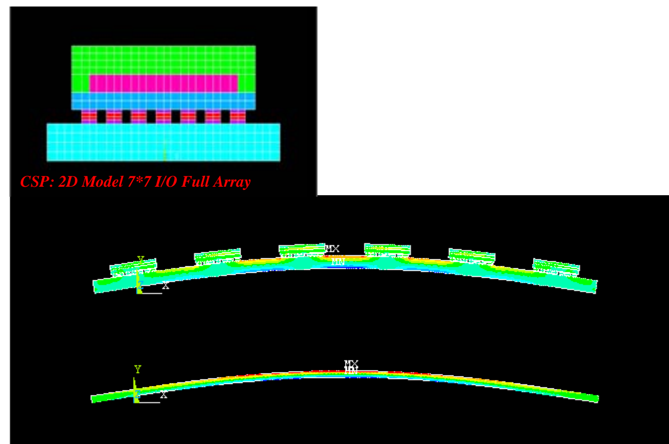

Figure4.9: Global Model for CSP Components Mounted on the PWB vs. PWB with No Components Mounted

To compare the K_{ratio} values for the three different types of BGA components the same gap size (locations) were used for each and K_{ratio} was evaluated.

$$K_{ratio} = \sigma_{ratio} = \frac{\sigma_{xx}^{component}}{\sigma_{xx}^{no\ component}} \qquad \text{Equation4.5}$$

The key point is that the stiffness order is CBGA>PBGA >CSP, as calculated from the following formula:

$$D = \frac{E^{*}h^{3}}{12(1-\upsilon^{2})} \qquad \text{Equation4.6}$$

where D is the rigidity. The rigidity values are as follows: CBGA=712701.9 MPa, PBGA= 9893.8 MPa, and CSP=3201.1 MPa. These values were calculated using material properties and geometries found in Chapter 3, section 3.4.1-3.4.3.

A summary our modeling test results are shown in Table4.3 and Figure4.9. To identify the maximum curvature (highest stress) that will occur in the PWB, we can select the stiffest component from the mixed component board and consider only that component in our model to arrive at a worst-case scenario for maximum stress. Developing a model that only accounts for the stiffest component will simplify the DOE analysis. Our approach of considering only the worst-case scenario allows us to simplify the model. Thus, our modeling approach will identify the stiffest component on a PWB containing multiple component types, and then arrive at a worst-case maximum stress level based upon the effects of that stiffest component.

Table4.3: Global Model Comparison of Single Packages and Mix Packages

Different types of BGA package mounted on the PWB	$K_{ratio} = \frac{\sigma_{xx}^{component}}{\sigma_{xx}^{no\ component}}$	Stiffest
PBGA_ PBGA_PBGA_ PBGA_ PBGA_ PBGA	1.039	
CBGA_ CBGA_CBGA_ CBGA_ CBGA_ CBGA	1.044	
CSP_ CSP_ CSP_ CSP_ CSP_ CSP	1.034	
PBGA_ CSP_ PBGA_ CSP _PBGA_ CSP	1.186	PBGA>CSP
PBGA_ CBGA_ PBGA_ CBGA_ PBGA_ CBGA	1.022	CBGA>PBGA
CBGA_ CSP_ CBGA_ CSP_ CBGA_ CSP	0.945	CBGA>CSP
PBGA_ CSP_CBGA_ PBGA_ CSP_CBGA	0.991	CBGA>PBGA >CSP
CBGA_CSP_CBGA_CSP_CSP_PBGA	0.995	CBGA>PBGA >CSP
CSP_PBGA_CBGA_PBGA_CBGA_CSP	0.946	CBGA>PBGA >CSP

The key point demonstrates Table4.3 is that no matter what types of BGA packages mounted on the PWB, the K_{ratio} is not greatly affected. It is almost the same value when all the components are the same and when they are mixed. For example, PBGA's K_{ratio} value =1.0, CBGA's value K_{ratio} =1.0, CSP's value K_{ratio} =1.0 and the mix components value K_{ratio} =1.0. That means in this research in order to reduce the computational time, one could use the same types of components to evaluate the value K_{ratio}.

4.2 DOE and ANOVA for Global Model

As explained in the previous section, this dissertation is not going to develop a completely new global model for the curvature response of a PWB assembly in a random

vibration environment. This dissertation is going to start with the curvature output from the *CALCE_PWA* software and modify it with a correction factor that accounts for the detailed stiffening influence of a BGA component and it's nearest neighbors. The correction factor C is simply the ratio between the curvature results of a detailed ANSYS 2D FE simulation and the curvature results from *CALCE_PWA*.

$$C = \frac{K_{ANSYS}}{K_{CalcePWA}} \qquad \text{Equation4.7}$$

Ultimately one needs to be able to estimate C without running a detailed ANSYS model. In order to do this, one needs to understand the key geometry and material parameters that influence the value and which parameters can be neglected without too much loss in accuracy; we will discuss these processes and approaches in this section. To accomplish this, general DOE and ANOVA techniques will be used. The modeling process is always composed of geometry modeling, material modeling, constraint, loading application, solution and post-processing. A modeling methodology is needed to accommodate the aforementioned modeling challenges.

As was discussed at the beginning of this chapter, the *CALCE_PWA* software for evaluating PWBs and their solder attaches has been demonstrated in the past to do an acceptable fatigue life assessment for most components. The problem with this model, since it is empirical, is that it must be calibrated for new components and new materials. Such calibration efforts are time consuming and require expensive experiments. Instead, this research intends to correct the curvature as calculated by the *CALCE_PWA* with a

multiplication factor that itself is a function of the critical geometry and material parameters.

Mathematically this multiplication factor, calibration factor, or transformation factor, C can be expressed as:

$$C = \frac{\mathrm{K}_{ANSYS}}{\mathrm{K}_{CalcePWA}} \qquad \text{Equation4.8}$$

where K_{actual} ($\sim K_{ANSYS}$) is the actual curvature, and K_{CALCE_PWA} is the curvature as calculated by the *CALCE* software.

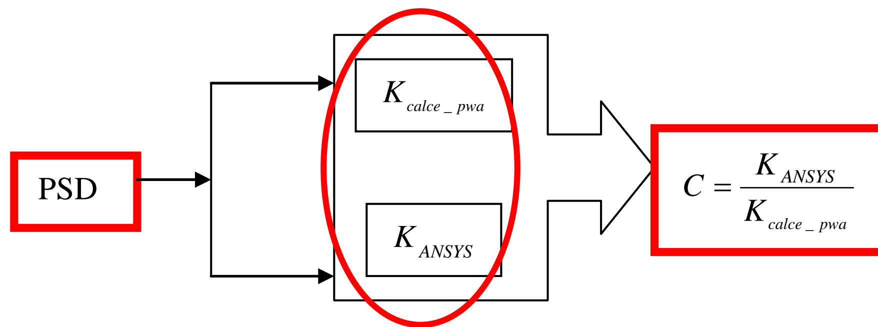

Figure4.10: Global Model Approach Output

In this research, the global model approach shown in Figure4.10, there are two distinct steps in the calculation of the vibration fatigue life of components mounted on a PWB. The next section will present the correction factor C distinct steps under the DOE and ANOVA and Response Surface Methodology approaches (RSM).

4.2.1 DOE and ANOVA Analysis for Model Development

Throughout the work, design of experiments (DOE) and ANOVA techniques will be used to determine the key parameters and help in the development of a rapid assessment model; this will be discussed in the following section. The approach for conducting design of experiment with finite element analysis data is illustrated in the below flowchart, Figure4.11.

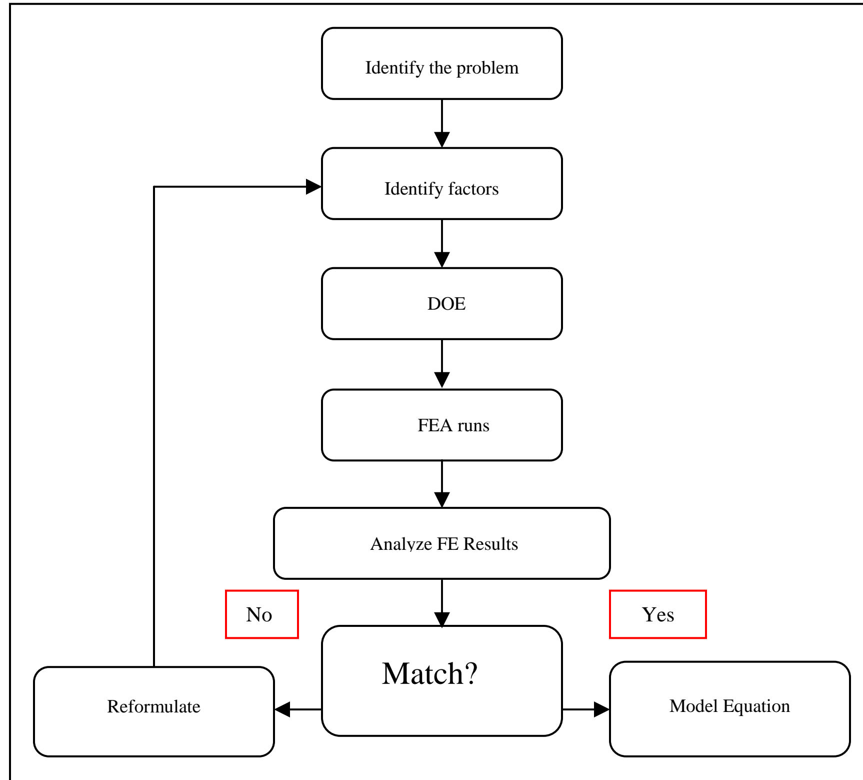

Figure4.11: Global Model's Flowchart of DOE

Step 1: Identify the problem: finding the correction factor in the global modeling

The underlying concept for developing rapid assessment methodology in the global modeling lies in finding the correction factor C. Our approach first adopted CALCE_PWA to calculate the curvature. The calculated curvature serves as an initial ballpark value. Then ANSYS is used to calculate the actual value of the curvature. The correction factor C is defined as:

$$K_{actual} = K_{ANSYS} = C \quad K_{CALCE_PWA} \qquad \text{Equation4.9}$$

$$C = \frac{K_{ANSYS}}{K_{CALCE_PWA}} \qquad \text{Equation4.10}$$

Limited sets of parameters are analyzed using *ANSYS* and a general form of the correction factor C will be derived as functions of the critical factors. Later on, once the material properties are given, one can use the general form to get the factor C without spending much time using *ANSYS*.

Step 2: Identify the Critical Factors: The conclusion from this section will show that $\frac{ball\ span\ length}{Neighboring\ component\ and\ location}, D_{ratio} = \frac{D_{component}}{D_{pwb}}$ are the two critical factors that influence the correction factor C. In the beginning we considered many more factors and slowly eliminated the non-critical factors.

i. First, we calculate the actual curvature by using a detailed ANSYS FEA model with enough resolution to accurately determine the curvature in the region of the component of interest as shown in Figure4.12. It was found that the curvature was a maximum near the mid-span of the PWB, but the curvature ratio

$K_{ratio} = \sigma_{ratio} = \frac{\sigma_{xx}^{component}}{\sigma_{xx}^{no\ component}}$ .was equal at the various other locations.

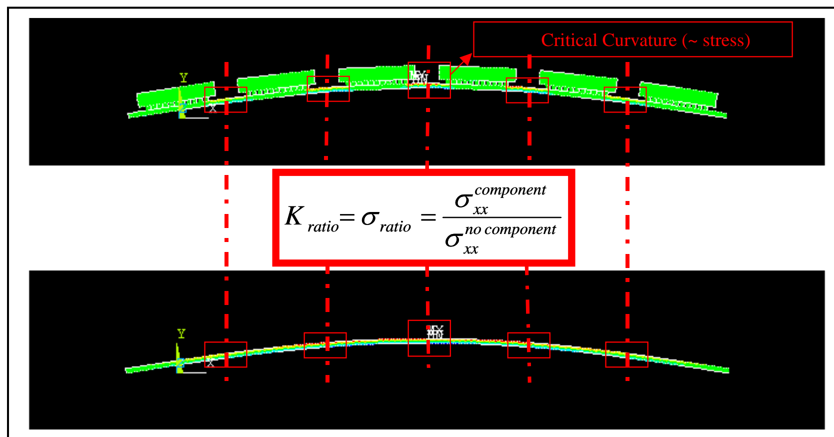

Figure4.12: Global Model Using by ANSYS

ii. For this problem the response variable, or dependent variable, is the curvature ratio and the independent variables, or factors, are a mixture of material properties and geometric dimensions.

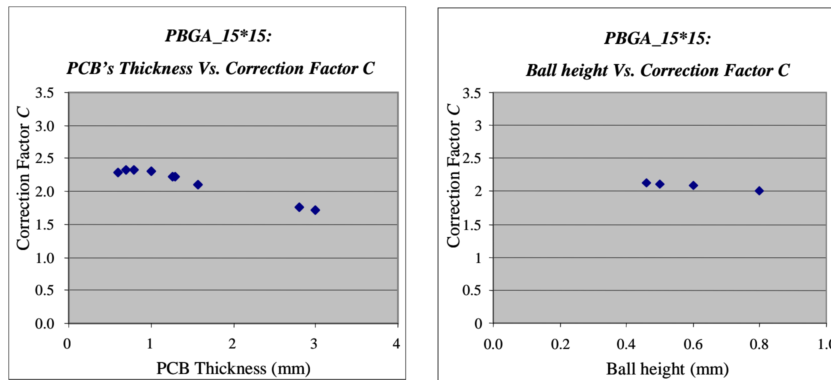

Figure4.13: PWB's Thickness Vs. Correction Factor C (Left);
Ball Height Vs. Correction Factor C (Right)

Table4.4 presents all possible factors. This list is too large and critical factors need to be identified. A series of preliminary calculations were performed to identify which factors influenced the curvature ratio. These calculations varied a single factor throughout its expected range and a plot was made of the curvature ratio as a function of the factor.

Figure4.13 is an example of two different factors; PCB thickness and ball height. Figure4.14 shows the results for PBGA over-mold thickness and component length. More plots are shown in the appendix B. From these plots one can quickly identify potential critical factors and they are identified in Table4.4.

Table4.4: Possible Critical Factors identify

Critical Factor	Possible Critical Factors
✓	PWB thickness
✓	PWB Young's Modulus
✓	PWB Poisson ratio
	PWB length
	PWB density
	Pitch size
	Solder joint height
	Solder joint diameter
	Solder joint Young's Modulus
	Solder joint Poisson ratio
✓	Solder Joint Span Length
✓	BT Young's Modulus
✓	BT thickness
✓	BT Poisson ratio
✓	BT length
✓	Die Young's Modulus
✓	Die thickness
✓	Die Poisson ratio
✓	Die length
✓	Overmolding Young's Modulus
✓	Overmolding thickness
✓	Overmolding Poisson ratio
✓	Overmolding length
✓	Neighboring component and location (gap size)

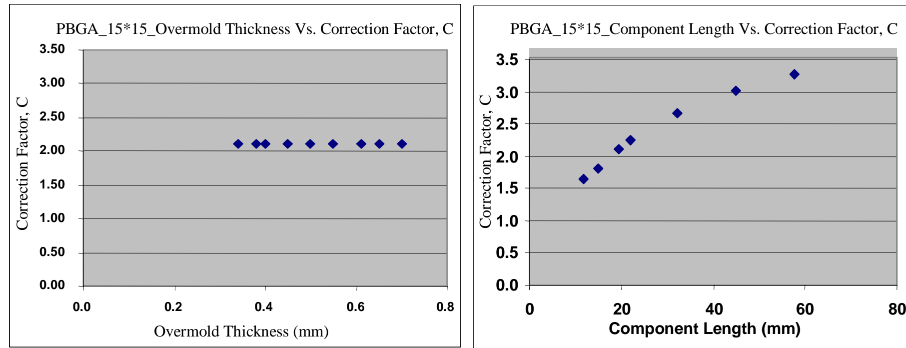

Figure4.14: Overmold Thickness vs. Correction Factor C (Left); Component Length vs. Correction Factor C (Right)

Obvious critical factors included: PWB and component young's modulus and thickness, neighboring component and location (also known as "gap size"), and component length (also known as "ball span length"). If we put all these factors into a DOE/ANOVA process there will be too many runs and the resulting formula may be too complicated. To further reduce the number of critical factors, some of these factors are grouped through known material relationships. For example, rigidity is related to Young's Modulus and the layer thickness as shown in Equation4.11. Thus, rigidity D will be used as a factor.

$$D_{pcb} = \frac{E_{pcb} \quad h_{pcb}^{3}}{12(1 - \nu_{pcb}^{2})} \quad and \quad D_{component} = \frac{E_{component} \quad h_{component}^{3}}{12(1 - \nu_{component}^{2})} \qquad \text{Equation4.11}$$

By doing so, the critical factors are reduced to $D_{component}$, D_{pcb}, ball span length and neighboring component and location. Since C is unit-less, we basically normalize these

four factors into two $D_{ratio} = \frac{D_{component}}{D_{pcb}}$ and $\frac{ball\ span\ length}{Neighboring\ component\ and\ location}$, for consistence of units.

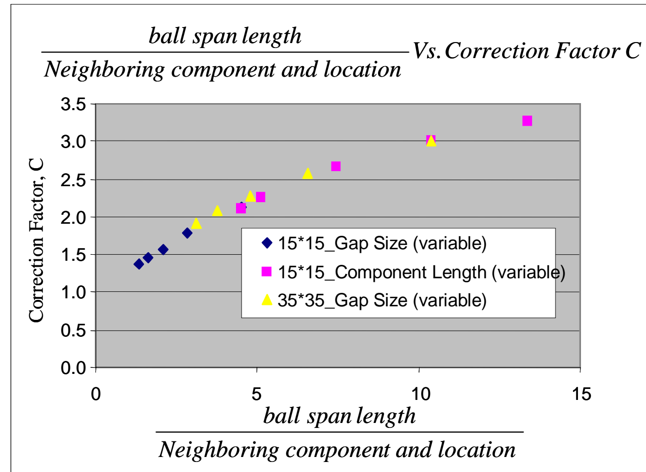

Figure4.15: $\frac{ball\ span\ length}{Neighboring\ component\ and\ location}$ Vs. Correction Factor, C

Similarly we use the ratio of $\frac{ball\ span\ length}{Neighboring\ component\ and\ location}$ to simplify the modeling. Preliminary modeling showed that this length ratio was a good choice as seen in Figure4.15. The figure includes the analysis for three cases: keeping the gap size between the component the same while varying the component length, keeping the component length the same while varying the gap size between components, and varying the number of interconnects for a given package size. When plotted as a function of the ratio of component length/gap size, the results seem to lie on a master curve.

Having preliminarily identified the key geometry and material parameters that influence the correction factor, DOE and ANOVA techniques will be more formally used in the next steps.

Step 3: Computation of the total runs required; decision on the design option:

To use RSM--three level factorials and two factors

$$(A: \frac{ball\ span\ length}{Neighboring\ component\ and\ location},\ B: D_{ratio})$$

The three level factorials can detect effectively in this step.

Step 4: Start to run design of experiment tool, and finite element analyses runs:

Three-level factorial design is written as a 3^2 factorial design in this dissertation. It means that 2 factors ($A: \frac{ball\ span\ length}{Neighboring\ component\ and\ location},\ B: D_{ratio}$) are considered, each at 3 levels. These are usually referred to as low, intermediate and high levels. All the low, intermediate, and high-level values are chosen based upon the specific PBGA, CBGA and CSP component of interest, i.e. a different model will be determined for each package type. The PWB's thickness range varied from 0.6m to 4.5m, and PWB's young's modulus ranged from 10000 MPa to 27924 MPa based upon a survey of available information. The other material and geometric data ranges were found in a similar manner. For example, the PBGA component ranged from 9*9 I/O to 41*41 I/O.

Table4.5: D_{ratio} Value for PBGA Package

Low Value	Intermediate Value	High Value
0.0041	0.0023	0.0435

For the factor A: $\frac{ball\ span\ length}{Neighboring\ component\ and\ location}$, we assume the PBGA component length is from 9*9 I/O counts to 41*41 I/O counts. We assume the gap between neighboring components is from 2.6 m to 9.0 m.

Table4.6: $\frac{ball\ span\ length}{Neighboring\ component\ and\ location}$ Value for PBGA Package

Low value	Intermediate value	High value
1.350829	7.47	13.34722

Using the DOE software tool (Design-Expert 7.0), we combine the ANSYS results with the CALCE_PWA as shown in Figure4.16 to get the functional relationship function of C:

$$C = f\left(\frac{ball\ span\ length}{Neighboring\ component\ and\ location}, D_{ratio} = \frac{D_{component}}{D_{PWB}}\right) \quad \text{Equation4.12}$$

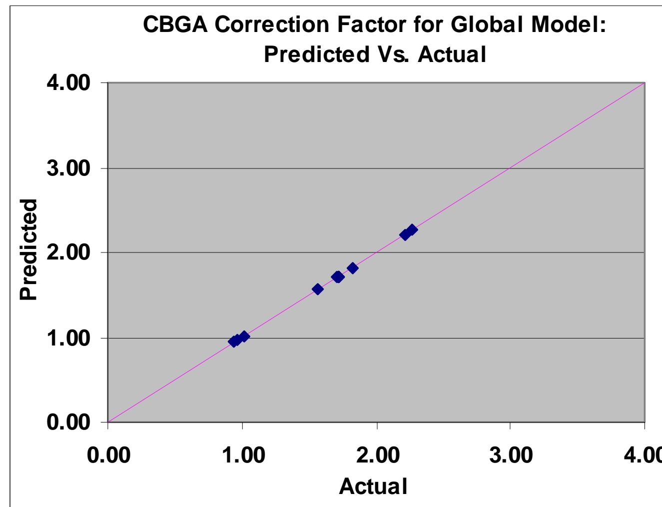

Figure4.16: CBGA Correction Factor for Global Model: Predicted Vs. Actual

Figure4.16 is the graph of the actual response values (curvature ratio) versus the predicted response values (RSM). This graph helps us detect a value, or group of values, that are not easily predicted by the model. The 45° line should split the data points evenly. The plot shows that the results seem to be a good fit for each case (the graphs of the actual response values versus the predicted response values for PBGA and CSP packages are shown in the appendix B).

Step 5: Analysis Process: Apply transformations to linearize fit as much as possible:

There are many transformations one can select, for example, square root, natural log, base 10 log, inverse square, inverse, power, logit, ArcSin square. In this case, diagnostics indicated that a square root transformation could potentially give the best results. Thus the analysis was restarted with transformed data.

Step 6: Perform ANOVA to identify the critical parameters and interactions:

Once the data were entered into the DOE matrix, all treatments and interactions were selected to be included in the ANOVA model. ANOVA was then performed to determine which factors were significant in the model. Based on *step 2*, we identified the possible critical factors from two methods. One method employed plot trends, which only considered a single factor at a time, holding all other factors constant. The second method used a 2-level full factorial DOE method based on the plot trends to confirm the possible critical factors. It is also important to consider interactions between the factors.

A three level "fractional factorial" design was employed with the previously identified critical factors of rigidity ratio and $\frac{ball\ span\ length}{Neighboring\ component\ and\ location}$. A three level analysis was chosen in order to handle non-linear responses. The three levels allow a quadratic response to be modeled.

Step 7: Confirm Design of Experimental Results (Confirmatory Runs)

When the analysis of the experiment is complete, one must verify that the predictions are good. These are called confirmation runs when one attempts to model factor values that were not used to generate the model. Here, we conducted 16 runs for CBGA component, 17 runs for PBGA component, and 15 runs for CSP component. In this case, the predicted value is calculated from RSM, and actual values are calculated from ANSYS and *CALCE_PWA*.

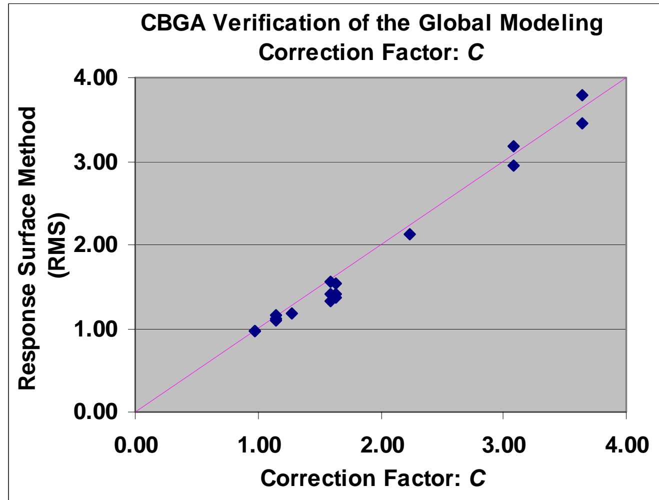

Figure4.17: Verification of Correction Factor *C* for PBGA

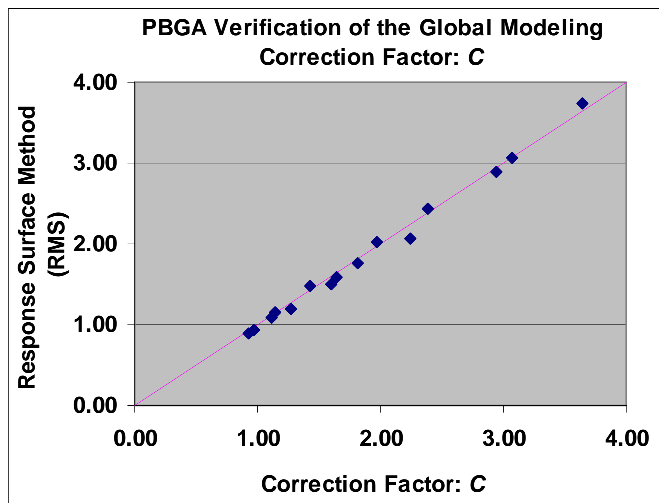

Figure4.18: Verification of Correction Factor *C* for CBGA

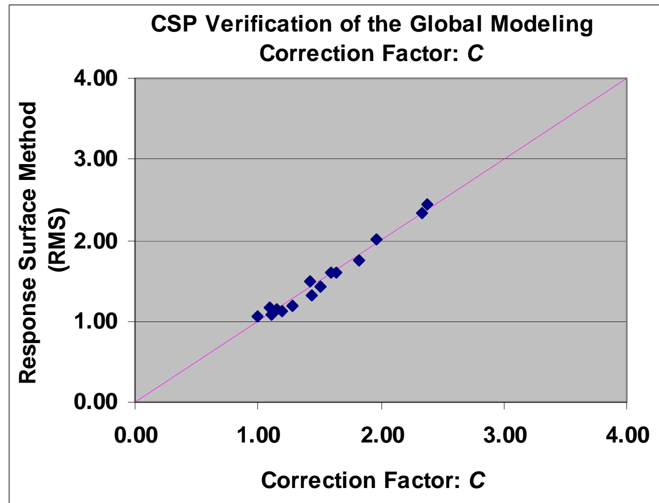

Figure4.19: Verification of Correction Factor *C* for CSP

Figure4.17 shows good agreement with less than 2.1% error between the predicted and actual values for the CBGA. Figure4.18 shows good agreement with less than 3.0% error between the predicted and actual values for the PBGA, and finally Figure4.19 shows good agreement with less than 3.3% error between the predicted and actual values for the CSP.

Step 8: Use/present the result*s: *Functional relationship for *C*

The response surface technique, with the identified critical parameters, gives us a functional relationship for C for the PBGA, CBGA and CSP cases.

$$C = f\left(\frac{ball\ span\ length}{Neighboring\ component\ and\ location}, D_{ratio} = \frac{D_{component}}{D_{PWB}}\right) \quad \text{Equation4.13}$$

$$C = f\left(\frac{ball\ span\ length}{Neighboring\ component\ and\ location}, D_{ratio}\right) \qquad \text{Equation4.14}$$

Once the model had been created and its appropriateness verified, the results are summarized in Table4.7 for the PBGA component. The process was repeated for CBGA and CSP, and shown in Table4.8 and Table4.9. The tables presented are for the PWB's thickness ranging from 0.6-1.6mm. It was found that a more accurate model could be created by splitting the PWB thickness into two different ranges. The functions for C, where the PWB thickness ranges from 1.6-4mm, are shown in Table4.10-Table4.12).

Table4.7: Functional relationship, Correction Factor: *C* for the PBGA

Final Equation in Terms of Actual Factors: *C* (0.6-1.6mm)	
Sqrt (PBGA Stress Ratio)	=
1.075216292	
0.052452684	* Component length/Gap size
-0.671710596	* D ratio
2.483034054	* Component length/Gap size * D ratio
-0.002373847	* Component length/Gap size^2
-23.34399238	* D ratio^2
-0.043092713	* Component length/Gap size^2 * D ratio
-19.32806298	* Component length/Gap size * D ratio^2

Table4.8: Functional relationship, Correction Factor: C for the CBGA

Final Equation in Terms of Actual Factors: C (0.6-1.6mm)	
Sqrt (CBGA Stress Ratio)	=
0.802092384	
0.130623619	* Component length/Gap size
-8.76086E-05	* D ratio
-7.8114E-06	* Component length/Gap size * D ratio
-0.001443644	* Component length/Gap size^2
1.7574E-08	* D ratio^2
-4.51852E-08	* Component length/Gap size^2 * D ratio
1.44384E-09	* Component length/Gap size * D ratio^2

Table4.9: Functional relationship, Correction Factor: C for the CSP

Final Equation in Terms of Actual Factors: C (0.6-1.6mm)	
Sqrt (CSP Stress Ratio)	=
0.918370774	
0.148282135	* Component length/Gap size
0.061756317	* D ratio
0.028451323	* Component length/Gap size * D ratio
-0.003209973	* Component length/Gap size^2
0.211650244	* D ratio^2
0.002477085	* Component length/Gap size^2 * D ratio
-0.311009683	* Component length/Gap size * D ratio^2

Table4.10: Functional relationship, Correction Factor: C for the PBGA

Final Equation in Terms of Actual Factors: C (1.6-3.5mm)	
Sqrt (PBGA Stress Ratio)	=
0.982085041	
0.108591668	* Component Length/Gap Size
-0.581334603	* D_ratio
0.681155571	* Component Length/Gap Size * D_ratio
-0.004590935	* Component Length/Gap Size^2
0.647419728	* D_ratio^2
-0.002762625	* Component Length/Gap Size^2 * D_ratio
-2.634566399	* Component Length/Gap Size * D_ratio^2

Table4.11: Functional relationship, Correction Factor: C for the CBGA

Final Equation in Terms of Actual Factors: C (1.6-3.5mm)	
Sqrt (CSP Stress Ratio)	=
0.908545227	
0.148945757	* Component Length/Gap Size
-0.327316609	* D_ratio
0.067948397	* Component Length/Gap Size * D_ratio
-0.003658408	* Component Length/Gap Size^2
0.813437015	* D_ratio^2
-0.001578836	* Component Length/Gap Size^2 * D_ratio
-0.161543108	* Component Length/Gap Size * D_ratio^2

Table4.12: Functional relationship, Correction Factor: C for the CSP

Final Equation in Terms of Actual Factors: C (1.6-3.5mm)	
Sqrt (CBGA Stress Ratio)	=
0.94356	
0.11377	* Component length/Gap size
-0.00081	* D ratio
0.00021	* Component Length/Gap Size * D_ratio
-0.00162	* Component length/Gap size^2
0.00241	* D_ratio^2
0.02025	* Component Length/Gap Size^2 * D_ratio
0.05046	* Component length/Gap size * D ratio^2

This dissertation is going to start with the curvature ratio output from *CALCE_PWA* software and modify it with a correction factor C that accounts for the detailed stiffening influence of a BGA component and its nearest neighbors. In the next section (4.2.2) we will calculate the curvature value from the *CALCE_PWA* software.

4.2.2 *CALCE_PWA for* K_{CALCE_PWA}

CALCE_PWA is a well documented software tool and will only be briefly discussed here. The primary purpose of this section is to show how the output from *CALCE_PWA* is used. *CALCE_PWA* calculates the modal response of a PWB and the dynamic response to a prescribed acceleration PSD as shown in Figure4.20. Unfortunately, the FEA mesh is not of sufficient density to capture the curvature information that is needed for an accurate local stress analysis model as seen in Figure4.21 and Figure4.22.

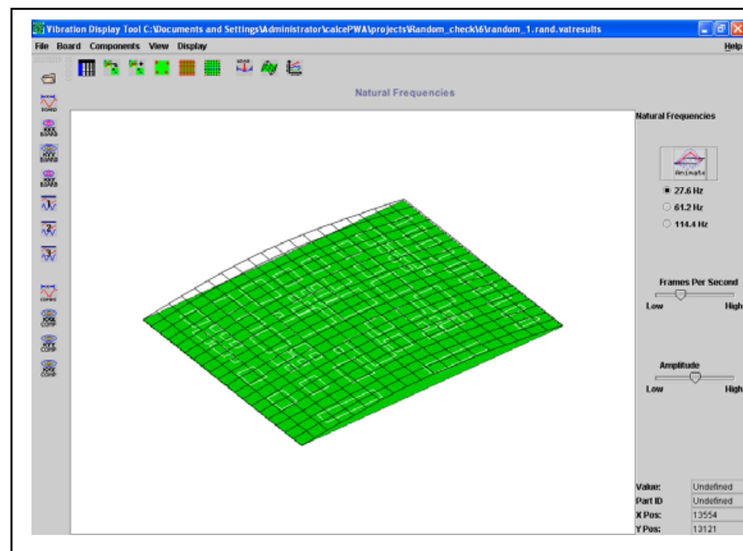

Figure4.20: Global Model form *CALCE_PWA*

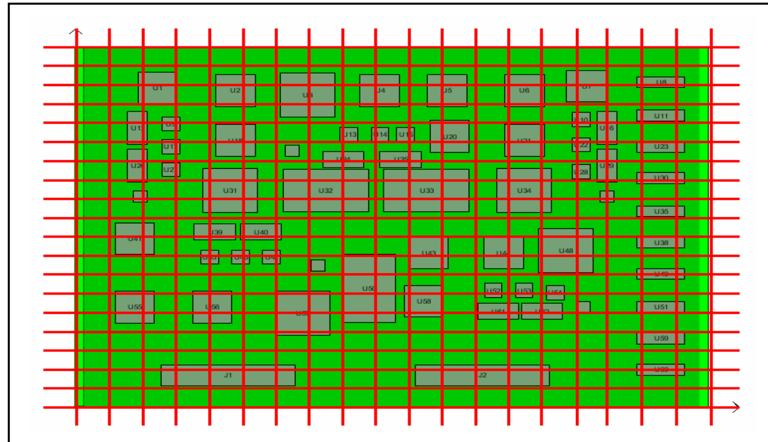

Figure4.21: *CALCE_PWA* FEA Mesh

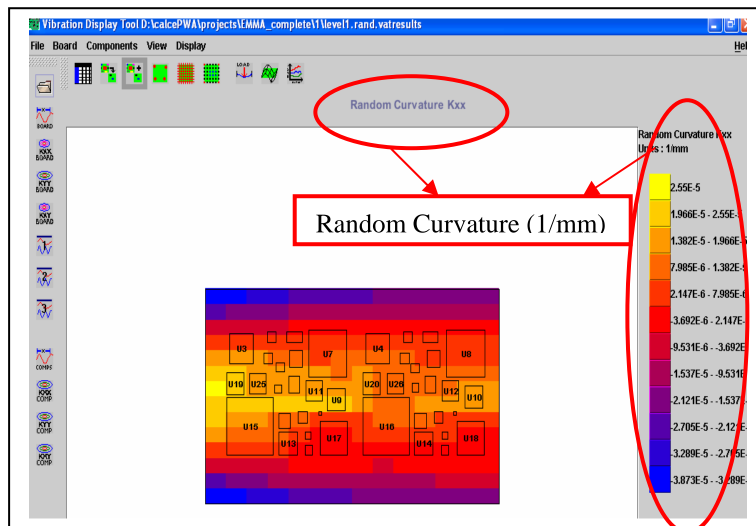

Figure4.22: *CALCE_PWA's* Random Curvature

Table4.13 is the components spreadsheet, showing the component ID and random curvature. From this table, we can get the curvature value for the component of interest.

Table4.13: *CALCE_PWA* Components Spreadsheet

Components SpreadSheet

File Edit

Part ID	Part Name	Placement Side	X Center (mm)	Y Center (mm)	Random Displacement (mm)	Random Curvature Kxx (1/mm)	Random Curvature Kyy (1/mm)	Random Curvature Kxy (1/mm)
U1	SOT23-8	top	4167.8	2614.1	0.022	[illegible]	-1.054E-6	[illegible]
U2	SOT23-8	top	9039.8	2614.1	0.01699	1.102E-5	[illegible]	-1.842E-6
U3	TQFP-144	top	1319.8	4496.5	0.02224	1.773E-5	-2.64E-6	-7.974E-6
U4	TQFP-144	top	6241.1	4496.5	0.01389	1.119E-5	5.129E-7	-3.004E-6
U5	TSSOP-56	top	3231.8	4842.5	0.01268	5.786E-6	-7.308E-7	-6.082E-6
U6	TSSOP-56	top	8153.0	4842.5	0.009191	4.347E-6	-5.863E-7	-2.366E-6
U7	PBGA-580	top	4430.6	4362.4	0.01731	[illegible]	[illegible]	[illegible]
U8	PBGA-580	top	9425.7	4362.4	0.01381	[illegible]	[illegible]	[illegible]
U9	PBGA-256	top	4747.6	3025.2	0.02263	[illegible]	[illegible]	[illegible]
U10	[illegible]	[illegible]	[illegible]	3099.0	0.01874	[illegible]	[illegible]	[illegible]
U11	[illegible]	[illegible]	[illegible]	3267.7	0.02431	2.117E-5	-7.191E-7	-8.31E-7
U12	[illegible]	[illegible]	[illegible]	3267.7	0.01853	1.655E-5	-2.044E-6	-2.622E-6
U13	[illegible]	[illegible]	[illegible]	1741.3	0.0166	9.717E-6	-1.864E-7	4.528E-6
U14	TBGA-256	top	7913.7	1741.3	0.01157	6.344E-6	-7.997E-8	1.75E-6
U15	TEBGA-560	top	1617.7	2242.7	0.02744	2.327E-5	-4.229E-6	-6.725E-8
U16	TEBGA-560	top	6539.6	2242.7	0.01666	1.601E-5	5.162E-7	2.092E-6
U17	CBGA-420	top	4649.5	1897.7	0.01506	5.48E-6	-1.704E-7	2.298E-6
U18	CBGA-420	top	9595.3	1897.7	0.01193	4.671E-6	-8.911E-7	-7.03E-7
U19	FLEXSCP-257	top	1096.3	3484.3	0.03446	2.33E-5	-4.208E-6	-1.031E-6
U20	FLEXSCP-257	top	6018.1	3484.3	0.02075	1.619E-5	5.461E-7	1.062E-6
U21	FLEXSC-64	top	2403.0	4842.5	0.01395	5.776E-6	-6.479E-7	-6.883E-6
U22	FLEXSC-64	top	7342.5	4842.5	0.009477	4.251E-6	-4.64E-7	-2.837E-6
U23	WBCSP-128	top	2874.0	2404.0	0.0233	1.624E-5	-6.098E-7	5.076E-7

Component ID

Random Curvature (1/mm)

4.2.3 Calculation of Moment through Curvature

Once the curvature is accurately determined from section 4.2.1 and section 4.2.2, the moment can be readily calculated through known equations. The following equations determine M in terms of K:

$$K_{actual} = C \quad K_{calce_pwa} \qquad \text{Equation4.15}$$

$$K_{actual} = \frac{1}{\rho} = \frac{M}{E_{pcb} \quad I_{pcb}} \qquad \text{Equation4.16}$$

With known K_{actual}, the accurate M for each component is obtained. Table4.14-Table4.16 shows three examples for different types of the components to calculate the M.

Table4.14: Actual Curvature and Moment's Relationship for PBGA

Vibration Level	***CALCE_PWA***	***Transformation parameter***	***Actual curvature***	***Moment***
Component	***Kxx (1/mm)***	C	***K (1/mm)***	***M (N*mm)***
U7 PBGA_580	0.0000264	2.68441	0.00007087	0.432
U9 PBGA_256	0.0000341	2.19257	0.00007468	0.455

Table4.15: Actual Curvature and Moment's Relationship for CBGA

Vibration Level	***CALCE_PWA***	***Transformation parameter***	***Actual curvature***	***Moment***
Component	***Kxx (1/mm)***	C	***K (1/mm)***	***M (N*mm)***
CBGA _225	0.0000264	2.68441	0.00007087	0.432
CBGA_381	0.0000341	2.19257	0.00007468	0.455

Table4.16: Actual Curvature and Moment's Relationship for CSP

Vibration Level	***CALCE_PWA***	***Transformation parameter***	***Actual curvature***	***Moment***
Component	***Kxx (1/mm)***	C	***K (1/mm)***	***M (N*mm)***
U19/U20 FlexCSP_257	0.0000388	2.16054	0.00008372	0.51
U23 WBCSP-128	0.0000269	1.24374	0.00003346	0.204
U25/U26 WBCSP_256	0.0000324	1.47332	0.00004769	0.29
U27 FC CSP-64	0.0000255	1.79744	0.0000458	0.279
U29 WFR CSP-98	0.0000276	1.40972	0.00003895	0.237
U31 WFR CSP-46	0.0000276	1.19977	0.00003316	0.202
U39 CSP BGA-64	0.0000288	1.26908	0.0000366	0.223
U41 RCCSP-150	0.0000237	1.44877	0.00003434	0.209

4.3 Uncertainty Issue

This section focuses on uncertainty analysis, that is, how the input data uncertainty affects the output data uncertainty. We are assuming the model is correct and are only dealing with uncertainties due to variations in inputs. Output uncertainty, uncertainty in the correction factor, is determined by Monte Carlo simulation. For the Monte Carlo simulation the various input parameters, both material property and geometric dimensions, are assumed to have a normal distribution. There was no special reason to choose a normal distribution other than most physical parameters measured in nature exhibit a normal distribution. Either a uniform, triangular, or any other distribution could have been chosen and easily implemented in a simulation. The actual Matlab code for the Monte Carlo simulations is provided in the appendix C.

Table4.17 lists the various input factors. For each factor a mean value and standard deviation was determined. It should be recognized that the various geometric factors are generally well know and have relatively tight distributions. If the width of the distribution is not well known, it is relatively easy to measure. Conversely the material properties and associated distributions are not as well known and are not easy (economical) to measure.

4.3.1 Global Life Uncertainty Issue Analysis

The uncertainty analysis is to estimate the error due to input data approximations rather than uncertainties associated with finite element modeling. We assume the model is an accurate model. In this subsection, estimates will be made on the amount of uncertainty

in the global modeling which basically involves the uncertainty in the value of the correction factor C derived in section 4.2.

Table4.17: Critical Factors

Critical Factors	***Possible Critical Factors***
✓	PWB thickness
✓	PWB Young's Modulus
✓	PWB Poisson Ratio
	PWB length
	PWB density
	Pitch size
	Ball span length
	Solder joint height
✓	Neighboring component and location (gap size)
	Solder joint Young's Modulus
	Solder joint Poisson Ratio
✓	BT Young's Modulus
✓	BT thickness
✓	BT Poisson Ratio
✓	BT length
✓	Die Young's Modulus
✓	Die thickness
✓	Die Poisson Ratio
✓	Dei length
✓	Overmolding Young's Modulus
✓	Overmolding thickness
✓	Overmolding Poisson Ratio
✓	Overmolding length
	Solder joint diameter

4.3.1.1 Uncertainty in the Correction Factor C

As an engineer, one can select or use nominal values of the input parameters, but actual values may be slightly different. This section examines how sensitive the output to input parameters. It also can be used to determine an acceptable range in input parameters, i.e. how accurately does one need to know the various input parameter values.

There are three types of components in this dissertation's formula: PBGA, CBGA, and CSP component (see Table4.7-Table4.12). This section discusses in detail the PBGA component. The results for the CBGA and CSP components are shown in the Appendix. The results indicate that the variation in the output is similar between the three different components.

Table4.18 lists the input nominal parameters and values for a typical PBGA. The standard deviations are also shown. The geometric factors have a much tighter distribution than the material properties.

Table4.18: Nominal Values for PBGA Packaging in Uncertainty Issue

	Nominal Value (Mean Value)	***Standard Deviation (% of mean value)***
Ball span length [mm]	17.78	0.1
Gap size [mm]	10.16	0.1
PWB thickness [mm]	1.57	0.2
Component thickness [mm]	0.81	0.2
PWB Young's modulus [N/mm^2]	18200	1.0
Component young's modulus [N/mm^2]	15200	1.0
PWB Poisson ratio	0.19	0.08
Component Poisson ratio	0.21	0.08

In Table4.18, the nominal values were found from various industry projects and/or various papers. I personally measured a variety of PWBs from the same vendor and same lot and found the thickness varied from the 1.591 (mm) to 1.601 (mm). The standard deviation was thus calculated to be about 0.2% if the nominal value or mean. Many of the other geometric dimensions have a tighter control on dimension since the component balls needs to fit on the PWB lands. The young's modulus of the FR-4 PWB can be found in various documents to range researches to be between the 17200 MPa and 27924 MPa range. This range is actually too large. It is assumed the young's modulus is around 18200 MPa and the standard deviation is 1% of the mean, similarly for the component. Later we will look more closely at the uncertainty in the Young's Modulus. The Poisson ratio in both the PWB and component, is not know to vary by much, thus we assume that the standard devotion is 0.8%. All the parameters in Table4.18 are important parameters, but from an uncertainty point of view, the material properties are more important than geometric parameters. The geometric parameters can always be measured and thus are known more accurately than the material properties.

When one uses the Monte Carlo simulation all input parameters shown in Table4.18 are varied in a random fashion for each calculation and the results for multiple calculations are presented in a histogram fashion to view the output distribution. Since the function for C involves the product of random variables, to output distribution is known not to be a normal distribution. Figure4.23 shows an example histogram of a Monte Carlo simulation for the correction factor C. This histogram exhibits some outlier points that skew the distribution far to the right. These outliers' points are due to our normal

distribution assumption for the input parameters and the fact that the functional form for C involves products of random variables and random variables raised to powers. With the normal assumption for the input parameters there is a finite probability for selecting one or more input parameters whose value is far into the tails of the distribution. With a Monte Carlo simulation with tens of thousands of replications, we are bound to have a calculated value for C that is not reasonable. To overcome this, the tails of the Monte Carlo simulation were clipped. Figure4.24 shows the same Monte Carlo simulation as the previous figure, but only 95% of the data is shown and plotted. The upper 2.5% and the lower 2.5% is eliminated. This histogram shows the range of the Correction Factor C with a 95% of data input parameters defined in Table4.18.

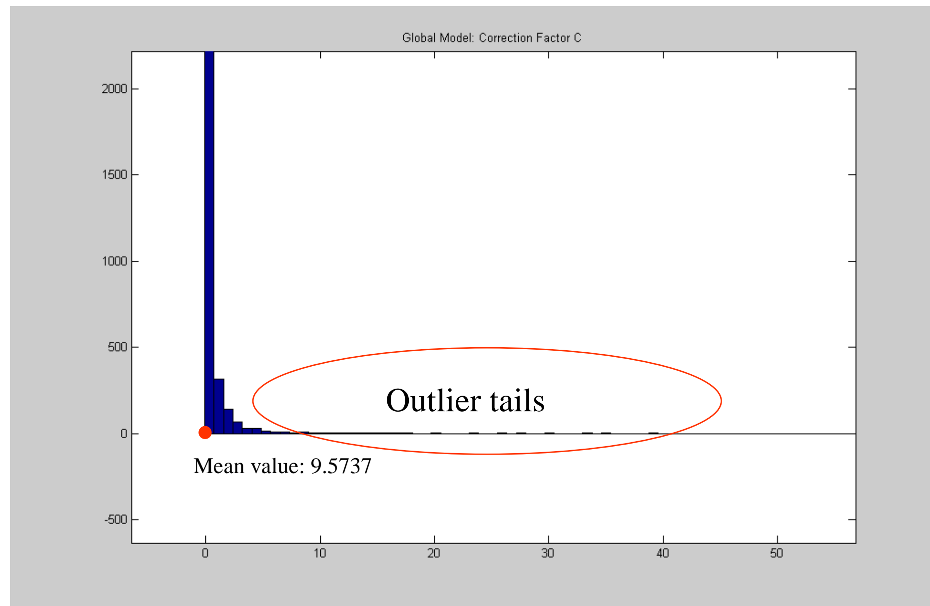

Figure4.23: Histogram of Monte Carlo Simulation for Correction Factor C

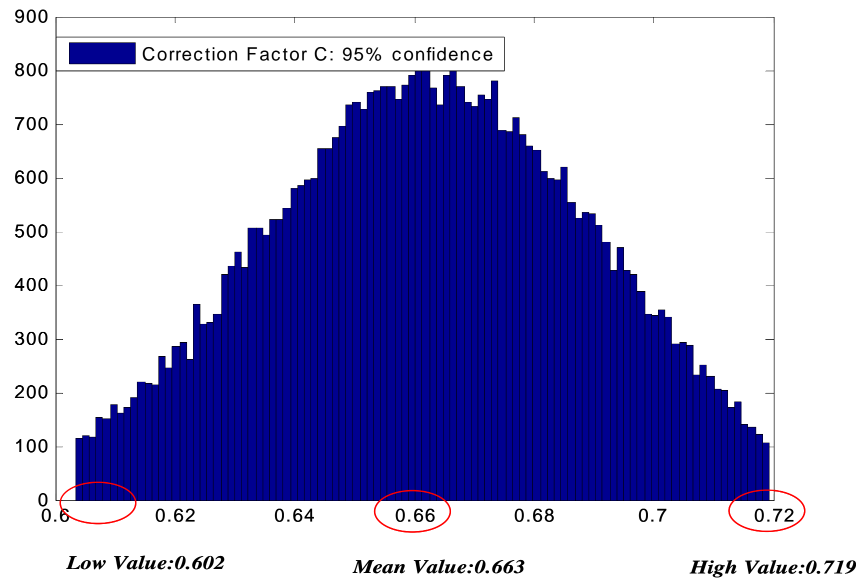

Figure4.24: Histogram of Monte Carlo Simulation for Correction Factor C Using Central 95% of Data

Figure4.24 shows the 95% of data range in the value of C. The mean value from the Monte Carlo simulation can also be calculated and compared to the nominal value calculated directly using the formula and nominal parameter values as shown in Table4.19. Table4.20 shows the comparison between the nominal value calculated directly from the formula and the mean value of C using the 95% of data range data from the Monte Carlo simulation.

Table4.19: The Correction Factor C in the Particular Parameter Value

Gap Size (mm)	10.17
Ball Span Length (mm)	17.78
E_c (MPa)	18,200
t_c (mm)	0.81
n_uc	0.20
D_c	840
E_pwb (MPa)	18,200
t_pwb (mm)	1.57
nu_pwb	0.20
D_pwb	6,114
A (mm^2)	1.778
D	0.137
Correction Factor C	***0.663***

Table4.20: Comparison of the particular nominal value and 95% of data Range with Monte Carlo simulation random variables for the correction factor C

	Correction Factor C	$\frac{N}{N_{nominal}}$ ratio
Particular Nominal Value	0.663	1.0
Monte Carlo Simulation Value	0.662	

Figure4.24 shows that from the Monte Carlo simulation the low correction factor C is 0.602, the mean value is 0.662, and the high correction factor C is 0.72. Table4.21 shows that the range in C varies from 0.9 to 1.1 times the nominal value. Table4.22 compares the ranges in for the 80% of data values and the 95% of data values.

Table4.21: The of data 95% Range in the correction factor C

	Correction Factor C	$\frac{N}{N_{nominal}}$ ratio
Low value	0.602	0.9
Nominal value	0.663	
High value	0.719	1.1

Table4.22: The 80% of data Range in the correction factor C

Nominal value =0.662	80% of data	95% of data	$\frac{N}{N_{nominal}}$ ratio
Low value	0.623	0.602	1
High value	0.700	0.719	1

Conclusions: Uncertainty Analysis for Correction Factor C :

We need to understand how small variations in the input parameters affect the output parameter C , and eventually the estimated life. As we know, measuring the geometric parameters is obviously the most accurate way to tighten up on these uncertainties. Material properties and in particular detailed information on the Young's modulus is difficult and/or expensive to obtain. Table4.23 and Table4.24 show the results when we only vary the Young's modulus' standard deviation of the PWB and PBGA package. For these calculations it is assumed that the critical solder joint stress is a function of the nominal Young's modulus, i.e. it is held constant as we vary it in the calculation for C . For a Young's modulus with a standard deviation of 1% of the mean, the life can vary by almost a factor of two. Tightening up the Young's modulus to a standard deviation of 5% of the mean improves the life calculation. This example shows that the final life cycle is very sensitive to the young's modulus of PWB and PBGA. If one wants to get

the most accurately life assessment, knowledge of the actual young's modulus is very important.

Table4.23: The 95% of data Range in the Correction Factor C and Final Life Cycle for the ***Young's Modulus' Standard Deviation 1% of Mean Value***

Value	Correction Factor: C	$\frac{X}{X_0}$ ratio	Critical Solder Joint Stress S	Life Cycle	$\frac{N}{N_{nominal}}$ ratio
Low	0.602	1	1.803	14,245,080	0.5
Nominal	0.662			26,166,069	
High	0.720	1.1		44,789,408	1.7

Table4.24: The 95% of data Range in the Correction Factor C and Final Life Cycle for the ***Young's Modulus' Standard Deviation 5% of Mean Value***

Value	Correction Factor: C	$\frac{X}{X_0}$ ratio	Critical Solder joint Stress S	Life Cycle	$\frac{N}{N_{nominal}}$ ratio
Low	0.398	0.6	1.803	1,008,089	0.04
Nominal	0.662			26,166,069	
High	0.892	1.3		176,434,056	7

This uncertainty discussion is not the complete result. It is only considering the global model independent from the local model. These results need to be combined with the local model for calculating the critical solder joint stresses. This will be treated in Chapter 7 when the predictions are compared to the experiment results.

4.3.1.2 Uncertainty in CALCE_PWA Curvature Calculation

The uncertainty section started with a discussion of the uncertainty in the correction factor C, given uncertainties in the input parameters. The correction factor is applied to the curvature as calculated by *CALCE_PWA*. We must understand the uncertainty in the curvature value calculated by *CALCE_PWA*.

It was quickly discovered that the *CALCE_PWA* curvature calculation is not sensitive to variations in the input parameters as shown in Table4.18. For example, Table4.25 shows the results in curvature, K_{rms}, when the PWB's young's modulus varies by +/- 10% or 20% while keeping the other parameters constant. Other previously identified critical parameters were also varied with little change in the curvature.

Table4.25: *CALCE_PWA* Curvature as a Function of PWB Young's Modulus

	PCB_E (MPa)	K_rms (1/mm)	$\frac{N}{N_{nominal}}$ ratio
-20	14560	0.0000944	1.0
-10	16380	0.0000916	1.0
0	18200	0.0000922	
10	20020	0.0000886	
20	21840	0.0000997	

	Ball Diameter (mm)	K_rms (1/mm)	$\frac{N}{N_{nominal}}$ ratio
-20	0.60	0.0000922	1
-10	0.68	.0000922	1
0	0.75	0.0000922	1
10	0.83	0.0000922	1
20	0.90	0.0000922	1

Conclusions: Uncertainty Analysis for CALCE_PWA:

It was determined that the most critical parameters for the *CALCE_PWA* analysis are Young's modulus, thickness, and PWB density. Even though they were identified as critical parameters, the variability in the curvature calculation from the *CALCE_PWA*

software is small compared to the uncertainty in the curvature ratio correction factor C discussed in the previous section.

4.4 Summary

The *CALCE* software, *CALCE_PWA*, currently has a simple FEA based vibration analysis tool that calculates the modal response of a PWB and the dynamic response to a prescribed acceleration PSD. The tool has been well received by the industry and has been previously validated against various experiments and other FEA codes. The important point for us is that the tool is easy to use and fast. Unfortunately, the FEA mesh is not of sufficient density to capture the curvature information that is needed for an accurate local stress analysis model. Instead this research intends to correct the curvature as calculated by the *CALCE_PWA* with a multiplication factor that itself is a function of the critical geometry and material parameters. Mathematically this correction factor C can be expressed as:

$$K_{actual} = C * K_{calce_pwa}$$

where is K_{actual} the actual curvature, and K_{calce_pwa} is the curvature as calculated by the *CALCE* software.

DOE and ANOVA techniques were used to help identify the critical parameters that are included in the functional relationship for the transformation factor C. The global model

gives us an accurate curvature value in the region of the component of interest. This information is then fed into a local stress analysis and eventually a damage model for accurate assessment of fatigue life is created.

Finally, in order to understand how small variations in the input parameters affect the output parameter, and eventually the estimated life, Monte Carlo simulations were run to understand the variations in the correction factor where the input factors were assumed to have a normal distribution. It was found that the most critical factor that influences the correction factor is knowledge of the Young's modulus for both the PWB and the component.

Chapter 5: Local Model

As introduced in Chapter 4—Global model, a coarse model of the entire PWB, with particular attention to the boundary conditions, needs to be built to determine the response of the PWB to the vibration environment. The next step is to construct a detailed model of the particular component of interest, using boundary condition inputs from the global model. This is the local model. This local model of a particular component has enough resolution to determine the critical location and value of the stresses in the solder joints. Once the critical solder ball stress has been determined, a damage model or law is used to calculate the fatigue life.

The expected life of the solder ball in a random vibration environment is easily in excess of 100,000 cycles. For perspective purposes, a typical PWB natural frequency is on the order of 100 Hz and 100,000 cycles will occur in 1,000 seconds or less than 17 minutes. The fatigue failure is in the region known as high cycle fatigue. High cycle fatigue is driven by elastic stresses, and plastic stresses are negligible to non-existent.

The local stress analysis will be a simple linear elastic analysis. This is a reasonable assumption because the life of the solder attaches that we will be looking at will be in the hundreds of thousands of cycles to tens of millions of cycles. There may be very small amounts of plastic deformation, but the extra effort of an elastic-plastic stress analysis is questionable. It is recognized that this may limit the use of the model to only vibration applications where large numbers of cycles to failure are expected. With this assumption

the model may not be usable for simple bending type applications where small numbers of cycles are expected, but the goal of the research is an easy to use rapid model for vibration environments. All calculations for the local curvature of the PWB and then the value of the critical stress in the component attachment will be expressed in terms of a probability distribution. A simple linear damage superposition technique will be used knowing the probability or percent of time that the stress will be of a certain magnitude, to calculate the total time that a component will last in the random vibration environment. Using finite element models, the effective stress in the outmost solder joint is calculated according to

$$\sigma_0 = \left[\sigma_{xx}^2 - \sigma_{xx} \cdot \sigma_{yy} + \sigma_{yy}^2 + 3 \cdot \sigma_{xy}^2\right]^{1/2} \quad \text{Equation5.1}$$

where σ_0 is the effective stress or also commonly known as the Von Mises Stress. The stress values of the solder joint of interest are averaged among the elements in each joint and the average value is used in a damage, or life calculation. The stress life relationship, proposed by Basquin high cycle fatigue power law, is used for estimating solder fatigue life and will be discussed in Chapter 6.

The *CALCE* software staff recently wrote a new finite element program, *CALCE_FEA*. This software is a simple FEA program with very coarse mesh density that can be used to determine the location and value of the maximum solder joint stress. The important point for us is that the tool is easy to use and fast. I also conducted a series of parametric studies with *ANSYS* and determined that this simple software was accurate enough for our

modeling. The problem with the ANSYS based approach is that it first requires an experienced modeler to conduct the analysis. Meshing the PWB would involve thousands of elements in order to obtain the required resolution to eventually find the critical stress locations and values. The time required building the model, conducting the analysis, and post-process the results would take at least a few days which is very time consuming and can not be afforded in the industry.

The goal of this research is to determine an empirical response surface model. We started out criticizing the current *CALCE* fatigue model because it was an empirical model. The problem with the *CALCE* fatigue model, since it is empirical is that it must be calibrated for new components and new materials. Such calibration efforts are time consuming and require expensive experiments. This research is an attempt to move in a direction to improve the current *CALCE* model by breaking up the current empirical model into a stress analysis, which then feeds into a classic fatigue damage model. By breaking up the current model into a stress analysis and a damage analysis, one can more directly investigate and predict the influence of new component families and new materials.

In this chapter, the local stress analysis will determine the critical stress in the critical solder joint. Section 5.1 will illustrate the complete local modeling approach, as shown in Figure5.1on the right-hand side. In our local modeling approach, a simulation tool, *CALCE_FEA* is adopted and discussed in section 5.2. Similar to the global model, DOE and ANOVA techniques will be used to determine the key parameters and help in the development of a rapid assessment model throughout the process of local modeling.

Again, at each level we will need to understand the key geometry and material parameters that need to be included in a rapid assessment approach and which parameters can be neglected without too much loss in accuracy. This is similar to the global modeling cases. Section 5.3 estimates the error due to structural approximations rather than those due to the finite element technique. The focus of section 5.4 is on errors resulting from geometry and material properties representation. The obtained critical stress is then fed into a damage model to determine the fatigue life of such components that will be calculated.

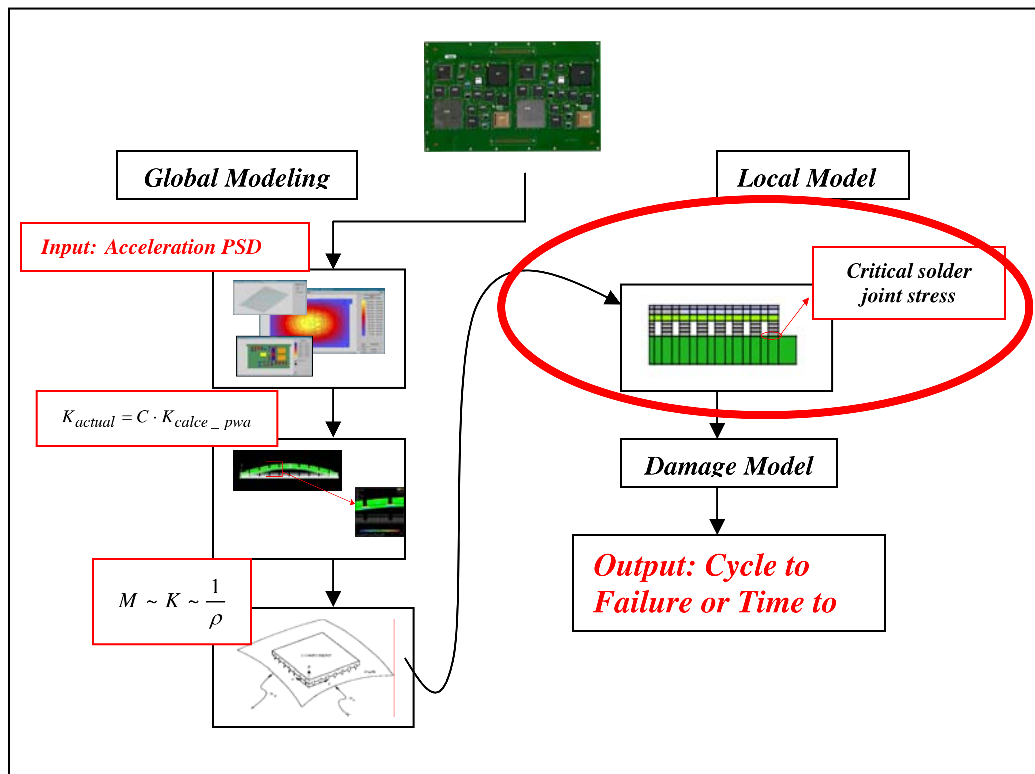

Figure5.1: Complete Local Model Approach

5.1 Local Model Approach

The approach in this dissertation will involve global (entire PWB) and local (particular component of interest) modeling approaches. The global model should give us the accurate curvature, which in turn can easily be converted into the accurate bending moment executed at specific locations of interest. This accurate moment is then fed into a local stress analysis for accurate assessment of fatigue life prediction for particular components.

The *CALCE* local model is a very simplified local FEA model, and in this model the region of interest is the maximum stress in the solder ball. This critical stress is actually the Von Mises Stress, which occurs at the outer corner of a solder joint as shown in Figure5.2. In *CALCE_FEA* software, all calculations are carried out at the gauss points.

In this research, *Von Mises Stress* in 2D is adopted as shown in the Equation5.2 below:

$$\sigma_0 = \frac{1}{\sqrt{2}}\left[(\sigma_{xx}-\sigma_{yy})^2 + (\sigma_{yy}-\sigma_{zz})^2 + (\sigma_{zz}-\sigma_{xx})^2 + 6\cdot\left(\sigma_{xy}{}^2 + \sigma_{yz}{}^2 + \sigma_{zx}{}^2\right)\right]^{1/2} \quad \text{Equation5.2}$$

In this dissertation, we only deal with the 2D finite element model, thus

$$\sigma_{zz} = \sigma_{zx} = \sigma_{yz} = 0 \quad \text{Equation5.3}$$

$$\sigma_0 = \frac{1}{\sqrt{2}}\left[\sigma_{xx}{}^2 - 2\cdot\sigma_{xx}\sigma_{yy} + \sigma_{yy}{}^2 + \sigma_{xx}{}^2 + 6\cdot\sigma_{xy}{}^2\right]^{1/2}$$
$$= \frac{1}{\sqrt{2}}\left[2\cdot\left(\sigma_{xx}{}^2 - \sigma_{xx}\sigma_{yy} + \sigma_{yy}{}^2 + 3\cdot\sigma_{xy}{}^2\right)\right]^{1/2}$$

$$\sigma_0 = \left[\sigma_{xx}{}^2 - \sigma_{xx}\cdot\sigma_{yy} + \sigma_{yy}{}^2 + 3\cdot\sigma_{xy}{}^2\right]^{1/2} \qquad \text{Equation5.4}$$

Once the critical solder joint stress is known, one can estimate the fatigue life from the damage model. Before getting into the local model approach, we will first discuss some preliminary issues such as ball shape (rectangular, circular) and mesh issue (simple or complicate).

5.1.1 Solder Joint Shape

Solder joint shapes on PWB vary from rectangular to circular with traces. In the presence of solder volume variations, different solder joint shapes may have different sensitivities. A 2D rectangular solder joints case using *CALCE_FEN* and a 2D circular one using ANSYS are analyzed and the results are compared in Table5.1, in this study, a "stress volume-average" was used. This is defined as the volume-average between the total 25% volume of all solder rectangular in the bottom joint and the 25% of volume average occupied by the solder circular in the axisymmetric model.

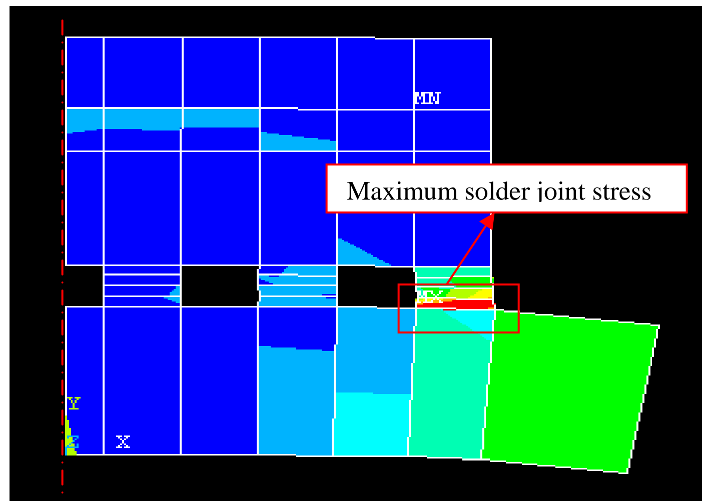

Figure5.2: Local FEA Model of Solder Joint

Figure5.2 shows the 2D slice model has been employed to study the BGA package solder joint fatigue performance in this dissertation. To shorten the computation time and memory space, a coarse mesh of the local slice model (without details of copper bond pads and solder mask) was first constructed in *CALCE_FEN*. The most critical solder joint location was determined as shown in Figure5.2. The stress volume averaging method was thus employed at the joint interface between the joint and the PWB in Equation5.5.

Stress Volume Average:

$$\frac{\sigma_1 V_1 + \sigma_2 V_2 + \sigma_3 V_3 + \dots\dots\dots\sigma_n V_n}{\sum_{i=1}^{n} V_i} \qquad \text{Equation5.5}$$

Figure5.2 shows the CBGA slice model 36 I/O full array and compares the different values of the 2D “rectangular” shapes using the *CALCE_FEN* software with the 2D “circular” shape using ANSYS, as calculated from the formula in Equation5.5. Except in the CBGA case, we have also done some tests (for example, change number of solder joint: 6*6 I/O counts, 9*9 I/O counts, 15*15 I/O counts, and 19*19 I/O counts; different types of components: PBGA, and CSP; change component’s thickness, and PWB’s thickness) to double check those comparisons of 2D rectangular and ball shapes results and determined that those results would not cause the stress volume-average results to be different. Fortunately, the results had shown a very good comparison and revealed that we could use the rectangular shape instead of the circular shape to calculate the volume-average stress in this local model case.

Table5.1: Comparison of 2-D Rectangular and Ball Shapes in solder joint

CBGA: slice model 36 I/O full array	***Volume-Average Stress***
2D Shape Rectangular with *CALCE_FEN*	0.770667
2D Shape Circular with ANSYS	0.752413
% Difference	-2.4

Figure5.3 shows the analyzed plots for both cases, rectangular and circular solder joint, as calculated in Equation5.5. Figure5.3 shows the location between the bottom joint and printing wiring board interface where we compare the rectangular and ball shapes’ stress volume-average. A difference of 2.4% is observed when using the CBGA slice model 36 I/O full arrays, as in Figure5.3, which compares the 2D “rectangular” shape using the *CALCE_FEA* software and the 2D “circular” shape using *ANSYS*. Even though the solder

joint is now transformed into a circle; it is shown that this does not diminish the model's ability to accurately capture the experimentally observed behavior. In both cases, for the purpose of fair comparison, the stress volumes average of solder joints is kept the same and the cross section area for the 2D shapes are normalized to the same volume.

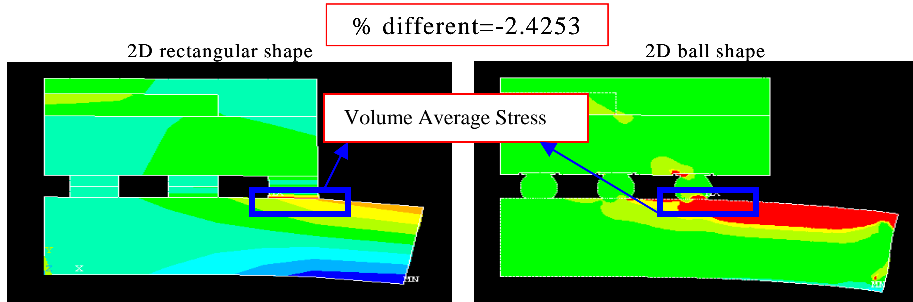

Figure5.3: Left: *CALCE_FEA* and Right: *ANSYS*

Thus, we find that we can easily use the rectangular shape instead of circular shape, based on saving computation time and memory space, which can be applied for the parametric study of the package's fatigue life to get acceptable enough in this dissertation. After discussing the solder joint "shape problem," the next subsection will consider the "mesh resolution problem".

5.1.2 Mesh Problem

The finite element mesh is generated automatically for a given geometrical shape in *CALCE_FEA*. The key parameters for the generation of the FEA model includes PWB's thickness, overmold's thickness, die's thickness, height of the solder joint, and etc. Mesh parameters are defined as the number of divisions along geometric edges. The mush

uniformity is maintained in the present procedure by a careful choice of the edges on which the mesh density is defined, and through pre-defined relationship between mesh parameters.

Figure5.4 shows the mesh comparison between *CALCE_FEA* with the very coarse mesh density and *ANSYS* with more complex mesh density; both models can be used to determine the location and value of the maximum solder joint stress. In this example, the PBGA slice model 121 I/O full arrays will be analyzed. In the *CLACE_FEA* software, there is a total of 129-mesh density in this model. Except for the number of mesh density, the material properties and geometry in this whole BGA structure are kept the same. Again, *CALCE_FEA* is a very coarse mesh density, and only 129-mesh density will be used. In this case, we will only change the number of mesh density in the *ANSYS* software to compare the final maximum solder joint Von Mises Stress value to see how much difference there is between *CALCE_FEA* and *ANSYS*.

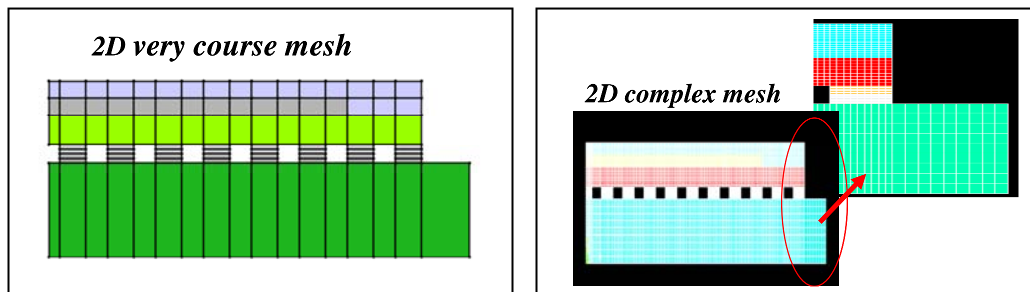

Figure5.4: Mesh Comparison, Left: *CALCE_FEA* (simple mesh);
Right: *ANSYS* (complex mesh)

As shown in Figure5.4, a plot of maximum Von Mises Stress versus number of mesh density shows the changes in maximum solder joint Von Mises Stress results for the different mesh densities.

The Von Mises Stress results at the corner of the solder joint converged upon a solution as the mesh density increased. The maximum solder joint volume-average stresses are as follows in Table5.2:

Table5.2: CACLE_FEN&ANSYS' Mesh Density and Von Mises Stress Results

CALCE_FEN: Mesh Density	*CALCE_FEN:* Von Mises Stress	*ANSYS:* Mesh Density	*ANSYS:* Von Mises Stress	% Difference
129	***47.309***	129	49.31	4.1
		516	49.221	3.9
		645	49.191	3.8
		774	49.304	4.0
		903	49.397	4.2
		1032	49.304	4.0
		1161	49.304	4.0
		1290	49.304	4.0
		1419	49.304	4.0
		1548	49.304	4.0
		1677	***49.304***	4.0

As shown in Table5.2, a difference of 4.0% is observed. This 4.0% means this does not diminish the model's ability to accurately capture the experimentally observed behavior. Although this example shows maximum solder joint Von Mises Stress results, the same general method can be used to perform a mesh convergence study for other types of results.

We will use a new finite element program that was written by the *CALCE* software staff, *CALCE_FEA*. Figure5.5 shows the cross section of the structure after meshing by *CALCE_FEA*. This software is a simple FEA program with very coarse mesh density that can be used to determine the location and value of the maximum solder joint stress.

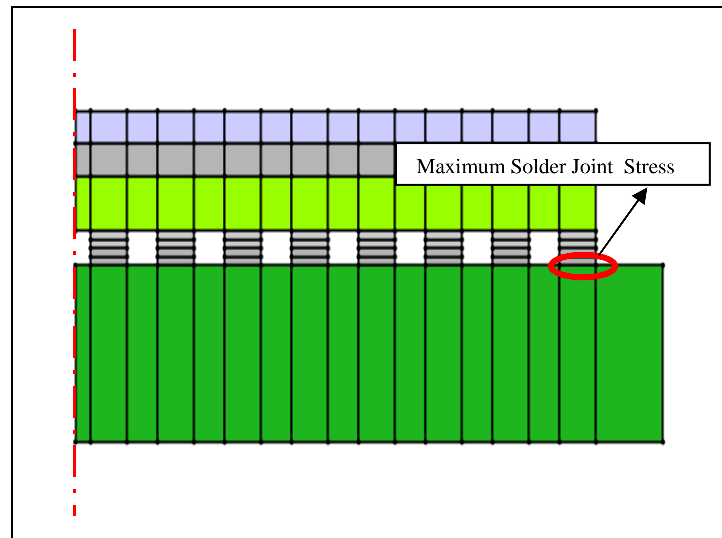

Figure5.5: Local Model for *CALCE_FEA*

The argument for using the *CACLE_FEA* is based on:

1. Wanting to demonstrate *CACLE_FEA* software that it is accurate enough for predicting the solder joint failures (i.e. *CALCE* center's industrial members can use it without any doubt or equation about this *CACLE_FEA* software)
2. Time and cost savings are not important since one only needs to do the DOE once to find a closed form equation

3. Eventually there are plans to directly incorporate *CACLE_FEA* in to *CACLE_PWA* directly and remove the empirically derived closed form equation that is the basis of this research.

Similar to the global modeling effort discussed in the previous chapter, I will use DOE and ANOVA techniques to determine the critical geometric and material parameters that influence the critical solder joint stress.

5.2 DOE and ANOV Approach for Local Model

In Chapter 4, we corrected the curvature as calculated by the *CACLE_FEA* with a multiplication factor that is a function of the critical geometry and material parameters. The results from the global model are used as a boundary condition to load the local model. This local model boundary condition load is a bending moment M applied to the outside edge of the PWB. This bending moment M is calculated knowing the PWB curvature. After determining the critical stress in the critical solder joint attach, a power law fatigue damage model is used to calculate the fatigue life that will be discussed in Chapter 6.

Before getting in to the local model issue, we need to point out that the solder joint stress, actually a *rms* value, is proportional to the bending moment, $\sigma \propto M$, modified by geometry factor. The critical solder joint stress (σ_{rms}) can be expressed as:

$$\sigma_{rms} = M \cdot S \quad \text{Equation5.6}$$

where M is the bending moment applied to the edges of a component board assembly. Mathematically this geometry factor, multiplication factor, or transformation factor, S can be expressed as:

$$S = \frac{\sigma_{rms}}{M} \qquad \text{Equation5.7}$$

CALCE_FEA will be the tool used to determine this geometry factor S as illustrated in Figure5.6.

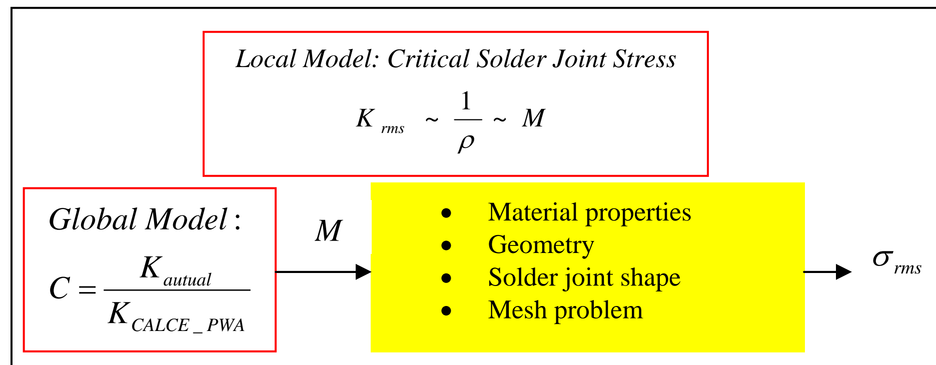

Figure5.6: Local model Approach

We will use the same DOE approach as discussed in Chapter 4 to identify the critical factors and ultimately arrive at a function form for the geometry factor S .

5.2.1 DOE and ANOVA Analysis for Model Development

Following the same methodology as discussed in Chapter 4, we broke the DOE/ANOVA/RSM approach into steps.

Step 1: Identify the problem:

The local model boundary condition load is a bending moment M applied to the outside edge of the PWB component assembly. This bending moment M is calculated from the global model and the basic moment-curvature relationship. *CALCE_FEA* will be used to determine the maximum solder joint stress.

$$S = \frac{\sigma_{rms}}{M} \qquad \text{Equation5.8}$$

where S is geometry factor in this equation. Our problem is to determine a functional form for S .

Step 2: Identify the factors:

Material properties and geometric information is know for each of our BGA typical components (PBGA, CBGA, and CSP), and then the model are built in *CALCE_FEA* shown in Figure5.7.

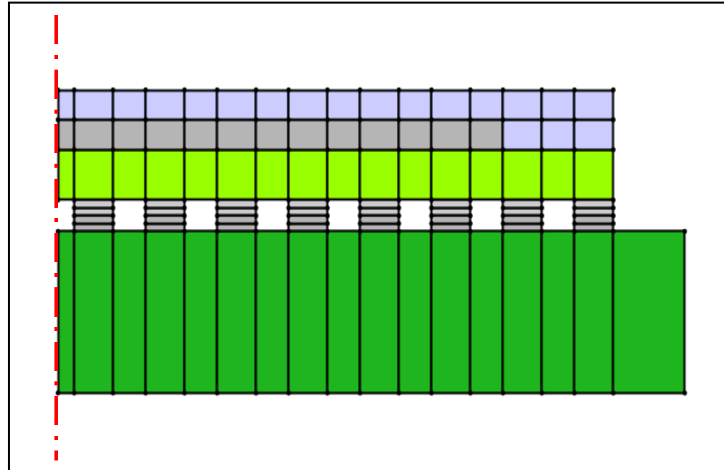

Figure5.7: PBGA Slice Model 256 I/O Full Array

From the element Gauss point output of *CALCE_FEA*, the critical solder joint Von Mises Stress was found to occur at the outer corner of a solder joint as shown in Figure5.8.

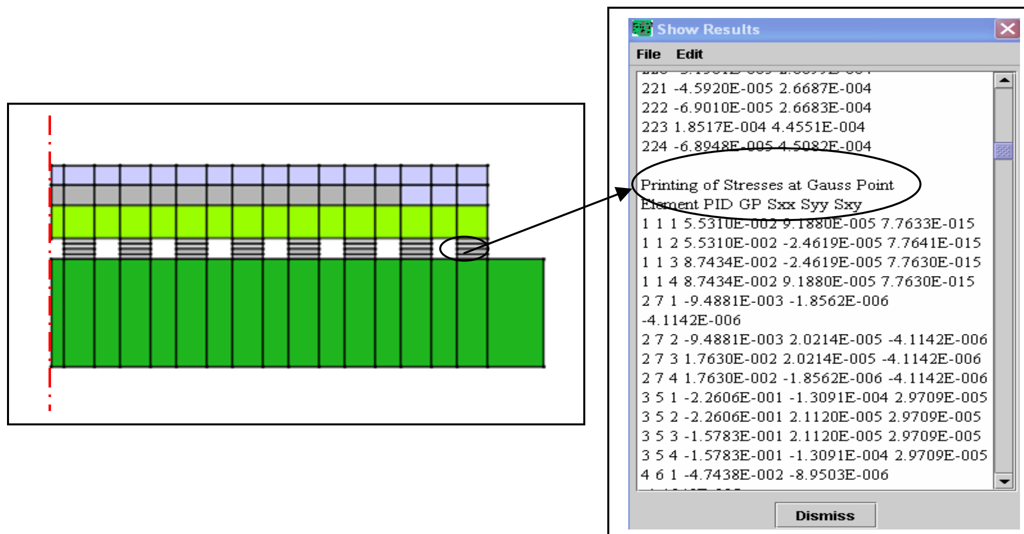

Figure5.8: Local Model Solder Joint Von Mises Stress

An analysis procedure similar to that in the global modeling case is performed to define the dependent variable (response variable) and the independent variables. The response variable is critical solder joint stress. As was done in the global model, various trend plots were made for the various independent variables. Each possible independent variable was varied over its expected range, while keeping the others constant, to preliminarily determine critical factors. Figure5.9 shows a typical plot.

From Table4.4 the number of solder joints is seen not to be a critical factor, but the ball diameter is. Table5.3 presents a summary of all the possible critical factors and identifies which ones are potential critical factors. Note that the identified critical factors are the same as those found in global model, with the exception that gap size from the global model is not present in the local model, and the solder ball diameter is identified as critical in the local model and not in the global.

Table5.3: Possible Critical Factors Identified by Using Plot Trend in Local Model

Critical Factors	***Possible Critical Factors***
✓	PWB thickness
✓	PWB Young's Modulus
✓	PWB Poisson Ratio
	PWB length
	PWB density
	Pitch size
	Ball span length
	Solder joint height
	Neighboring component and location (gap size)
	Solder joint Young's Modulus
	Solder joint Poisson Ratio
✓	BT Young's Modulus
✓	BT thickness
✓	BT Poisson Ratio
✓	BT length
✓	Die Young's Modulus
✓	Die thickness
✓	Die Poisson Ratio
✓	Dei length
✓	Overmolding Young's Modulus
✓	Overmolding thickness
✓	Overmolding Poisson Ratio
✓	Overmolding length
✓	Solder joint diameter

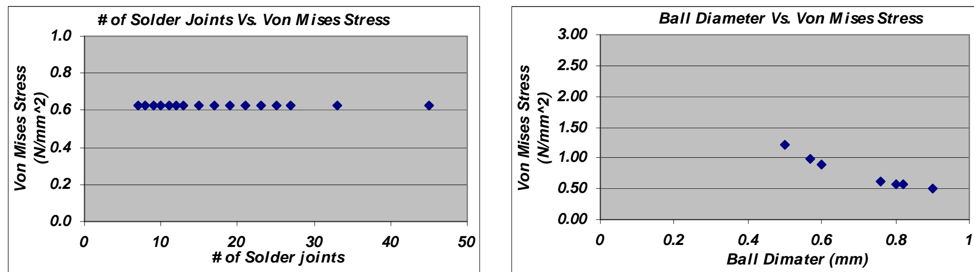

Figure5.9: Left: Number of Solder Joints vs. Von Mises Stress; Right: Ball Diameter Vs. Von Mises Stress

Unfortunately, the trend plots are not enough to judge whether the factors are truly critical. The trend plots only consider a single factor at a time while keeping the others constant. It does not consider interactions between possible factors. For this reason, DOE is used to identify the critical factors and also identify possible interactions. A 2-level factorial DOE will be used during the second step. This means 2-levels of each factor will be studied at once. The resulting identified critical factors are shown in Table5.4.

Table5.4: Possible Critical Factors Identify by 2-level factorial DOE in Local Model

Critical Factors	***Possible Critical Factors***
✓	PWB thickness
✓	PWB Young's Modulus
✓	PWB Poisson Ratio
	PWB length
	PWB density
✓	Pitch size
	Ball span length
✓	Solder joint height
	Neighboring component and location (gap size)
	Solder joint Young's Modulus
	Solder joint Poisson Ratio
✓	BT Young's Modulus
✓	BT thickness
✓	BT Poisson Ratio
✓	BT length
✓	Die Young's Modulus
✓	Die thickness
✓	Die Poisson Ratio
✓	Dei length
✓	Overmolding Young's Modulus
✓	Overmolding thickness
✓	Overmolding Poisson Ratio
✓	Overmolding length
✓	Solder joint diameter

Comparison of Table5.3 and Table5.4 shows that the 2-level DOE only eliminated the Poisson ratio factors for the overmold, die, BT, and PWB. This step did not really gain

us much. As was done in Chapter 4, a reduction in the number of factors can be accomplished by combining the factors together into physical parameters like stiffness and various dimensionless ratios.

To improve the curve fitting efficiency and the stability of convergence in RSM, it is important to identify the critical variables, which we define as the independent factors. These factors are the ones that will have major impact on the response variable. The number of such factors should be minimized to guarantee a unique fitting result with required accuracy level without getting into a local minimum while optimizing the error functions involved in RSM. Adding too many factors without careful examination will waste the computational resources and run the risk of getting inaccurate results.

The identified potential critical parameters are grouped to reduce the number of factors. Here the functional relationship of the Von Mises Stress for local model geometry factors can be written as:

$$D_{pcb} = \frac{E_{pcb} \cdot h_{pcb}{}^{3}}{12(1-\nu_{pcb}{}^{2})} \quad and \quad D_{component} = \frac{E_{component} \cdot h_{component}{}^{3}}{12(1-\nu_{component}{}^{2})} \qquad \text{Equation5.9}$$

$$D_{ratio} = \frac{D_{component}}{D_{pwb}} \qquad \text{Equation5.10}$$

$$S = f\left(D_{ratio} = \frac{D_{component}}{D_{pcb}}, \frac{Ball\ Diameter}{Ball\ Span\ length} \right) \qquad \text{Equation5.11}$$

$$\sigma_{ratio} = M \cdot S \qquad \text{Equation5.12}$$

Step 3: Computation of the total runs required; decision on the design options:

To use RSM-three level factorials and two factors ($A: \frac{Ball\ Diameter}{Ball\ Span\ length}$, $B: D_{ratio}$), were used in a similar manner for each of the three component types (PBGA, CBGA, CSP) as we discussed in section 4.3 for the global model. A full factorial design with 9 runs was executed.

Step 4: Start to run DOE tool, and FEA runs:

All the low, intermediate, and high-level values for each factor (A & B) are calculated for the specific PBGA, CBGA and CSP package. For example, the rigidity ratio of our typical PBGA package $D_{ratio} = \frac{D_{component}}{D_{pcb}}$ is shown in Table5.5.

Table5.5: D_{ratio} Value for PBGA Package in Local Model

Low Value	Intermediate Value	High Value
0.0041	0.0023	0.0435

For all these values in A (ball diameter), we assume the ball diameter is from 0.35(mm) to 0.9 (mm) as shown in Table5.6.

Table5.6: Ball Diameter Value for PBGA Package in Local Model

Low Value	Intermediate Value	High Value
0.35	0.65	0.9

The Design-Expert 7.0 software tool was used to help conduct the DOE analysis and determine the final functional relationship for S :

$$S = f\left(D_{ratio} = \frac{D_{component}}{D_{pcb}}, \frac{ball\ diameter}{component\ length} \right) \qquad \text{Equation5.13}$$

Figure5.10 shows a preliminary graph of the actual response values versus the predicted response values (more plots are shown in the appendix B). These graphs help us detect a value, or group of values, that are not easily predicted by the model. The 45° line should split the data points evenly. In this plot the horizontal axis is the actual values and vertical is predicted values. If the predicted values agree exactly with actual values, everything would lie on straight line with slope equals to 1. The plot shows that the result seems to be very good fit for each case, but further work can improve upon the fit.

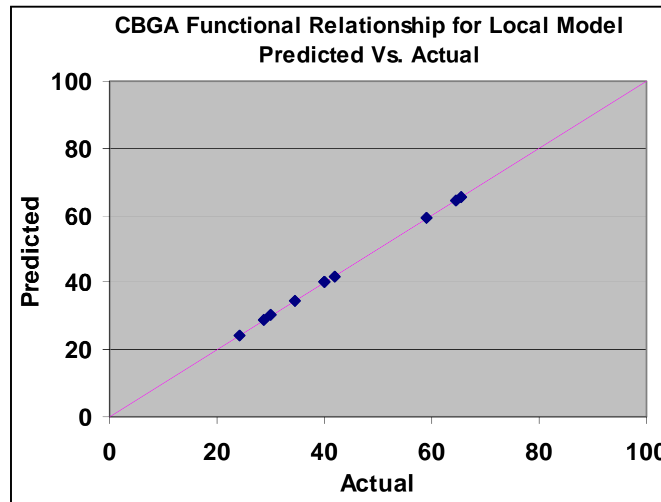

Figure5.10: CBGA Functional Relationship Factor for Local Model: Predicted Vs. Actual

Step 5: Apply the transformations to linearize the fit as much as possible

In this case, diagnostics indicated that an "Inverse Square Root" transformation would be appropriate, so the analysis was restarted with transformed data.

Step 6: Perform the ANOVA to identify the critical parameters and interactions affecting the response variable and quantifying the same:

Once the data were entered into the DOE matrix, all treatments and interactions were selected to be included in the ANOVA model. ANOVA was then performed to determine which factors were significant effects in the model. As each of the remaining Sources (A, B, AB) was statistically significant (Prob>F is less then 0.05), one can conclude that (A: the ball diameter/ PWB's length) and (B: D_{ratio}) both have an effect on the Von Mises Stress. Perhaps more importantly, the interaction between these two treatments is important, i.e. certain combinations (ball diameter/ PWB's length) and (D_{ratio}) may have significant effects.

As mentioned, ANOVA can help to quickly identify the possible critical factors. Based on *step 2*, we got the possible critical factors from two methods. One is from the plot trends, which only considered a single factor to determine the effect of one factor on a process. The other method is from the 2-level full factorial DOE method based on the plot trends to get the possible critical factors again, because there are still multiple factors involved and it is typically important to consider them together in case they interact

(influence each other). Both methods represented the rigidity ratio $D_{ratio} = \frac{D_{component}}{D_{pcb}}$, and

$\frac{Ball\ Diameter}{Ball\ Span\ length}$ are the critical factors in the local model process.

Step 7: Confirm Design of Experimental Results (Confirmatory Runs)

When the analysis of the experiment is complete, one must verify that the predictions are good. The interpretation and conclusions from an experiment may include a "best" setting to use to meet the goals of the experiment. Even if this "best" setting were included in the design, we should run it again as part of the confirmation runs to make sure nothing has changed and that the response values are close to their predicted values. Here, we conducted 10 runs for CBGA component, 12 runs for PBGA component, and 15 runs for CSP component. In this case, the predicted value is calculated from RSM, and actual values are calculated from the *CALCE_FEA*.

The derived factors S as a function of D_{ratio} and $\frac{Ball\ Diameter}{Ball\ Span\ length}$ is tested using the following examples. Figure5.11 shows that we test any material properties and geometries to validate the correction factor S in the validation runs to see how the results look. The plotted responses in Figure5.11 show a very good agreement with less than 4.3% error between the predicted and actual values for all CBGA case. Figure5.12 shows a very good agreement with less than 5.3% error between the predicted and actual values for all PBGA case, and finally Figure5.13 shows a very good agreement with less than 4.53% error between the predicted and actual values for all CSP case.

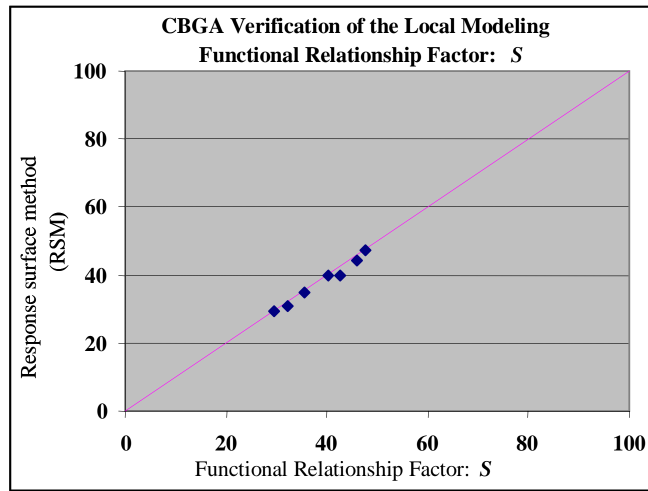

Figure5.11: Verification of Functional Relationship Factors: Critical Solder Joint *S* for CBGA

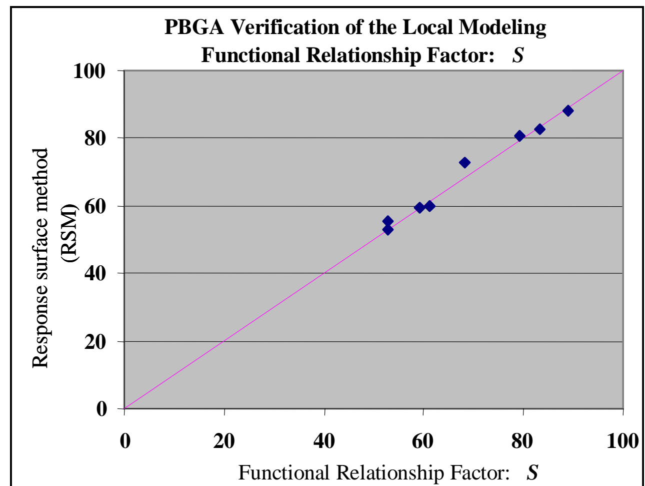

Figure5.12: Verification of Functional Relationship Factors: Critical Solder Joint *S* for PBGA

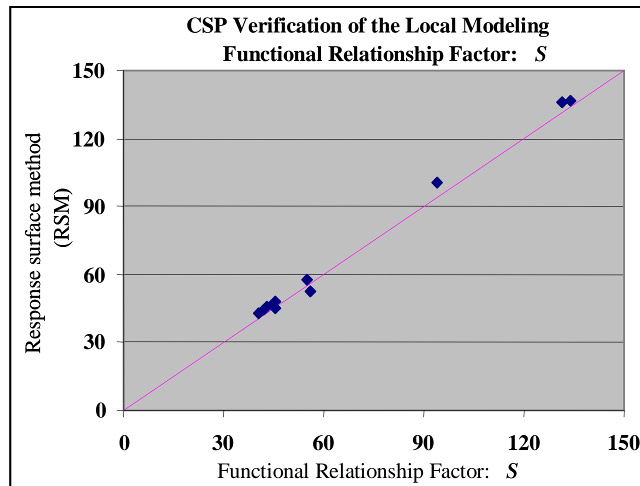

Figure5.13: Verification of Functional Relationship Factors: Critical Solder Joint *S* for CSP

***Step 8: Use/Present the Result*s: *Functional Relationship for Critical Solder Joint,* S**

Eventually response surface techniques with the identified critical parameters will give us a functional relationship for S as listed in Equation 5.11-Equation 5.13 for PBGA, CBGA and CSP cases, respectively.

Transformations of variables are again applied for accuracy control. In this case, inverse square root for both PBGA and CSP and inverse for CSP are found to be appropriate. The final functional relationship for local modeling is tabulated in Table5.7-Table5.9.

Table5.7: Functional Relationship in Critical Solder Joint S for the PBGA

Final Equation in Terms of Actual Factors: S	
1.0/Sqrt (PBGA Von Mises Stress)	=
-0.017483805	
29.70607565	* Ball Diameter/PCB Length
0.082097493	* D_ratio
-45.61270524	* Ball Diameter/PCB Length * D_ratio
-1104.825999	* Ball Diameter/PCB Length^2
-0.036898518	* D_ratio^2
765.3569837	* Ball Diameter/PCB Length^2 * D_ratio
134.7674615	* Ball Diameter/PCB Length * D_ratio^2

Table5.8: Functional Relationship in Critical Solder Joint S for the CBGA

Final Equation in Terms of Actual Factors: S	
1.0/(CBGA Von Mises Stress Ratio)	=
-0.013838513	
3.678244861	* Ball Diameter/PCB Length
0.037535522	* D_ratio
-5.971462924	* Ball Diameter/PCB Length * D_ratio
4.66697384	* Ball Diameter/PCB Length^2
-0.0363092	* D_ratio^2
39.90020585	* Ball Diameter/PCB Length^2 * D_ratio
5.729361585	* Ball Diameter/PCB Length * D_ratio^2

Table5.9: Functional Relationship in Critical Solder Joint S for the CSP

Final Equation in Terms of Actual Factors: S	
1.0/Sqrt (CSP Von Mises Stress)	=
0.000813862	
23.20142168	* Ball Diameter/PCB Length
0.00526788	* D_ratio
-5.440044411	* Ball Diameter/PCB Length * D_ratio
-649.2855275	* Ball Diameter/PCB Length^2
-0.028317082	* D_ratio^2
270.8558078	* Ball Diameter/PCB Length^2 * D_ratio
19.8857439	* Ball Diameter/PCB Length * D_ratio^2

Accurate critical solder joint stress can then be calculated using equation in Table5.7-Table5.9, once the functional relationship S for the local model is obtained. After determining the critical stress in the critical solder joint attach, a power law fatigue damage model is used to calculate the fatigue life that will be discussed in Chapter 6. In the next section, we will explore how the uncertainty issue affects the final local model results.

5.3 Local Life Uncertainty Issue Analysis

In this section, similar to section 4.4.2 the focus will be only on the model detail. Basically the model derived in this chapter comes from a FEA. To use this model an engineer can nominal value data to assess the life of the BGA component, but if the new components are used to in a new build or design, those parameters could be slightly different. In this section, we will discuss how much the output of the local model changes with small expected changes in the input parameters.

There are three types of components in this dissertation's local model formula: PBGA, CBGA, and CSP component (see Table5.7-Table5.9). The PBGA formula is used in this section to calculate the local critical solder joint stress S . The uncertainty issue is also relevant to the CBGA and CSP components. The results for the CBGA and CSP components are shown in the Appendix C and found to be similar to the PBGA component.

The first step in the discussion of critical solder joint stress S is to setup the nominal parameters and values. Table5.10 lists the input nominal parameters and values, which include the geometries and material properties and also show the realistic variations. This table is identical to Table4.18 with the addition of solder ball diameter in this table and the elimination of the gap size from Table4.18. The parameter values and standard deviations were previously explained for Table4.18 and will not be repeated here.

Table5.10: Nominal Values (PBGA) for Uncertainty Issue in Local Model

	Nominal Value (Mean Value)	***Standard Deviation***
Component length [mm]	17.78	0.001
Ball Diameter [mm]	0.76	0.002
PWB thickness [mm]	1.57	0.002
Component thickness [mm]	0.81	0.001
PWB Young's modulus [N/mm^2]	18200	0.01
Component Young's modulus [N/mm^2]	15200	0.01
PWB Poisson ratio	0.19	0.008
Component Poisson ratio	0.21	0.008

As was done in section 4.4.2, a Monte Carlo simulation was conducted using the developed formula for the critical solder joint stress S, assuming each of the input parameters having a normal distribution. Figure5.14 shows a histogram from such a simulation including all trials. As before, due to the normal distribution assumption it is not surprising to find outlier points that skew the histogram. Figure5.15 is the same histogram using only the central 95% of the trial values for S.

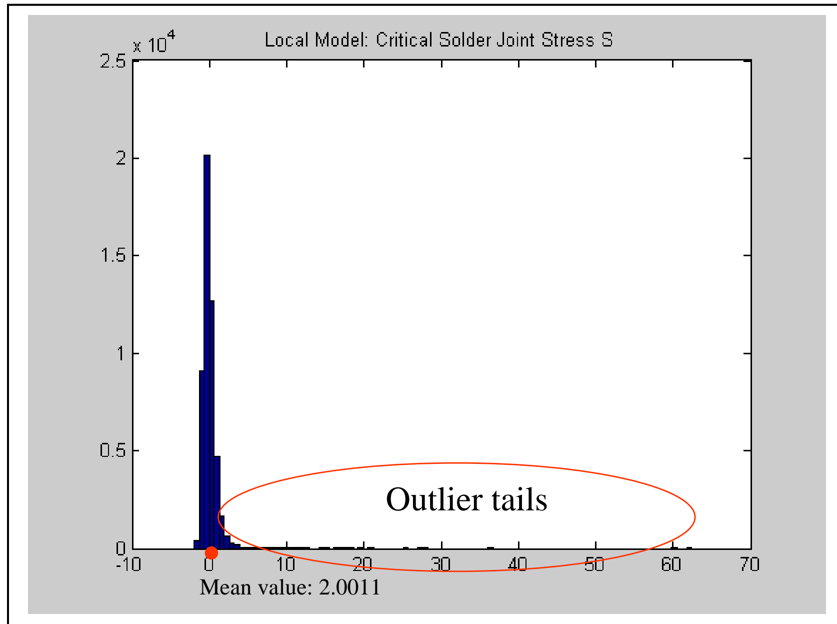

Figure5.14: Histogram of Monte Carlo Simulation for the Critical Solder Joint Stress S

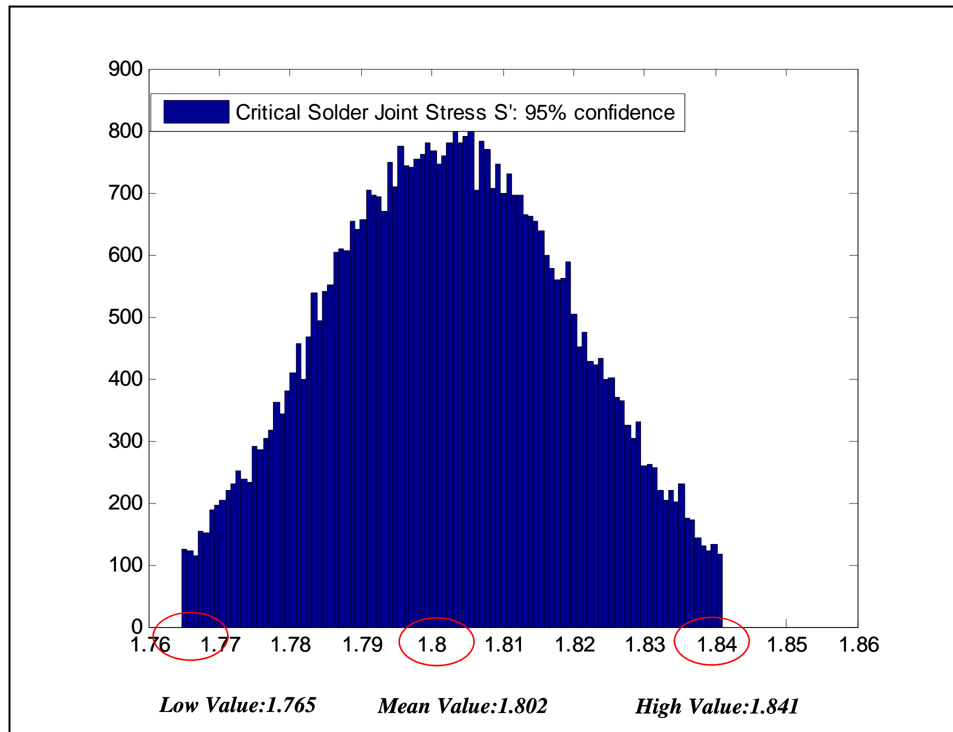

Figure5.15: Histogram of Monte Carlo Simulation for Critical Solder Joint Stress S using central 95% of Data

Table5.11 compares the value of S calculated using the nominal values of the input parameters and the mean value from the Monte Carlo simulation using the central 95% of values (95% of data). Even though it is understood that the Monte Carlo simulation distribution is not a normal distribution, the mean value is very close to the value calculated by using only nominal values.

Table5.11: Comparison the particular nominal value and Monte Carlo simulation random variables for the critical solder joint stress S

	Critical solder joint stress S	% Difference
Particular Nominal Value	1.803	0.1
Monte Carlo Simulation Value	1.802	

The important thing is the range in the S values from the Monte Carlo simulation. Table5.12 lists the low and high value for S using an 80% of data and a 95% of data. Note that critical solder joint stress S does not vary by much. This is also seen in Figure5.15 that the distribution is relatively narrow.

Table5.12: The 80% and 95% of data Range in the Local Solder Joint Stress, S

Nominal value=1.914	80% of data	95% of data	% Different
Low value	1.778	1.765	0.73
High value	1.827	1.841	-0.77

Conclusion: Uncertainty Analysis for the Critical Solder Joint Stress S

In Table5.13, the range of the critical solder joint stress S is shown as well as the percent difference from the mean or nominal value. Ultimately we are interested in life

assessment. Considering only the stress generated from the local model, the power law fatigue life model shows the effect on life for this small change in stress. The approximate 1 variation time the nominal value in stress implies approximately 1 variation difference in life. To follow what was done in section 4.3.1, and Table5.13. Table5.14 shows the results for a 5% standard deviation in the material properties. Note that the certainty in the local model is much less than the uncertainty exhibited by the global model as shown in Table5.13 and Table5.14.

Table5.13: 1% of Material Properties of the Standard deviation in the Local Model Solder Joint Stress S

	S	$\frac{X}{X_{nominal}}$ ratio	Life Cycle to Failure	$\frac{N}{N_{nominal}}$ ratio
Low value	1.765	1	22,912,580	0.8
Nominal value	1.802		26,166,069	
High value	1.841	1	30,009,039	1.1

Table5.14: 5% of Material Properties of the Standard deviation in the Local Model Solder Joint Stress S

	S	$\frac{X}{X_{nominal}}$ ratio	Life Cycle to Failure	$\frac{N}{N_{nominal}}$ ratio
Low value	1.767	1.94	23,079,254	1
Nominal value	1.802		26,166,069	
High value	1.838	-2	29,697,445	1

5.4 Summary

This research is an attempt to move in a direction to improve the current *CALCE* model by breaking up the current empirical model into a stress analysis, which then feeds into a

classic fatigue damage model. By breaking up the current model into a stress analysis and a damage analysis, one can more directly investigate and predict the influence of new component families and new materials. Ultimately a new finite element program was written by the *CALCE* software staff, *CALCE_FEA*. This software is a simple FEA program with very coarse mesh density that can be used to determine the location and value of the maximum solder joint stress. A series of parametric studies with ANSYS determined that this simple software was accurate enough for our modeling.

Similar to the global modeling effort DOE and ANOVA techniques were used to determine the critical geometric and material parameters that influence the critical solder joint stress. Using response surface techniques a functional relationship for the critical stress was determined. This final functional relationship is necessary for complete software automation so that the component life can be calculated. The robustness of the final functional relationship for the critical stress was examined assuming that the input parameters could be expressed as random variables with a normal distribution. It was found that the local stress analysis model is much more robust than the global model, yet for best accuracy the material properties and particularly the young's modulus were identified being critical.

Chapter 6: Damage Model

The rapid assessment approach in this dissertation uses a global model to analyze the dynamic response of a PWB assembly to a prescribed acceleration PSD. The key output of the global model is the root mean square curvature K_{rms} of the PWB in the vicinity of the BGA component of interest. The curvature information is used as a boundary loading condition for a local stress model that determines stresses in the critical solder ball of the component. The stresses of interest are the root mean square stresses because they are directly proportional to the curvature due to the simple elastic relation. The local model calculates the actual stresses; but the effective stress or Von Mises stress is used as an input to a solder fatigue damage model for calculating life.

Section 6.1 of this chapter briefly reviews the Basquin high cycle fatigue power law model and provides some limitations and reasons for choosing this model. Section 6.2 reviews the linear damage superposition assumption. Section 6.3 starts to discuss the uncertainties in the final life calculations caused by the uncertainties of the material fatigue constants. This uncertainty discussion continues in Chapter 7, where it is presented with the data analysis from vibration experiments.

6.1 Basquin High Cycle Fatigue Power Law Model

Once the critical solder ball stress has been determined, a damage model is required to calculate the fatigue life. The expected life of a solder ball in a random vibration environment easily exceeds 100,000 cycles. For perspective purposes, a typical PWB natural frequency is on the order of 100 Hz; therefore, 100,000 cycles will be reached in 1,000 seconds or less than 17 minutes. Thus the fatigue failure will be in the region known as High Cycle Fatigue. High cycle fatigue is driven by elastic stresses.

The goal of this research is not to develop a new fatigue damage model, but to use the simple Basquin power law relation for high cycle fatigue damage simulations. Basquin power law model is a very simple model; and yet it has been well accepted in the fatigue community as a simple law that captures the primary features of high cycle fatigue. The power law states:

$$\sigma^b \cdot N = C \qquad \text{Equation6.1}$$

where σ is the critical solder joint stress, N is the total number of cycles to failure, b is the fatigue exponent, and C is a constant. Both b and C are considered to be material constants. Commonly high cycle fatigue data is presented on a $S-N$ diagram, which is simply a plot of the stress amplitude (S) versus the number of cycles to failure (N). A power law plots as a straight line in a log-log space. The Basquin power law is often plotted or visualized as a straight line on a log-log plot of a $S-N$ diagram. Figure6.1 is

such a $S-N$ diagram and the slope of the straight line in the diagram is $-\frac{1}{b}$ as shown in the following equation:

$$\log\sigma = -\frac{1}{b}\log N + \log C \qquad \text{Equation6.2}$$

In this dissertation the solder fatigue exponent b will be assumed to have the value of 6.4. This value is basically a historical value [Steinberg, 1988] but it has been successfully used in *CALCE_PWA*. Various sources have reported or specified values for the fatigue exponent ranging from 4 to 6. Life uncertainties in terms of uncertainties in the fatigue exponent will be discussed later in this chapter.

The value for the fatigue constant C is not available or quoted in the literature. Most researchers do not bother to calculate the fatigue constant, but use the power law model in a form that compares two different load conditions as shown in Equation6.3:

$$\sigma_1^b N_1 = C = \sigma_2^b N_2$$

$$\left(\frac{\sigma_1}{\sigma_2}\right)^b = \frac{N_2}{N_1} \qquad \text{Equation6.3}$$

The underlying assumption in this dissertation is that the acceleration load G is directly proportional to the critical stress σ; thus Equation6.3 can be modified as:

$$\left(\frac{G_1}{G_2}\right)^b = \frac{N_2}{N_1} \qquad \text{Equation6.4}$$

If the failure time for a part during testing is known, then the failure time in the field can be determined using only the fatigue exponent b. A stress analysis is unnecessary when only the G level of loading is required. In this dissertation the solder material fatigue constant C will be calculated from some of the vibration experimental data.

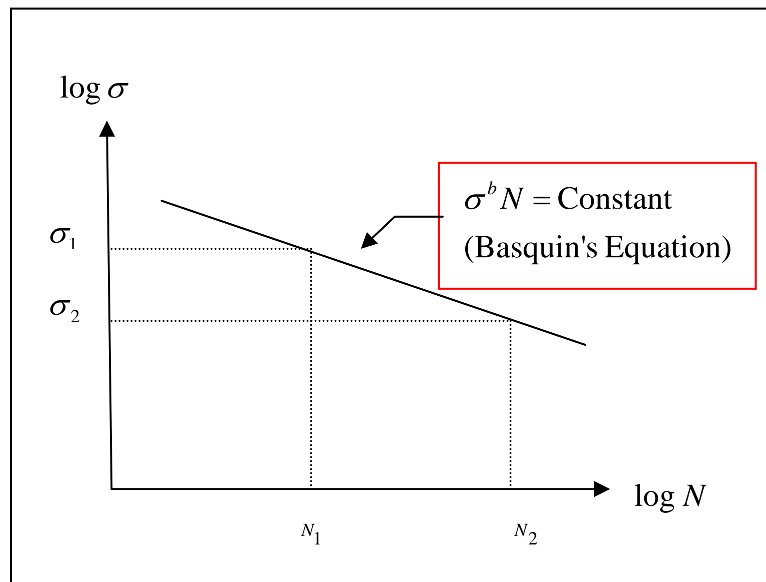

Figure6.1: $S-N$ Curves

6.2 *Accumulation of Fatigue Damage*

The Basquin power law fatigue damage model was originally formulated for constant stress amplitude loading. Therefore, a damage superposition technique needs to be used for random vibration loading. As discussed in section 3.2.3, this dissertation assumes

linear damage superposition and uses Miner's Rule assuming the random vibration amplitude distribution is Gaussian. By combining Equations 3.3, 3.4, and 6.1, the Damage Ratio can be written as:

$$Damage\ Ratio = \frac{t \cdot f_n \cdot (\sigma_{rms})^b}{C} \qquad \text{Equation6.5}$$

where σ_{rms} is the root mean square effective stress due to random vibration, t is the total vibration exposure time, f_n is the natural frequency of the PWB assembly, b is the solder material fatigue exponent, and C is a material constant.

Typically the linear damage superposition equation is not used in the above form, but used in a form where the time to failure, *t*, is the unknown:

$$t = \frac{Damage\ Ratio \cdot C}{f_n \cdot (\sigma_{rms})^b} \qquad \text{Equation6.6}$$

It is assumed that failure occurs when the damage ratio equals a certain constant. Typically one sets this constant equal to 1, which implies that different types of damage are truly linearly independent. The following section further explores this issue.

6.2.1 Critical Fatigue Damage Ratio

Suppose a body can tolerate only a certain amount of damage D. If that body experiences different types of damage D_i ($i = 1, ..., N$) from N sources, then we might expect that failure will occur if:

$$\sum_{i=1}^{N} D_i = D \qquad \text{Equation6.7}$$

or, equivalently

$$\sum_{i=1}^{N} \frac{D_i}{D} = 1 \qquad \text{Equation6.8}$$

where D_i/D is defined as the fractional damage received from the ith source.

When a component is subjected to n_1 cycles at stress σ_1, n_2 cycles at stress σ_2, and n_N cycles at stress σ_N, the linear damage concept can be used in a fatigue setting by allowing the fractional damage at stress level σ_i to be n_i/N_i. According to the Miner's rule, fatigue failure would occur when:

$$\sum_{i=1}^{N} \frac{n_i}{N} = 1 \qquad \text{Equation6.9}$$

When the damage ratios are all added together, a sum of 1.0 or greater means that all of the life has been used up and the structure would fail.

Many experiments were carried out to confirm Miner's rule. These experiments showed a significant scatter in the value of D at the instant of failure [Curtis, 1971; Gertel, 1976]. Miner [1945] specifies that the value of 1 is only an average. A book by Forrest [1974] summarizes multiple works that examine the scatter of $\sum \frac{n_i}{N}$. Even with its imperfections, Miner's rule remains the simplest, most general, and most used fatigue life model that gives life predictions with sufficient accuracy for many applications. Many authors consider that there is no rule more applicable than Miner's even though it sometimes produces coarse results. The Miner's hypothesis remains a good first approximation confirmed by experiments. The error depends not only on the rule itself, but also on the precision of the $S-N$ curve used. Finally, Miner's rule is widely used for the calculation of fatigue strength of mechanical structures and electronic equipment. Therefore, for simplicity and for generating predictions that are on average correct, we will assume failure occurs when the damage ratio is equal to 1.

6.3 Summary

The local model of a particular component will have enough resolution to determine the critical location and the value of stresses in the solder joint. Once the critical solder ball stress has been determined, a damage model is required to calculate the fatigue life. The goal of this research is to use the existing Basquin high cycle fatigue power law relation for calculating fatigue life of a BGA component. We will assume a value for b and use the calculated value of the material constant, C from EMMA experimental data. A simple linear damage superposition technique will be used to calculate the total time a component will last in a random vibration environment. The next chapter will discuss the case studies for EMMA and JGPP using all the steps of the rapid assessment approach.

Chapter 7: Case Study

In this chapter, the developed rapid assessment approach is applied to two real cases with well characterized experimental data; the Electric Miniaturization for Missile Applications (EMMA) [Ferdie, Shah, 2000] and Joint Group on Pollution Prevention (JGPP) [J-01-EM-026-P1, 2003]. In both cases, we will focus on the BGA type components including Plastic Ball Grid Array (PBGA), Ceramics Ball Grid Array (CBGA) and Chip Scale Package (CSP) components. Only the data for the eutectic PbSn solder will be used, the Pb free solder data will be ignored for now in both projects. Complete approaches as described in the previous chapters—Chapter 4, Chapter 5 and Chapter 6, will be discussed in a step-by-step manner here starting with global modeling, moving to local modeling and finally to the fatigue life prediction. Predicted life cycles for our rapid assessment methodology from EMMA project in the section 7.1 and JGPP project in the section 7.2 will then be compared with the experimental results.

For the fatigue life prediction, it should be noted that some of the experimental data from the EMMA project is used to determine the material constant C in the basic Basquin fatigue life power law equation. Thus the agreement between the predicted and measured experimented life are expected to be good for the EMMA data. Once the material constant C has been determined, it is then used with the JGPP experimental data. Since C is theoretically a material property, the JGPP experimental data should be a good test of the developed approach.

Finally, the goal in this chapter is to demonstrate that the rapid assessment methodology is easy to use, rapid, and better accurate than the existing *CALCE_PWA* rapid assessment model for fatigue life assessment of BGA solder joints under vibration loading.

7.1 Case Study 1: EMMA Project

The EMMA project has been widely referenced by researchers and engineers in the field of electronic packaging (Ferdie, 2000). This project documents the vibration testing of circuit boards that was performed under the EMMA program. These circuit boards were populated with daisy chained, Ball Grid Array (BGA), Chip Scale Package (CSP), and Direct Chip Attach (DCA) components as seen in Figure7.1. The fatigue characteristics as a function of component type, board construction and manufacturing processes, and vibration level were determined in the study. The program originally evaluated various empirical correlations that were available to predict component field fatigue life and to provide general design guidelines for the use of area array packages in high vibration environments. In the following subsections, a step-by-step application of the rapid assessment methodology will be presented in detail using the geometry and material information of the test boards as presented in the EMMA project.

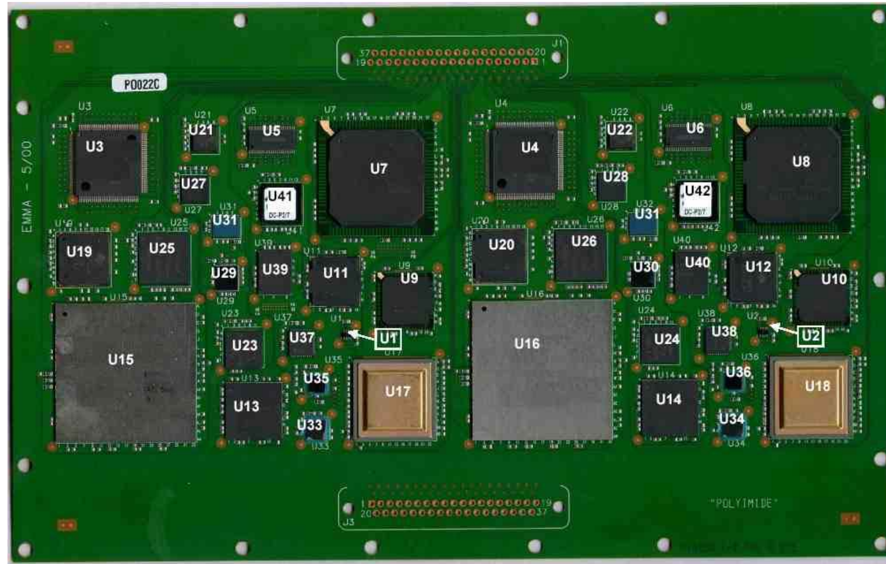

Figure7.1: EMMA test Board

7.1.1 Case Study 1: EMMA—Global Model

In the global model approach (Chapter 4), the vibration response of the PWB is determined. This global model gives us the response of the PWB at specific component locations of interest. Detailed discussions on each step of the global and local modeling processes have been described in Chapter 4 & 5. Table7.1- Table7.3 gives the geometric and material properties for the PBGA, CBGA, and CSP components. The results calculated from the global model are shown in Table7.4-Table7.6 and the local model results are shown in Table7.7-Table7.9.

The final functional relationship that were developed in Chapter 4 for the correction factor C in the global model is shown again in Table7.4-Table7.6 for the three different types of BGA components, CBGA, PBGA, and CSP, where the ratio C ,

$C = f\left(\frac{component\ lengh}{gap\ size}, D_{ratio} = \frac{D_{component}}{D_{pwb}}\right)$, is a function of geometry and material properties. The two critical factors in the global model are the $\frac{component\ length}{gap\ size}$, $D_{ratio} = \frac{D_{component}}{D_{pwb}}$.

Table7.1: PBGA 580 Geometry and Material Properties

U7/U8 PBGA_580	***PCB***	***Ball***	***BT***	***Die***	***Overmold***	
E (MPa)	18200	32000	19000	130000	15100	
h (mm)	1.57		1.200	0.450	0.750	
poission ratio	0.19	0.4	0.195	0.278	0.3	
L (length,mm)	100		30.990		30.990	
				13.460	17.530	
Diameter		0.635				
Pitch Size		1.27				
A (area, mm^2)	1.5700E+02		37.188	6.057	31.131	
A_total (bt, die, overmold)						74.38
D	6089.156258		2844.14	1069.87144	583.361950	
D_component (bt, die, overmold)						1753.38
D_component/ D_pcb	0.28795					

Table7.2: CBGA 256 Geometry and Material Properties

U9/U10 PBGA_256	***PCB***	***Ball***	***BT***	***Die***	***Overmold***	
E (MPa)	18200	32000	19000	130000	15100	
h (mm)	1.57		0.360	0.300	0.550	
poission ratio	0.19	0.4	0.195	0.278	0.25	
L (length,mm)	100		20.830		20.830	
				8.380	12.450	
Diameter		0.50				
Pitch Size		1.00				
A (area, mm^2)	1.5700E+02		7.499	2.514	15.192	
A_total (bt,die,overmold)						25.20
D	6089.1562		2844.148	1069.87144	583.361950	
D_component (bt,die,overmold)						1304.52
D_component/ D_pcb	0.21424					

Table7.3: CSP BGA64 Geometry and Material Properties

CSP_ PBGA_64	PCB	Ball	BT	Die	Overmold	
E (MPa)	18200	32000	19000	130000	15500	
h (mm)	1.57		0.340	0.500	0.700	
poission ratio	0.3	0.4	0.2	0.28	0.25	
L (length,mm)	60		8.000		8.000	
				6.400	1.600	
Diameter		0.50				
Pitch Size		1.00				
A (area, mm^2)	9.4200E+0		2.720	3.2000	6.4000E+00	
A_total (bt,die,overmold)						1.23E+0
D	6089.1562		239.9957	374.90324	64.2857142	
D_component (bt,die,overmold)						183.759
D_component/ D_pcb	0.0301780					

Table7.4: Functional Relationship in Correction Factor: *C* for the CBGA

Final Equation in Terms of Actual Factors:	Global Model: *C*
Sqrt (CBGA Stress Ratio)	=
0.802092384	
0.130623619	* Component length/Gap size
-8.76086E-05	* D ratio
-7.8114E-06	* Component length/Gap size * D ratio
-0.001443644	* Component length/Gap size^2
1.7574E-08	* D ratio^2
-4.51852E-08	* Component length/Gap size^2 * D ratio
1.44384E-09	* Component length/Gap size * D ratio^2

Table7.5: Functional Relationship in Correction Factor: *C* for the PBGA

Final Equation in Terms of Actual Factors:	Global Model: *C*
1.0/Sqrt (PBGA Von Mises Stress)	=
-0.017483805	
29.70607565	* Ball Diameter/PCB Length
0.082097493	* D_ratio
-45.61270524	* Ball Diameter/PCB Length * D_ratio
-1104.825999	* Ball Diameter/PCB Length^2
-0.036898518	* D_ratio^2
765.3569837	* Ball Diameter/PCB Length^2 * D_ratio
134.7674615	* Ball Diameter/PCB Length * D_ratio^2

Table7.6: Functional Relationship in Correction Factor: C for the CSP

Final Equation in Terms of Actual Factors:	Global Model: C
Sqrt (CSP Stress Ratio)	=
0.918370774	
0.148282135	* Component length/Gap size
0.061756317	* D ratio
0.028451323	* Component length/Gap size * D ratio
-0.003209973	* Component length/Gap size^2
0.211650244	.* D ratio^2
0.002477085	.* Component length/Gap size^2 * D ratio
-0.311009683	.* Component length/Gap size * D ratio^2

The local model functional relationship for S, which can be used to determine the critical stress in the critical solder joint as $S = \frac{\sigma_{rms}}{M}$, is shown again in Table7.7-Table7.9 for the three different types of the components. The critical factors in local model are the $\left(\frac{ball\ diameter}{pwb\ length}, D_{ratio} \right)$.

Table7.7: Functional Relationship in Critical Solder Joint *S* for the PBGA

Final Equation in Terms of Actual Factors:	Local Model *S*
1.0/Sqrt (PBGA Von Mises Stress)	=
-0.017483805	
29.70607565	* Ball Diameter/PCB Length
0.082097493	* D_ratio
-45.61270524	* Ball Diameter/PCB Length * D_ratio
-1104.825999	* Ball Diameter/PCB Length^2
-0.036898518	* D_ratio^2
765.3569837	* Ball Diameter/PCB Length^2 * D_ratio
134.7674615	* Ball Diameter/PCB Length * D_ratio^2

Table7.8: Functional Relationship in Critical Solder Joint *S* for the CBGA

Final Equation in Terms of Actual Factors: *S*	Local Model
1.0/(CBGA Von Mises Stress Ratio)	=
-0.013838513	
3.678244861	* Ball Diameter/PCB Length
0.037535522	* D_ratio
-5.971462924	* Ball Diameter/PCB Length * D_ratio
4.66697384	* Ball Diameter/PCB Length^2
-0.0363092	* D_ratio^2
39.90020585	* Ball Diameter/PCB Length^2 * D_ratio
5.729361585	* Ball Diameter/PCB Length * D_ratio^2

Table7.9: Functional Relationship in Critical Solder Joint S for the CSP

Final Equation in Terms of Actual Factors: S	Local Model,
1.0/Sqrt (CSP Von Mises Stress)	=
0.000813862	
23.20142168	* Ball Diameter/PCB Length
0.00526788	* D_ratio
-5.440044411	* Ball Diameter/PCB Length * D_ratio
-649.2855275	* Ball Diameter/PCB Length^2
-0.028317082	* D_ratio^2
270.8558078	* Ball Diameter/PCB Length^2 .* D_ratio
19.8857439	* Ball Diameter/PCB Length .* D_ratio^2

Table7.10-Table7.12 shows how the curvature determined from *CALCE_PWA* is modified by the correction factor C to arrive at the final actual curvature: $K_{Actual} = C \cdot K_{CALCE_PWA}$. Table7.10 presents the two different PBGA components mounted on the EMMA assembly PWB. These use different I/O counts and different locations. Each represents the PBGA_580 and PBGA_256, which can be seen in Table7.10. The results for selected CBGA and CSP packages are shown in Table7.11and Table7.12 respectively.

Table7.10: Functional relationship C for PBGA

	CALCE_PWA	***Correction Factor***	***Actual Curvature***
Component	***Kxx (1/mm)***	***C***	***K (1/mm)***
U7 PBGA_580	0.0000264	2.68441	0.00007087
U9 PBGA_256	0.0000341	2.19257	0.00007468

Table7.11: Functional relationship C for CBGA

	CALCE_PWA	***Correction Factor***	***Actual Curvature***
Component	***Kxx (1/mm)***	***C***	***K (1/mm)***
CBGA _225	0.0000264	2.68441	0.00007087
CBGA_381	0.0000341	2.19257	0.00007468

Table7.12: Functional relationship C for CSP

	CALCE_PWA	***Correction Factor***	***Actual Curvature***
Component	***Kxx (1/mm)***	***C***	***K (1/mm)***
U19/U20 FlexCSP_257	0.0000388	2.16054	0.00008372
U23 WBCSP-128	0.0000269	1.24374	0.00003346
U25/U26 WBCSP_256	0.0000324	1.47332	0.00004769
U27 FC CSP-64	0.0000255	1.79744	0.0000458
U29 WFR CSP-98	0.0000276	1.40972	0.00003895
U31 WFR CSP-46	0.0000276	1.19977	0.00003316
U39 CSP BGA-64	0.0000288	1.26908	0.0000366
U41 RCCSP-150	0.0000237	1.44877	0.00003434

7.1.2 Case Study 1: EMMA Project Calculation of Bending Moment

The global model gives the boundary condition loading, M for a local detailed stress analysis. The final functional relationship as developed in section 5.2 for local modeling was tabulated in Table7.4-Table7.6. The critical solder joint stress can now be calculated. The calculated results are listed in Table7.13-Table7.15.

Table7.13: Critical Solder Joint Stress for PBGA in Functional Relationship S

Vibration Level	***Moment***	***RMS***
Component ID	(N*mm)	Von Mises Stress
U7 PBGA_580	0.432	2.128
U9 PBGA_256	0.455	2.826

Table7.14: Critical Solder Joint Stress for CBGA in functional relationship S

Vibration Level	***Moment***	***RMS***
Component ID	(N*mm)	Von Mises Stress
CBGA_361	0.798	1.308
CBGA_1089	0.233	0.566

Table7.15: Critical Solder Joint Stress for CSP in functional relationship S

Vibration Level	***Moment***	***RMS***
Component ID	(N*mm)	Von Mises Stress
U19/U20 FlexCSP_257	0.50979	1.502194311
U23 WBCSP-128	0.20372	0.684352792
U25/U26 WBCSP_256	0.29040	0.864611622
U27 FC CSP-64	0.27888	1.085023661
U29 WFR CSP-98	0.23718	0.920740649
U31 WFR CSP-46	0.20193	0.777552697
U39 CSP BGA-64	0.22287	0.661747704
U41 RCCSP-150	0.20908	0.619673334

7.1.3 Case study 1: EMMA—Damage Model

Once the critical stress in the local component of interest is found, a damage model can be used to calculate the life. The Basquin Power Law relation for high cycle fatigue is used in our case. As discussed in chapter 3 and chapter 6, the Basquin Power Law relation for high cycle fatigue can be expressed as:

$$Damage\ Ratio = \frac{t \cdot f_n \cdot (\sigma_{rms})^b * 21.68}{C} \qquad \text{Equation7.1}$$

where we assume failure when the $Damage\ Ratio = 1$. Knowing the critical solder joint stress σ_{rms}, natural frequency of the PWB, f_n and the material fatigue constant C and

exponent b, one can calculate the fatigue life or time to failure t (cycles to failure = $t \cdot f_n$).

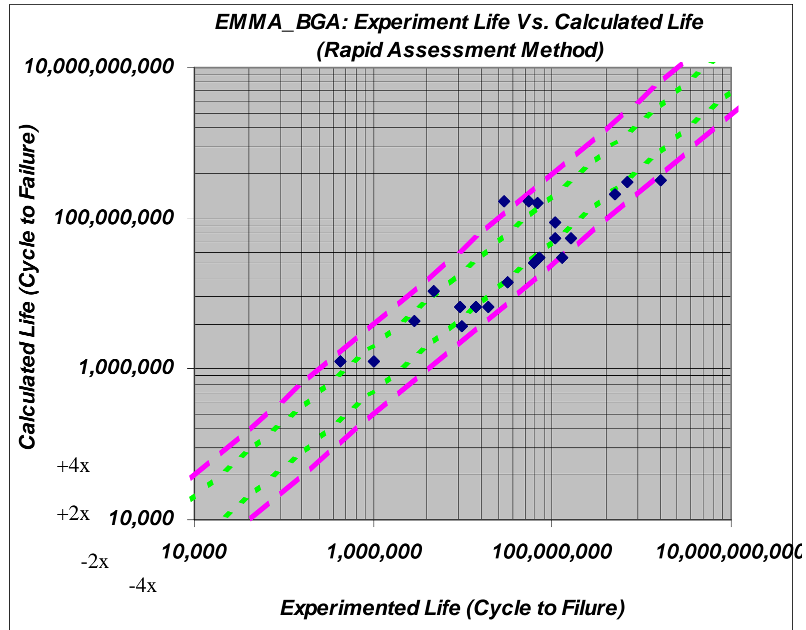

Figure7.2: EMMA Report: Rapid Assessment Model for Experiment Life Vs. Calculated Life

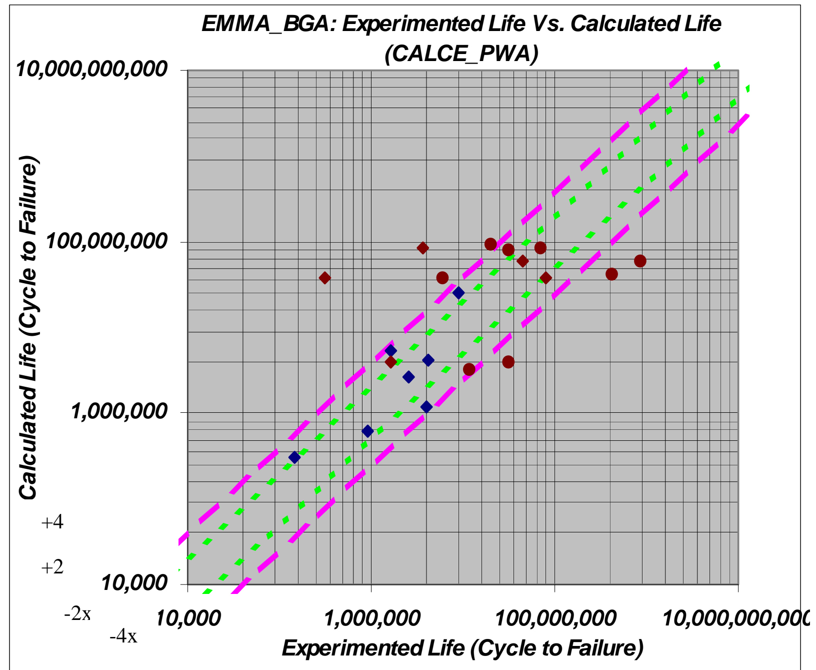

Figure7.3: EMMA Report: *CALCE_PWA* Model for Experiment Life Vs. Calculated Life

Figure7.2 and Figure7.3 compare the predicted cycles to failure to the experimentally measured time to failure for the new rapid assessment model and the existing *CALCE_PWA* model. The horizontal axis is the measured experimented life, and the vertical axis is the predicted life. Figure7.2 shows our rapid assessment predicted life while Figure7.3 shows the results from the current *CALCE_PWA* software. If the predicted life agrees exactly with the experiment life, everything would lie on a straight line with slope equal to 1. Errors can occur during either the vibration testing, vibration life assessment or modeling. When dealing with fatigue, one must be aware of natural scatter in any fatigue data. In addition to the natural scatter due to fatigue, one must be also conscious of potential biasing problems due to the test setup. Equally one must be aware of potential problems with the vibration simulation including issues with geometric, or material detail input information, and characterization of the vibration environment itself. The error bands of +2x, -2x, +4x, and –4x are also plotted in these figures to help gage the accuracy of the results.

In these two plots, each data point corresponds to a particular style or family of BGA and CSP type packages. For the experimental data there are 21 components comprising each particular style. These 21 failures were used to determine the two-parameter Weibull failure distribution and from this the mean value was calculated. These 21 failures are show in the figure as a single data point indicating the mean value of the experimental results. For the calculated life, when we input loading, geometry, and material properties we get a single data point. We assume that this value represents a median time to failure.

Looking only at these median times to failure, the predicted times to failure using the new rapid assessment approach in Figure7.2 shows a tighter grouping about the exact fit line than the predicted lives from the *CALCE_PWA* software in Figure7.3. Thus we can say that the rapid assessment model developed in this dissertation appears to be more accurate than the *CALCE_PWA* model.

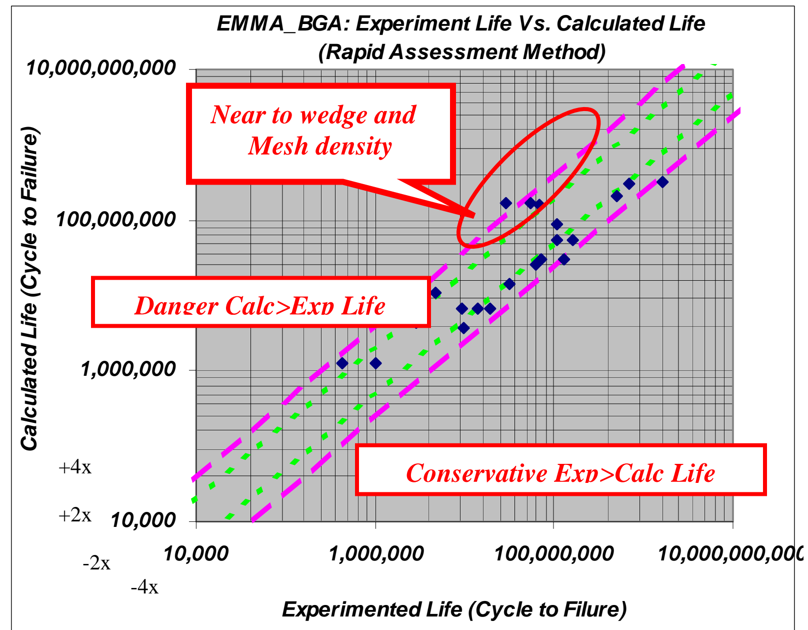

Figure7.4: EMMA Report: Rapid Assessment Model for Experiment Life Vs. Calculated Life

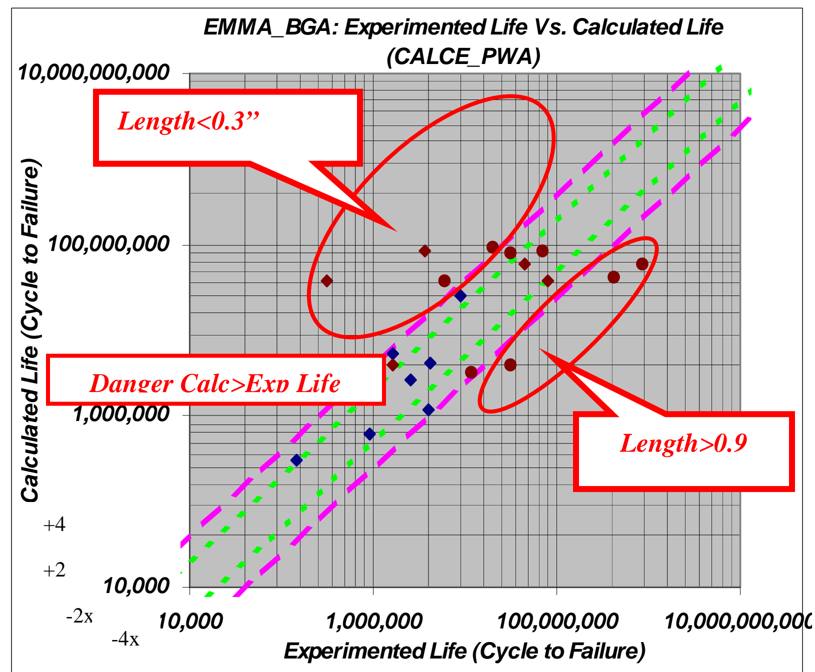

Figure7.5: EMMA Report: *CALCE_PWA* Model for Experiment Life Vs. Calculated Life

One can see that there is a single data point within the one or two different circles shown in Figure7.4 and Figure7.5. The results in Figure7.5 were calculated using the empirical model in the existing *CALCE_PWA* software. The major shortcoming of this empirical model is that it requires tweaking the calibration constant for component family type, as well as the component size. This model does seem to capture the load influence, but it does not capture the component style and size as well as it should. These two circles imply that the *CALCE_PWA* does not account for component lengths less than 0.3" or greater than 0.9". Contrary to Figure7.5, the rapid assessment model developed in this dissertation calculates an actual stress in the critical solder joint and considers all package geometry and material details and the results are shown in Figure7.4. This rapid assessment approach conducts an actual stress analysis, where the empirical model only considers package size and style. One can see that in Figure7.4, there is only one single data point that appears to be an "outlier". Re-examination of this component determined that the component was located very near the PWB edge. Due to the course meshing in *CALCE_PWA*, the curvature calculation in this area is not as accurate as it should be. We need an accurate curvature from *CALCE_PWA* to input into our model.

7.2 Case Study 2: JGPP Project

In the case study 2, vibration test data information will be used from the JGPP project to demonstrate the rapid assessment methodology developed in this dissertation. In the JGPP as shown in Figure7.6, vibration testing was conducted by Boeing Phantom Works for the JGPP. Only the results of SnPb balls assembled with SnPb paste are used.

7.2.1 Case Study 2: JGPP—Global Model

The objective of the JGPP project was to determine the effects of high vibration environments on the relative reliability of lead-free and lead solder joint [J-01-EM-026-P1, 2003]. Modal data and strain data were also collected during this project in an effort to provide data that would be useful to those that may want to try to model the behavior of the JGPP/JCAA test vehicle. After completion of the modal analysis, thirty test vehicles were subjected to the vibration test conditions. The input PSD was increased during the test at 60 minutes intervals in an effort to fail as many components as possible within the time allotted for the test.

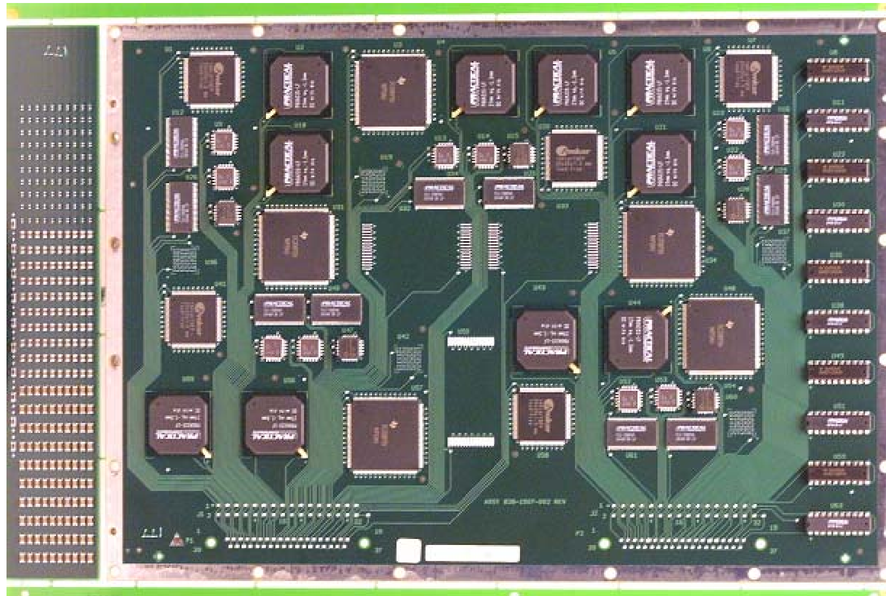

Figure7.6: JGPP Assembly Vibration Completed Test Vehicle

Table7.16 lists typical material properties and geometry for PBGA 225 component in JGPP project. In the JGPP report it is very important to understand that during vibration testing, the vibration environment at a given location on a test vehicle can be very different from the vibration environment at a different location on the same vehicle during the same test. This means that only identical components in identical locations on identical test vehicles can be directly compared. It also implies that the test solder must be used on one set of test vehicles and the control solder on a second set of test vehicles [Woodrow, 2005].

Table7.16: PBGA 225 Material Properties and Geometry in JGPP

PBGA_225 (15*15)	PCB	Ball	BT	Die	Overmold	
E (MPa)	17200	32000	15200	130000	15900	
h (mm)	2.362		1.650	0.600	1.000	
poission ratio	0.3		0.195	0.278	0.25	
L (length,mm)	100		22.500		22.500	
				13.460	9.040	
Diameter		0.750				
Pitch Size		1.50				
A (area, mm^2)	236.20		37.125	8.076	27.924	
A_total (bt,die,overmold)						73.13
D	20756.08729		5914.940617	2535.991573	1413.333333	
D_component (bt,die,overmold)						3822.752
D_component/ D_pcb	0.18417					

In JGPP, there are a total of seven vibration test levels, which involve $9.9\,G_{rms}$, $12\,G_{rms}$, $14\,G_{rms}$, $16\,G_{rms}$, $18\,G_{rms}$, $20\,G_{rms}$, and $28\,G_{rms}$ as shown in Table7.17 (more tables are shown in the appendix B).

Table7.17: JGPP Correction Parameter ***C*** for Global Model

JGPP: Vibration Level_1 (9.9 Grms)	***CALCE_PWA***	***Correction parameter***	***Actual Curvature***
Component	***Kxx (1/mm)***	***C:***	***K (1/mm)***
U2	0.0000924	**1.32780**	0.00012268
U4	0.0001265	**1.36349**	0.00017248
U5	0.0001344	**1.16130**	0.00015608
U6	0.0000960	**1.45034**	0.00013917
U18	0.0000928	**1.24204**	0.00011530
U21	0.0000878	**1.29603**	0.00011384
U43	0.0001080	**1.17882**	0.00012731
U44	0.0000822	**1.96377**	0.00016142
U55	0.0000346	**1.17885**	0.00004080
U56	0.0000435	**1.08097**	0.00004699

In this report, using these seven vibration test levels we will focus only on the BGA components. As Figure7.6 shows, there are a total of 10 identical PBGA components mounted on the PWB at different locations. We use the rapid assessment methodology to determine the transformation parameter $K_{Actual} = C \cdot K_{CALCE_PWA}$ shown in Table7.17. Once the transformation parameter is calculated, the next step will be to calculate the curvature of the PWB in the region of the component of interest. Note: the curvature K_{rms} is directly proportional to the M .

7.2.2 Case Study 2: JGPP—Local Model

The global model gives us the curvature that is then fed into the local stress analysis model. Table7.18 shows the critical solder joint stress results (more tables are included in the appendix B). Note: the curvature K_{rms} is proportional to the σ_{rms} .

Table7.18: Critical Solder Joint Stress for PBGA in *CALCE_FEA*

JGPP: Vibration Level_1 (9.9 Grms)	***Moment (N*mm)***	***Rapid Assessment Method***
Component	***M***	***: (Von Mises Stress)***
U2	2.546	1.078
U4	3.580	1.516
U5	3.240	1.372
U6	2.889	1.223
U18	2.393	1.013
U21	2.363	1.000
U43	2.643	1.119
U44	3.350	1.418
U55	0.847	0.359
U56	0.975	0.413

7.2.3 Case study 2: JGPP—Damage Model

Once the critical stress in the local component of interest is found, the damage model is used to calculate the life. Table7.19 (more tables are shown in the appendix B) shows the fatigue life calculated from the damage superposition due to the different σ_{rms} levels. For example, in Table7.19, one can see that t (time to failure) was caused by total 132 minutes under the different vibration levels. Remember in the JGPP experiments the vibration level was increased every 60 minutes. This value, 132 minutes, is calculated as the total time of exposure to random vibration:

$$D_{ratio} = \sum_{i=1}^{p} \frac{n_i}{N_i} = f_n \cdot t \cdot \sum_{i=1}^{p} \frac{\alpha_i}{N_i}$$ Equation7.2

$$\begin{aligned} D_{ratio} &= D_1 + D_2 + D_3 + \ldots\ldots \\ &= \frac{t_1 \cdot f_n \cdot 60(\sec) \cdot 21.68}{N_1} + \frac{t_2 \cdot f_n \cdot 60(\sec) \cdot 21.68}{N_2} + \ldots = 1 \end{aligned}$$ Equation7.3

There are a total of 10 PBGA 15*15 I/O components at different locations on the same test vehicles as shown in Table7.19 (more tables are shown in the appendix B).

Table7.19 uses the component name U2 as an example and lists the data for the eutectic SnPn solder. Seven vibration levels were used to estimate the fatigue life and 30 test vehicles were subjected to the vibration test conditions. The input PSD was increased during the test at 60-minute intervals in an effort to fail as many components as possible within the time allotted for the test. Table7.19 shows the seven vibration levels that were tested and the time to fail for each.

Table7.19: Damage Ratio for Time to Failure in JGPP

U2						
SnPb/SnPb	***Von Mises Stress (N/mm^2)***	***Constant***	***N (number of cycles)***	***t (min)***	***Miners Rule***	***Damage Ratio***
Vibration Level_1 (9.9 Grms)	1.680	977,171,616	35,317,621	60	0.160879874	1.008820296
Vibration Level_2 (12 Grms)	2.037	977,171,616	10,290,305	60	0.552159947	
Vibration Level_3 (14 Grms)	2.376	977,171,616	3,841,967	12	0.295780475	
Vibration Level_4 (16 Grms)	2.715	977,171,616	1,636,228			
Vibration Level_5 (18 Grms)	3.054	977,171,616	770,565			
Vibration Level_6 (20 Grms)	3.394	977,171,616	392,116			
Vibration Level_7 (28 Grms)	4.751	977,171,616	45,556			
Total time to failure				132		

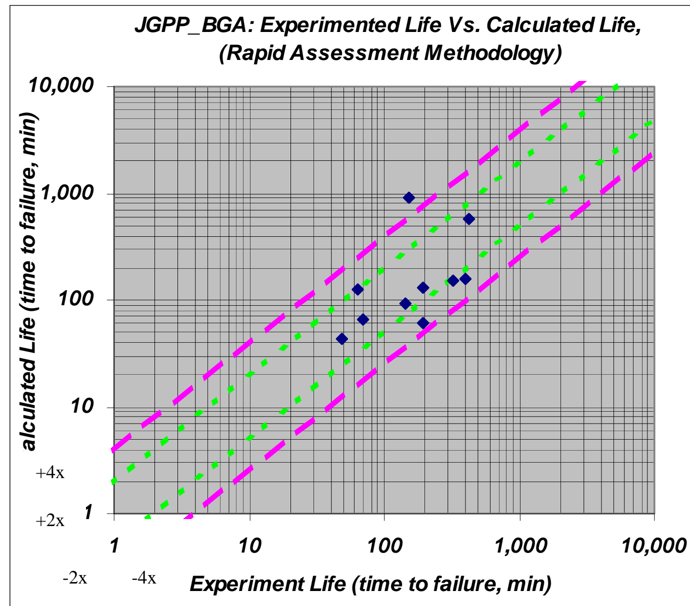

Figure7.7: JGPP Project's Rapid Assessment Methodology for Experimented Life Vs. Calculated Life

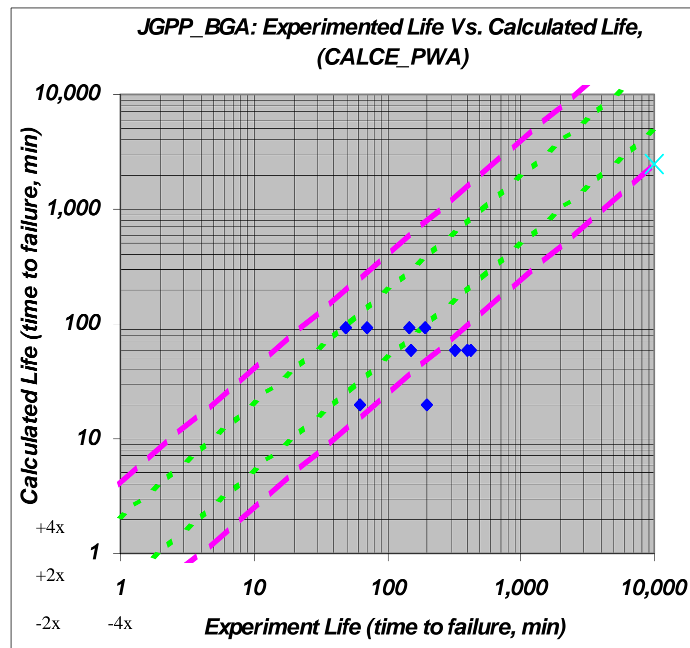

Figure7.8: JGPP Project's *CALCE_PWA* Model for Experiment Life Vs. Calculated Life

Figure7.7 shows our rapid assessment predicted life while Figure7.8 shows the results from the current *CALCE_PWA* software. In the plots the horizontal axis is the measured experimented life, and the vertical axis is the predicted life. Again, a perfect fit would lie upon the line with a slope of 1. As we discussed with the EMMA project, each data point corresponds to a particular location of the PBGA package. In the horizontal direction this single data point is the measured median time to failure, calculated from a two-parameter Weibull distribution of 10 replicate packages. In the vertical direction the single data point is the calculated life from our rapid assessment model using nominal loading, geometry, and material properties as input. This calculated value is assumed to be the median time to failure. Looking only at these median times to failure, the predicted times to failure using the new rapid assessment approach in Figure7.7 shows a tighter grouping about the exact fit line than the predicted lives from the *CALCE_PWA* software in Figure7.8.

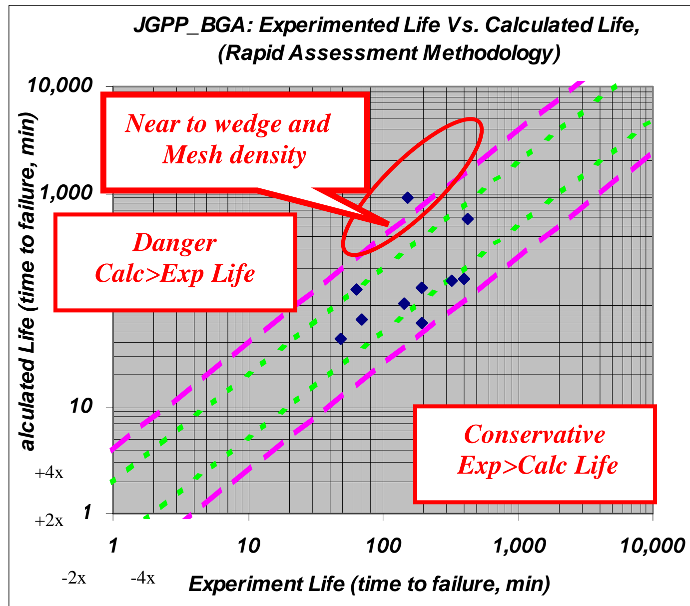

Figure7.9: JGPP's Rapid Assessment Model for Experiment Life Vs. Calculated Life

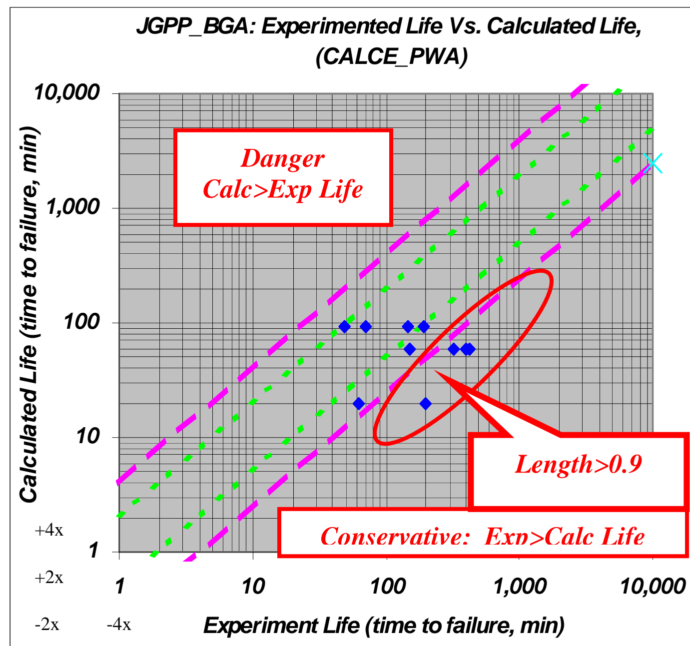

Figure7.10: JGPP Project's *CALCE_PWA* Model for Experiment Life vs. Calculated Life

This are three single data point “outlier” in Figure7.10 circled that implies the *CALCE_PWA* does not accurately account for the curvature in the region of component of interest. In Figure7.9, there is only one “outlier” data point, and again this component is located near the PWB’s edge. We do not expect the curvature as calculated by *CALCE_PWA* to be as accurate as it should be in the region and our rapid assessment model uses the *CALCE_PWA* curvature in the global model. These plots do not unquestionably show that the rapid assessment model developed in this dissertation is better than *CALCE_PWA*. One reason is the JGPP project test boards only had 10 PBGA components. This is not enough data to conclusively compare these two assessment models. The primary advantage of the developed rapid assessment model is that it is based solidly on a stress analysis followed by a damage assessment. This approach is much more receptive to new technologies and new package designs than the empirical model currently embedded in the *CALCE* software that requires experimentally derived calibration factors for it accuracy.

7.3 Uncertainty Issue Analysis in the Lifetime distribution

The previous section discussed the cycle to failure only in reference to a single measured and calculated data point for each package style of package location. The next section, 7.3.1, will discuss the failure distribution for the measured (experimental) life in terms of uncertainties. Similarly the predicted (calculated) life will be discussed in terms of uncertainties in section 7.3.2.

7.3.1 Uncertainty Analysis in the Measured (Experimented) Life

The theoretical population models used to describe unit lifetimes are known as Lifetime Distribution Models. A lifetime distribution model can be any probability density function (or PDF), $f(t)$ defined over the range of time from $t = 0$ to $t =$ infinity. The corresponding cumulative distribution function (or CDF), $F(t)$ is a very useful function. The 2-parameter Weibull distribution is an example of a popular $F(t)$ and is used in both the EMMA and JGPP projects to characterize the failures. The Weibull CDF and PDF equations are:

$$f(t) = \frac{\beta}{\lambda}\left(\frac{t}{\lambda}\right)^{(\beta-1)} e^{-\left(\frac{t}{\lambda}\right)^{\beta}} \qquad \text{Equation7.4}$$

$$F(t) = 1 - e^{-\left(\frac{t}{\lambda}\right)^{\beta}} \qquad \text{Equation7.5}$$

$$R(t) = 1 - F(t) = e^{-\left(\frac{t}{\lambda}\right)^{\beta}} \qquad \text{Equation7.6}$$

where β is the "shape" parameter and λ is a scale parameter called the characteristic life. The Reliability Function $R(t)$, also known as the Survival Function and is defined by: $R(t)$=the probability a unit survives beyond time *t*.

In the EMMA project, the number of cycles to failure was estimated by multiplying the first resonant frequency of the circuit board times the number of seconds of mechanical vibration until failure. The failure data was then analyzed in terms of a Weil bull distribution to estimate the relationship between number of cycles of mechanical vibration and the expected fraction of components that would fail. From Equation7.7 one can calculate the time it takes for 50% to fail.

$$R(t) = 0.5 = e^{-\left(\frac{t}{\lambda}\right)^{\beta}}$$
$$\text{In}(0.5) = -\left(\frac{t}{\lambda}\right)^{\beta}$$
$$\text{In}(2) = -\left(\frac{t}{\lambda}\right)^{\beta}$$
$$t = \lambda(\text{In}(2))^{\frac{1}{\beta}} = 5{,}431{,}363 \cdot (\text{In}(2))^{\frac{1}{2.3493}} = 4{,}636{,}840$$

Equation7.7

Where λ and β are determined from the EMMA project data.

To gain a better understanding of the range of failure times, one can calculate the time it takes for 5%, 50% and 95% to fail. All calculations are shown in the Appendix B. Figure7.11 shows measured time to fail (time for 5%, 50% and 95% to fail) versus the calculated time to fail using our rapid assessment model. This plot is a better plot in that is shows the distribution range as well as the median value for the experimental data and does not show the experimental data as a single point. 90% of the failure data will fall within the range shown in the plot. One must always appreciate and understand the amount of natural scatter in fatigue data. The choice to show the 90% range was

somewhat arbitrary. The appendix B shows the results for the 60% range (20% fail and 80% fail).

This plot shows the experimental data independent from the calculated data. The next section will show the range in the calculated time to failure, and finally in section 7.3.3 both ranges will be combined together in a single plot.

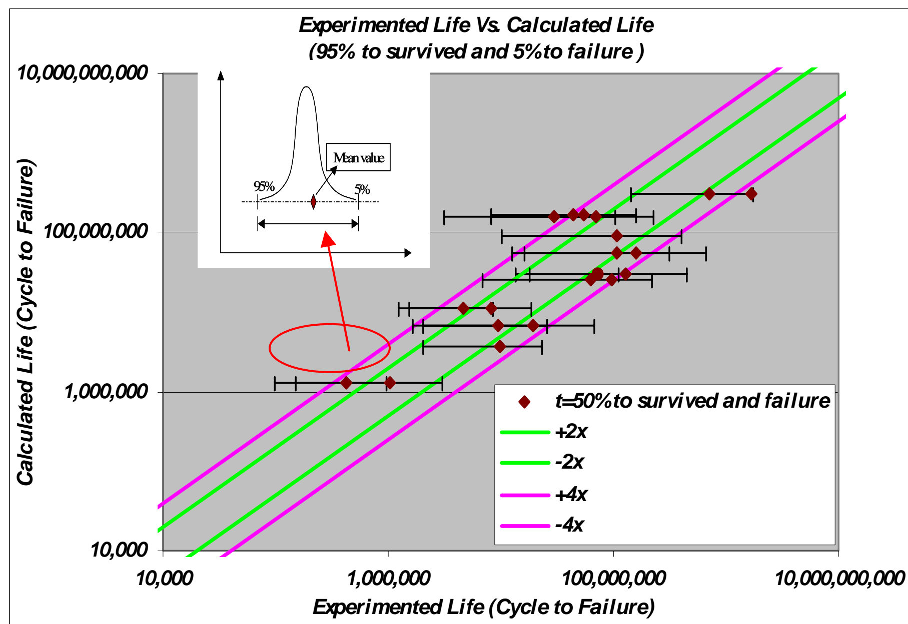

Figure7.11: Measured (Experimented) Life- Life Cycle in the Uncertainties Issue for 5%, 50% and 95% survive

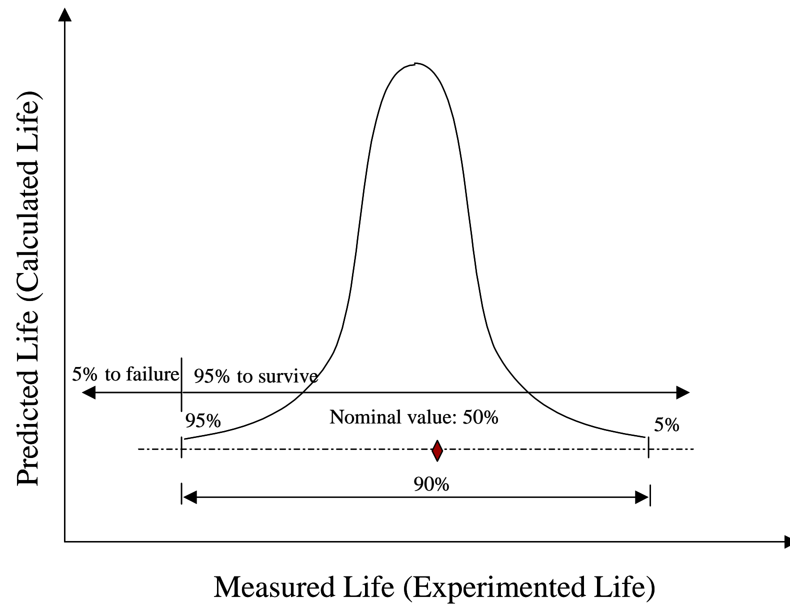

Figure7.12: Uncertainties Issue for 5%, 50% and 95% survive

7.3.2 Uncertainty Analysis in the Predicted (Calculated) Life

As discussed in section 4.2.3, regarding the global model uncertainties, one can calculate the correction factor C . Using the correction facto C , the actual curvature and then the bending moment is calculated. The bending moment is the loading condition for the local model. In section 5.3 on the local model uncertainties, one can see how the critical solder joint stress value S , affects the final life. Chapter 4 and chapter 5 treated the uncertainties independently, this is not completely correct because they are not independent. For example the modulus used in the global model is the same modulus used in the local model. One needs to use the same random variable and same trial selection of the random variable in the Monte Carlo simulation for the combined global and local model. This combined result will be discussed in this section.

From the Monte Carlo simulation with an assumed normal distribution on the input parameters, we have previously discussed the distribution and ranges in the global model correction factor C and the ranges in the local model critical solder joint factor S while holding the correction factor C constant. The Monte Carlo simulation results plotted in Figure7.13 recognize that the final critical stress is proportional to the correction factor C from the global model times the solder joint factor S from the local model. In the Monte Carlo simulation the same trial choice of the random input parameters were used for calculating C and S and then the product $C * S$. As we did before, the histogram in Figure7.13 contains 90% of the simulation results. The 5% of the data in the tails were clipped. This particular figure used the input data as previously shown and discussed in Tables 4.18 and 5.10. Careful studying of this figure and others show that the distribution range of the final critical solder joint stress is slightly smaller than the range seen for correction factor C only from the global model. The actual Matlab code for the Monte Carlo simulation is provided in the appendix E.

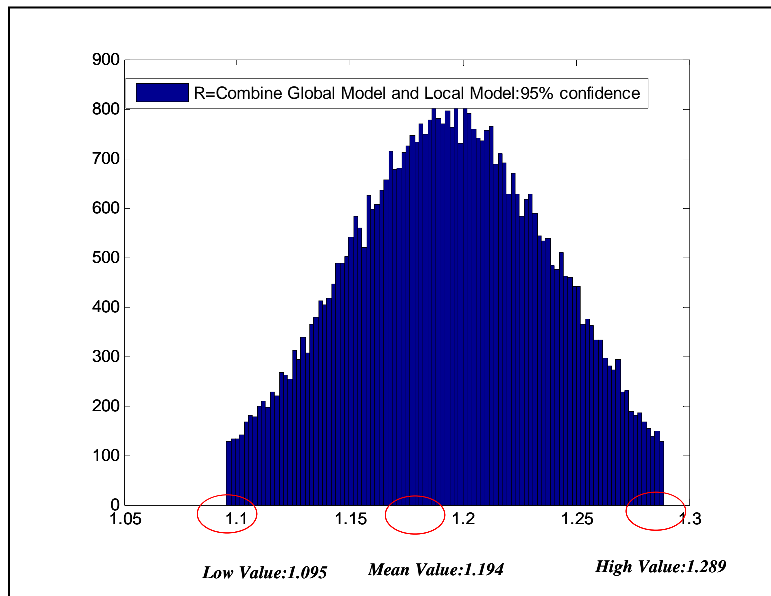

Figure7.13: Uncertainty Issue for the Combine Global and Local Model's functions for PBGA Package

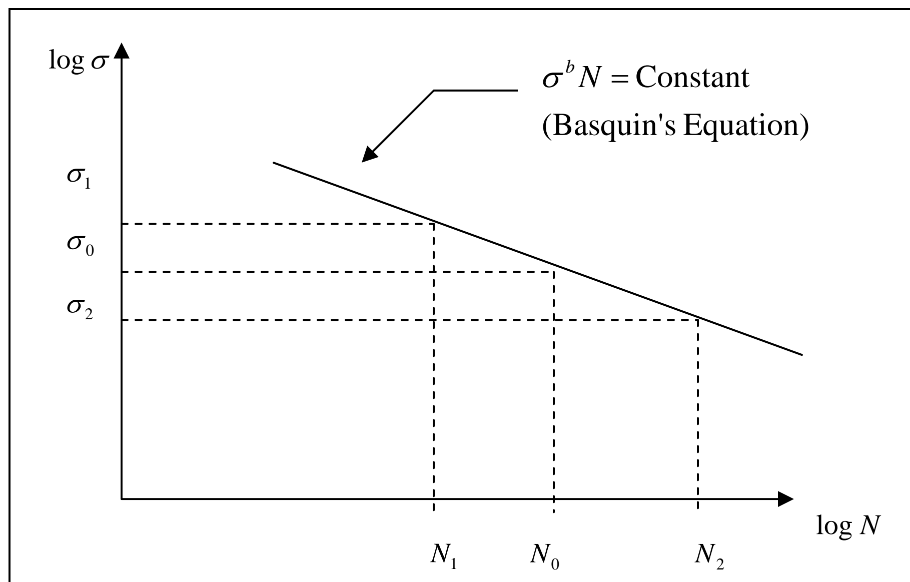

Figure7.14: Log-Log S-N Curve

Figure7.14, which is a log-log stress versus cycles to failure plot of the Basquin fatigue model, visually shows the large variation in cycles to failure for small changes in stress levels. Mathematically the fatigue power law is expressed as:

$$N \cdot \sigma^b = \text{constant} \qquad \text{(Ref. Equation 6.1)}$$

where the fatigue exponent is assumed to be $b = 6.4$. Manipulating the equation for two different stress conditions, we can calculate the ratio in life as a function of the ratio in stress levels. Note that material fatigue constant does not need to be known.

$$\sigma_0{}^b N_0 = \sigma_1{}^b N_1 \qquad \text{Equation7.8}$$

$$\left(\frac{N_1}{N_0}\right) = \left(\frac{\sigma_0}{\sigma_1}\right)^b \qquad \text{Equation7.9}$$

The uncertainties in the fatigue exponential and its influence on the life were discussed in Chapter 6, section 6.3. In this chapter the fatigue constant will be considered to be a constant equal to 6.4.

Table7.20 shows the variation in the life from the range in critical solder joint stress shown in the distribution plot as shown in Figure7.14, σ_{rms} and life cycle's relationship. The results are expressed as a ratio of the lives calculated using the upper and lower range value of the critical stress and comparing it to the life calculated using the mean

critical stress. Note that for the lower value of the critical stress; the life is 2 time longer than that for the mean value of critical stress. Similarly for the upper range of the critical stress, the life is 0.71 times shorter than that calculated using the median value of critical stress. With a random variation in the input parameters to the global and local model as defined in Table4.18 and Table5.10, we are 90% confident that the calculated fatigue life is between 18,470,380 and 52,461,916 cycles.

Table7.20: Combine Global and Local model Critical Solder Joint Stress in ***1%*** of Material Properties of the Standard Deviation for the PBGA package

	$C*S$	% Difference	Life Cycle	N_x/N_0
Low value (σ_1, N_1)	1.095	8.3	52,461,916	2
Median value (σ_0, N_0)	1.194		26,166,069	
High value (σ_2, N_2)	1.289	-8	18,470,380	0.71

From the section 4.1.1 and section 5.3's conclusions, the material properties are the major parameters that affect the calculated life. The Table7.20 is the results with an assumed standard deviation of 1% in the material properties. The next table, Table7.21 shows the results for an assumed standard deviation of 5% in the material properties.

Table7.21: Combine Global and Local Model's Final Critical Solder Joint Stress in ***5%*** of Material Properties of the Standard Deviation for the PBGA package

	$C*S$	% Difference	Life Cycle	N_x/N_0
Low value (σ_1, N_1)	0.749	36.9	571,117,141	21.8
Median value (σ_0, N_0)	1.186		26,166,069	
High value (σ_2, N_2)	1.563	-31.8	5,153,133	0.2

This table confirms that knowledge of the material properties is critical to accurate modeling.

Figure7.15 and Figure7.16 is again a plot of the calculated life versus the measured life. This time the range and mean value for the calculated life is indicated on the plot. The error bars represent 5% and 95% failure for a range of 90%. The experimental life is represented using only the calculated median value for each components failure distribution.

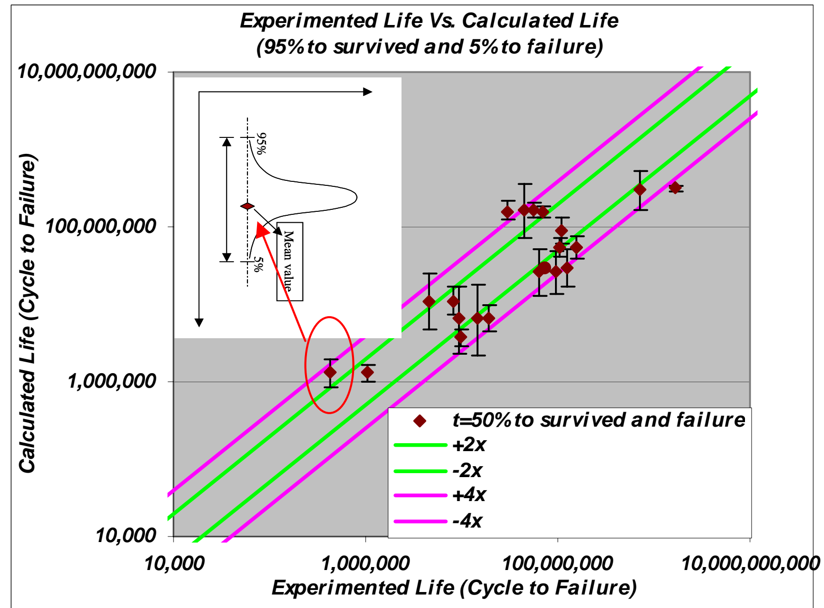

Figure7.15: Uncertainty in the Calculated (Predicted) Life

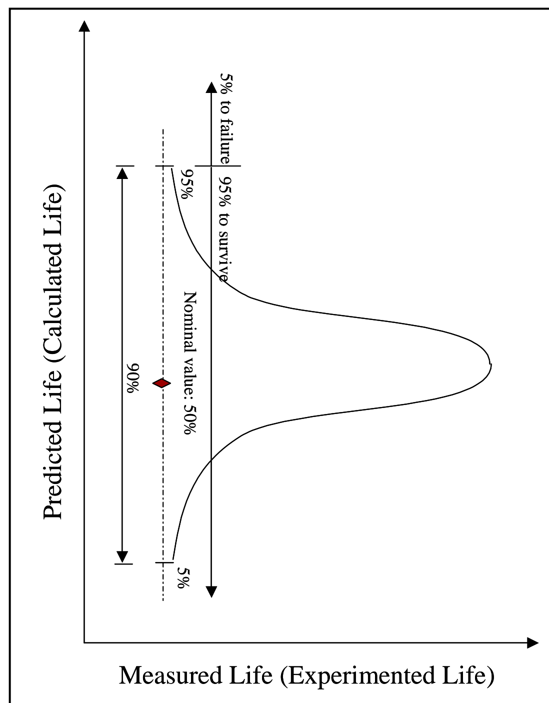

Figure7.16: Uncertainties Issue for 90% of Data

7.3.3 Uncertainty Analysis Combined the Predicted Life and Measure Life

Figure7.17 joins together the results from the two preceding sections. Error bars representing the 5% and 95% failure for both the calculated life and the experimental life are shown in the plot. The central median value point is the only point that is typically shown. Viewing this plot with the 90% of data ranges shown for the experimental life as well as the calculated life, gives one a better feel on the accuracy of the model. With the uncertainties as indicated in the plot, the model is doing a reasonable job. One could judge the adequacy of the model better, if the experimental data had tighter ranges.

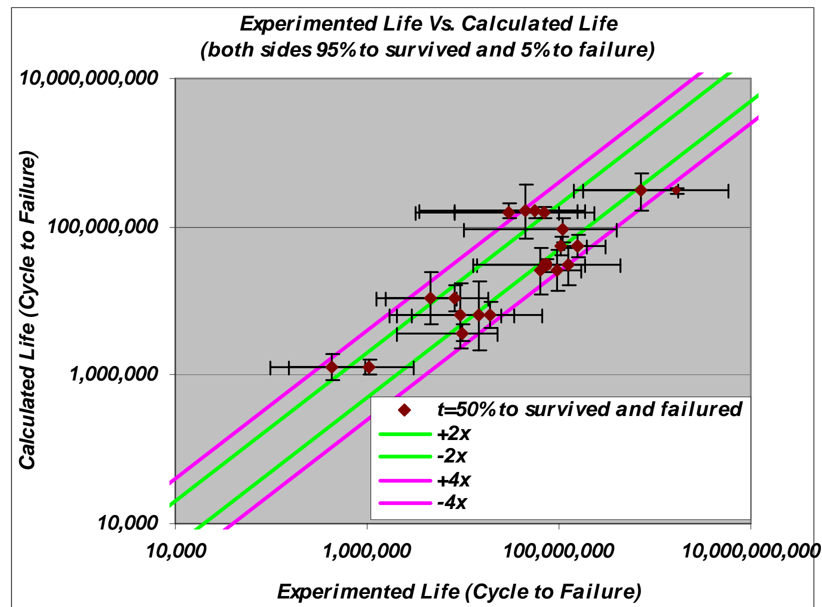

Figure7.17: Calculated and Measured Life: Life Cycle Uncertainty Issue

Chapter 8: Conclusion and Future work

This dissertation develops a rapid assessment methodology for evaluating the fatigue life of BGA packages in a vibration environment. A "rapid assessment methodology" implies that the complete fatigue life analysis can be conducted in real time by an average engineer with answers being generated immediately. If time were not a factor, it is recognized that the "best" approach would be the use of a general purpose FEA program to conduct a stress analysis of the critical solder joint in the BGA component of interest, but the rapid assessment approach developed in this dissertation digests the results of a parametric FEA study via DOE and response surface techniques. As long as the user is careful to keep the input parameters within the ranges specified in the development of the model, the accuracy of this rapid approach is basically the same as one would obtain with FEA.

The approach used in this dissertation is a physics of failure type approach to damage analysis. The methodology starts with a model of the complete PWB assembly. A global-local type of analysis is employed. The PWB including its support conditions is typically called the global model. A more detailed model that only deals with a local section of the PWB, including the component of interest, is the local model. These two levels of modeling are required since it is not possible to realistically model the complete PWB assembly in enough detail to accurately obtain the critical stresses in the BGA solder attach. Once the critical stress in the BGA solder attach is determined, a fatigue damage model assess the life of the component. Note that the approach in this

dissertation separates the stress analysis and the damage modeling and thus should not be as affected by new packages styles as many assessment models that combine the stress analysis and damage model together.

The global model starts with an analysis of the PWB using *CALCE_PWA* software where the vibration environment is specified with an acceleration power spectral density. The *CALCE_PWA* software calculates the PWB dynamic response using a simple FEA analysis. Unfortunately due to the relative course FEA mesh in the *CALCE_PWA* software, the calculated curvature, K_{rms} of the PWB is a smeared curvature and not very accurate near the component of interest. An accurate curvature of the PWB is needed in order to conduct a local stress analysis on the package. Through a series of DOE simulations using a much finer mesh in ANSYS, a functional form was determined for a correction factor that improved that accuracy of the *CALCE_PWA* calculated curvature. One of the primary contributions of this dissertation is to identify and qualify the influence of the various parameters that influence the global model correction factor and the local model stress analysis function. It was found that the global model correction factor is a function of the rigidity ratio between the BGA and the PWB, as well as the ratio of ball span length on a side to the gap length between a the package of interest and it nearest neighbor. Those these two factors may seem intuitive, ANOVA techniques were carefully used to identify the critical factors and their interactions. Note the correction factor as determined in the dissertation is not a function of component location on the PWB. This is due to the fact that it was assumed that the fundamental frequency dominated the response. The reader is cautioned that for PWB's where higher order

modes are strongly excited, such as with non-uniform acceleration PSD's and/or non rectangular boards, this assumption my need to be more carefully examined.

The local model takes the PWB calculated curvature, K_{rms} for the component of interest and converts it into a boundary condition moment load for a local model consisting of the BGA mounted on a small section of the PWB. A 2D finite element model was used to determine the critical solder joint and the maximum stress. Again through a series of DOE simulations and response surface fitting a functional form for the critical stress was determined. The critical stress was found to be a function of the rigidity ratio of the BGA to the PWB and a function of the ratio of the solder ball diameter over the ball span length on a package side.

Once the critical stress is determined, a simple fatigue power law damage model is used to calculate BGA life. The complete rapid assessment approach was demonstrated on two different sets of published experimental data and the predictions developed in this dissertation were shown to be more accurate than the currently used *CALCE_PWA* BGA prediction model. The models developed in this dissertation proved to be easy to use and are expected to be incorporated into a future version of the *CALCE_PWA* software.

For the solder fatigue damage model, the fatigue exponent used was 6.4, based upon past experience with this value from the *CALCE_PWA* software. The fatigue exponent can be viewed as the slope of the failure line in an S-N (log stress versus log life) diagram. Using the global and local models developed in the dissertation and available

experimental data, it was found that the final life assessment results were not very sensitive to variations in the fatigue exponent (+/- 5, 10, and 20%) due to the fact that the stresses were nearly unity in value. Using a subset of the experimental data, the fatigue constant was determined. This fatigue constant was then used successfully to predict the life of a completely different set of experimental data with good success. It appears that the fatigue constant is indeed a material property, but it must be recognized that the fatigue constant determined in this dissertation is determined for the volume averaged critical Von Mises Stress as calculated in this dissertation.

The following is a series of major conclusions and observations that became evident during the development of the rapid assessment approach for BGA package under vibration loading. Many of the more detailed observations, particularly with respect to the justification of the simulation FEA meshing and resulting accuracy, are left within the body of the various chapters. The major conclusions and observations became most evident during an uncertainty analysis where it was recognized that the input parameters were not fixed known values, but nominal values or "best guesses" that a designer or engineer would input to the model either from an existing product or a design yet to be built. Such nominal values or "best guesses" could be slightly different than the actual values of the final product.

The various dimensional parameters are either relatively well known or can be physically measured and the resulting distribution about the nominal value can be determined. Assuming reasonable normal distributions, it was found that the dimensional parameters

do not influence the resulting life calculation very much due to their relatively tight distributions. Material properties, particularly Young's Modulus for both the PWB and an effective Young's modulus for the BGA, are a different story. Material properties are rarely well characterized and actual values can differ substantially from nominal handbook values.

For the uncertainty analysis, the dissertation examined how the input data uncertainty affects the output data uncertainty. We are assuming that the model is correct and are only dealing with uncertainties due to variations in inputs. Output uncertainty, uncertainty in the correction factor (global model), and critical solder joint stress (local model) were determined by Monte Carlo simulation. For the Monte Carlo simulation the various input parameters, both material properties, and geometric dimensions are assumed to have a normal distribution. Note that the model developed in this dissertation is only valid over the particular parameters ranges used and cannot be used outside these ranges.

From the Monte Carlo simulations the global model was found to be very sensitive to small variations in the Young's modulus of both the PWB and the effective modulus of the BGA. The *CALCE_PWA* calculated curvature was found to be relatively un-sensitive to variations in the Young's modulus. It turns out that the formula for the curvature correction factor is very sensitive to the Young's modulus through the ratio parameter of the rigidities of the component to the PWB. This same ratio parameter is used in the

local stress analysis, but the critical stress model is not as sensitive as the curvature correction model.

For accurate assessment of BGA life, the Poisson's ratio and particularly the Young's modulus of the PWB and the effective modulus of the component need to be accurately known. If one assumes a normal distribution for all the input parameters where the dimensional parameters have a standard deviation of between 0.1% and 0.2% of the nominal values, Poisson's ratio have a standard deviation of 0.8%, and the Young's modulus of both the PWB and the component to have a standard deviation of 1% of the nominal value, the resulting life assessment can vary by almost a factor of +/- two. If the Young's modulus standard deviation increases to 5%, the resulting life assessment can vary by almost a factor of +/- ten.

It must also be emphasized that when comparing any prediction method to experimental results, one must understand the scatter or distribution of the experimental failure data. Many times a single data point is used to represent the experimentally measured median time to failure, or time to x% failure. Due to the typically limited number of experimentally measured failures at any load level, one needs to more carefully look at the range of the experimental failure distribution and then compare it to the range of the expected predicted distribution assuming a reasonable variation in the prediction input values. This was done for the prediction method developed in this dissertation when it was compared to various experimental data. The ranges for the predictions were generally less than the ranges for the experimental data. This demonstrated that the

accuracy of the prediction method is better than the natural scatter in the fatigue data, something that should be strived for.

Recommendations for the Further Work:

From the uncertainty analysis it is clear that the global model influences the final life much more than the local stress analysis. Thus it is strongly recommended that more effort is spent in understanding how to accurately determine a load or boundary condition that can be used to drive a local stress analysis model. This dissertation concentrated on determining the PWB curvature in the vicinity of a component. The global model developed in this dissertation is very sensitive to the ratio of the rigidities between the component and the PWB. More study need to be done to determine if this sensitivity can be toned down so that the engineer does not need to as accurately know the Young's modulus of the PWB and component as is now required. Most researchers want to continually improve upon the local stress analysis model; the uncertainty analysis in this dissertation demonstrates that this is not a major source of uncertainty in the final life calculation. Thus at this time it is not recommended to spend time improving the local stress analysis model.

Using a power law fatigue damage model, the final life is a function of the critical stress raised to an exponent. The final life is a strong function of the exact value of the fatigue exponent. In the dissertation a solder fatigue exponent of 6.4 was used based upon historical experience. One continually needs to evaluate the value of this exponent and the author is aware of a current research project in *CALCE* looking directly at measuring

the fatigue exponent for PbSn and Pb-free solder. Similarly the fatigue constant is also a material property that needs to be continually evaluated in light of new data and research.

Appendices A: Design of Experimental Methodology (RSM and ANOVA)

Design of experiment (DOE):

Design of experiment (DOE) with factorial analysis is adopted to obtain the sensitivity information of each parameter by the two-dimensional linear finite element models. In this research, we estimated the critical curvature of the three different types of solder joint components by associating the finite element analysis simulation with the design of experiment to obtain a parameter sensitivity analysis, and also optimized the process design by means of the response surface models (RSM) methodology. To this end, a virtual DOE process with two-dimensional linear finite element analysis simulation is set up.

The factorial designs mean that in each complete trial or replication of the experiment all possible combinations of the factors at all levels is investigated. The magnitude and direction of the factor's effects need to be examined to determine which variables are likely to be important. The analysis of variance (ANOVA) can generally be used to confirm this interpretation and significance. For a fixed effects model, test statistics (F distribution) for each main effect and interaction may be constructed by dividing the corresponding mean square for the effect or interaction by the mean square error. Moreover, the prediction of the response surface can be fitted through linear regression methods. The regression model representation maybe written as:

$$y = \lambda_0 + \lambda_1 x_1 + \lambda_2 x_2 + \lambda_{12} x_1 x_2 + \varepsilon$$

Where y is the response, $\lambda_0, \lambda_1, \lambda_2, \lambda_{12}$ are the coefficients to be determined, and x_1, x_2 are the variables that represent factors A and B, respectively. The ε is a random

error term. All the parameter estimates in this regression model are relative to the effect estimates. In this research there are two design parameters considered in the factorial analysis of the finite element model simulation. Because the ANOVA in Table 4.1.1 and the regression analysis will become more complicated, the DOE software of Design-Expert is adopted to deal with the calculation of statistics. In order to ensure that reliable effect estimates are obtained the distance between the low (-) and high (+) levels of the factor is increased. At the same time, the adjusted R^2 statistic, which measures the proportion of total variability explained by the regression model, is adopted to judge the significance of the effects as the number of factors increase in the model.

ANOVA:

The easiest way to understand ANOVA is through a concept known as value splitting. ANOVA splits the observed data values into components that are attributable to the different levels of the factors. ANOVA allows us to compare the effects of multiple levels of multiple factors. The analysis of variance (ANOVA) is used to detect significant factors in a multi-factor model. In the multi-factor model, there is a response (dependent) variable and one or more factor (independent) variables. This is a common model in designed experiments where the experimenter sets the values for each of the factor variables and then measures the response variable. Each factor can take on a certain number of values. These are referred to as the levels of a factor. The number of levels can vary between factors. For designed experiments the number of levels for a given factor tends to be small. Each factor and level combination is a cell. Balanced designs are those in which the cells have an equal number of observations and

unbalanced designs are those in which the number of observations varies among cells. It is customary to use balanced designs in designed experiments.

We say we have a one-way layout when we have a single factor with several levels and multiple observations at each level. With this kind of layout we can calculate the mean of the observations within each level of our factor. The residuals will tell us about the variation within each level. We can also average the means of each level to obtain a grand mean. We can then look at the deviation of the mean of each level from the grand mean to understand something about the level effects. Finally, we can compare the variation within levels to the variation across levels. It is easy to model all of this with an equation of the form:

$$y_{ij} = m + a_i + e_{ij}$$

This equation indicates that the *jth* data value, from level *i*, is the sum of three components: the common value, the level effect, and the residual. Estimation for the one-way layout can be performed one of two ways. First, we can calculate the total variation, within-level variation and across-level variation. These can be summarized in a table as shown and tests can be made to determine if the factor levels are significant. In general, the ANOVA table for the one-way case is given in Table 4.1.1

We will discuss the DOE and ANOVA global model approach, give examples and show how to use those DOE and ANOVA technique in our final results in section 4.4. The next section will describe the response surface methodology (RSM). The response surface methodology offers statistical design of experiment tools that lead to peak process

performance. RSM produces precise maps based on mathematical models. It can put all our responses together via sophisticated optimization approaches, which ultimately lead to the discovery of the spots where we meet all specifications at minimal cost. Section 4.3 will demonstrate how RSM fits into the overall framework of DOE and provide historical background.

Table 4.1.1: ANOVA Table for the one-way case

Source	Sum of Squares	Degrees of Freedom	Mean Square
Factor levels	$J\sum a_i^2$	I-1	$J\sum a_i^2 / (I-1)$
Residuals	$\sum\sum e_{ij}^2$	I (J-1)	$\sum\sum e_{ij}^2 / I(J-1)$
Corrected total	$\sum\sum y_{ij}^2 ....IJm^2$	IJ-1	

Response surface methodology (RSM):

Response surface methodology (RSM) is a very common method and is particularly useful for optimizing a running system. The traditional response surface methodology (RSM) is an iterative process involving experimental design, empirical model building, and analysis of the developed model. This iterative process of learning through RSM is roughly formalized by [Box, 1987] and [Khuri, 1987] and consists of the repeated use of the steps, conjecture, design, experiment, and analysis. With this approach, one must first conjecture where to conduct the experiments and the form of the model, which may be used to represent the system over a given portion of the solution space. The next step is to design a suitable experiment to test, estimate, and develop a current conjectured model. Finally, one runs the experiment and then conducts the analysis. The analysis leads to verification of the postulated model and the working out of its consequences, or to the

forming of a new or modified conjecture, [Box, 1987], and [Khuri, 1987]. The applications of the traditional RSM usually have one of three possible purposes: 1) To map a response surface over a particular region of interest; 2) To optimize the response; 3) To select operating conditions to achieve desired specifications, [Box, 1987] and [Myers, 2002].

The response surface methodology is a technique designed to optimize process control by the application of designed experiments in order to characterize a system [Myers and Montgomery, 1995]. The relationship between the response variable of interest (y), and the predictor variables ($\xi_1, \xi_2, \xi_3, ...\xi_k$) may be known exactly allowing a description of the system of the form

$$y = g(\xi_1, \xi_2, \xi_3, ...\xi_k) + \varepsilon$$

where ε represents the model error and includes measurement error, and other variability such as background noise. The error will be assumed to have a normal distribution with zero mean and variance σ^2. In general, the experimenter approximates the system function g with an empirical model of the form

$$y = f(\xi_1, \xi_2, \xi_3, ...\xi_k) + \varepsilon$$

where f is a first or second order polynomial. This is the empirical or response surface model. The variables are known as natural variables since they are expressed in physical units of measurement. In the response surface methodology (RSM), the natural variables are transformed into coded variables $x_1, x_2, x_3, ...x_k$ which are dimensionless, zero mean, and the same standard deviation. The response function now becomes

$$\eta = f(x_1, x_2, x_3, ...x_k)$$

The successful application of RSM relies on the identification of a suitable approximation for f. This will generally be a first order model of the form

$$\eta = \beta_0 + \beta_1 x_1 + \beta_2 x_2 ..... + \beta_k x_k$$

or a second order model of the form

$$\eta = \beta_0 + \sum_{j=1}^{k} \beta_j x_j + \sum_{j=1}^{k} \beta_{jj} x^2{}_j ..... + \sum_{i<j}\sum \beta_{ij} x_i x_j$$

It may be necessary to employ an approximating function grater than an order of two, based on the standard Taylor series expansion. The response surface methodology is intimately connected to regression analysis.

Earlier, we described the RSM objective. Under some circumstances, a model involving only main effects and interactions may be appropriate to describe a response surface when Analysis of the results revealed no evidence of "pure quadratic" curvature in the response of interest (i.e., the response at the center approximately equals the average of the responses at the factorial runs). The design matrix originally used included the limits of the factor settings available to run the process. In other circumstances, a complete description of the process behavior might require a quadratic or cubic model:

Quadratic:

$$\begin{aligned}\hat{y} &= b_0 + b_1 x_1 + b_2 x_2 + b_3 x_3 + b_{12} x_1 x_2 \\ &+ b_{13} x_1 x_3 + b_{23} x_2 x_3 + b_{11} x_1{}^2 + b_{22} x_2{}^2 + b_{33} x_3{}^2\end{aligned}$$

Cubic

$$\hat{y} = Quadratic\ Model + b_{123}x_1x_2x_3 + b_{112}x_1^2x_2 + b_{113}x_1^2x_3 + b_{222}x_1x_2^2$$
$$+ b_{133}x_1x_3^2 + b_{233}x_2^2x_3 + b_{233}x_2x_3^2 + b_{111}x_1^3 + b_{222}x_2^3 + b_{333}x_3^3$$

These are the full models with all possible terms--rarely would all of the terms be needed in an application. If the experimenter has defined factor limits appropriately and/or taken advantage of all the tools available in multiple regression analysis (for example, transformations of responses and factors), then finding an industrial process that requires a third-order model is highly unusual. Therefore, we will only focus on designs that are useful for fitting quadratic models. As we will see, these designs often provide lack of fit detection that will help determine when a higher-order model is needed.

Factor Levels for Higher-Order Designs

Figure 4.1.1 illustrates possible behaviors of responses as functions of factor settings. In each case, assume the value of the response increases from the bottom of the figure to the top and that the factor settings increase from left to right.

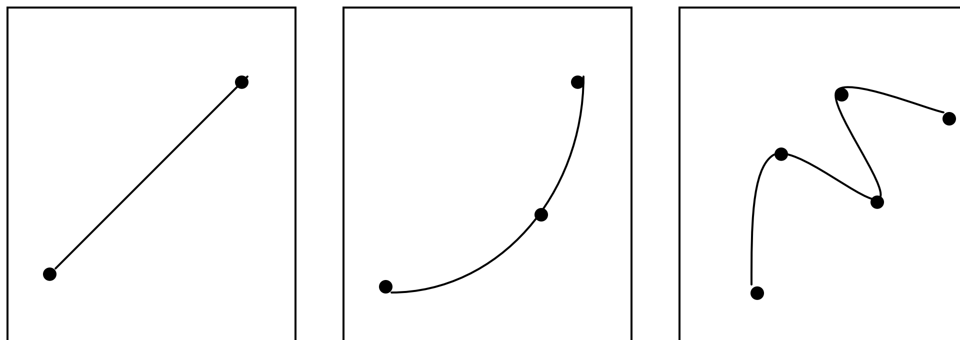

Figure 4.1.1: Left: Linear Function; Middle: Quadratic Function; Right: Cubic Function

If a response behaves as in Figure 4.1.1, left figure, the design matrix to quantify that behavior need only contain factors with two levels -- low and high. This model is a basic assumption of simple two-level factorial and fractional factorial designs. If a response behaves as the middle figure, the minimum number of levels required for a factor to quantify that behavior is three. One might logically assume that adding center points to a two-level design would satisfy that requirement, but the arrangement of the treatments in such a matrix confounds all quadratic effects with each other. While a two-level design with center points cannot estimate individual pure quadratic effects, it can detect them effectively. A solution to creating a design matrix that permits the estimation of simple curvature as shown in Figure 4.1.1 middle figure would be to use a three-level factorial design. Table 4.1.2 explores that possibility. Finally, in more complex cases such as illustrated in Figure 4.1.1, right figure, the design matrix must contain at least four levels of each factor to characterize the behavior of the response adequately.

Table 4.1.2: Three-Level Factorial Designs

Number of Factors	Treatment Combinations 3^k Factorial	Number of Coefficients Quadratic Empirical Model
2	9	6
3	27	10
4	81	15
5	243	21
6	729	28

Two-level factorial designs quickly become too large for practical application as the number of factors investigated increases. This problem was the motivation for creating `fractional factorial' designs. Table4.1.2 shows that the number of runs required for a 3^k

factorial becomes unacceptable even more quickly than for 2^k designs. The last column in Table4.1.2 shows the number of terms present in a quadratic model for each case.

With only a modest number of factors, the number of runs is very large, even an order of magnitude greater than the number of parameters to be estimated when k isn't small. For example, the absolute minimum number of runs required to estimate all the terms present in a four-factor quadratic model is 15: the intercept term, 4 main effects, 6 two-factor interactions, and 4 quadratic terms. The corresponding 3^k design for $k = 4$ requires 81 runs.

In this research, the experiment is designed to allow us to estimate interaction and even quadratic effects, and therefore give us an idea of the (local) shape of the response surface we are investigating. For this reason, they are termed response surface method (RSM) designs. RSM designs are used to:

- Find improved or optimal process settings
- Troubleshoot process problems and weak points
- Make a product or process more robust against external and non-controllable influences. "Robust" means relatively insensitive to these influences.

The three-level design is written as a 3^k factorial design. It means that k factors are considered, each at 3 levels. These are (usually) referred to as low, intermediate and high levels. These levels are numerically expressed as 0, 1, and 2. One could have considered the digits -1, 0, and +1, but this may be confusing with respect to the 2-level designs since 0 is reserved for center points. Therefore, we will use the 0, 1, 2 scheme. The reason that the three-level designs were proposed is to model possible curvature in the response function and to handle the case of nominal factors at 3 levels. A third level for a continuous factor facilitates investigation of a quadratic relationship between the response and each of the factors.

This is the simplest three-level design in Figure4.1.2. It has two factors, each at three levels. The 9 treatment combinations for this type of design can be shown pictorially as follows: A notation such as "20" means that factor A is at its high level (2) and factor B is at its low level (0).

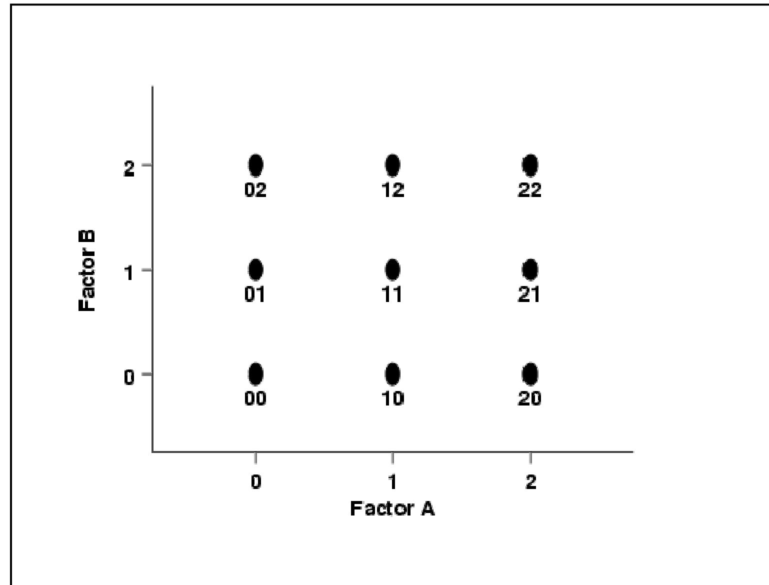

Figure 4.1.2: A 3^2 Design Schematic

Response surface methods are employed at the design and the analysis stages. The design stage is important because the design defines how the data are to be collected and how much data is to be collected. In the analysis of the data, the objective is to provide plausible explanations of the experimental evidence and to stimulate the process of conjecture on the part of experimenter. Thus, the design of the experiment and the analysis of the data go hand in hand in helping an experimenter learn which factors are important, what role each factor plays in the system, and why these factors are important. The next section, 4.4 will be discussed the detail about design of experiment and ANOVA for our global model.

Appendices B: Additional Figures and Tables in Chapter 4-Chapter7

Chapter 4: Figures and Tables

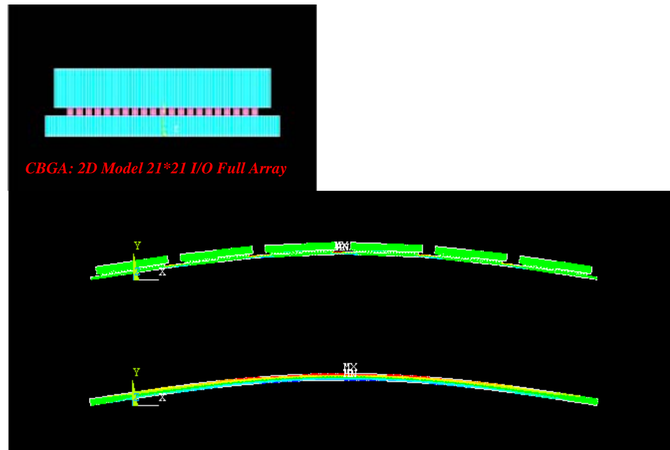

Ref Figure 4.8: Global Model for CBGA Components Mounted on the PWB Vs. PWB

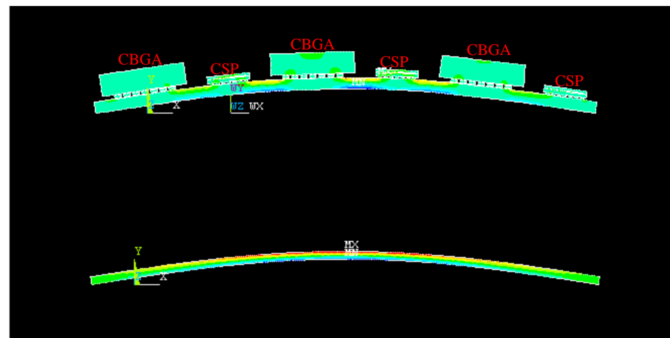

Ref Figure 4.8: Global Model for Mix Components (CBGA and CSP) Mounted on the PWB Vs. PWB

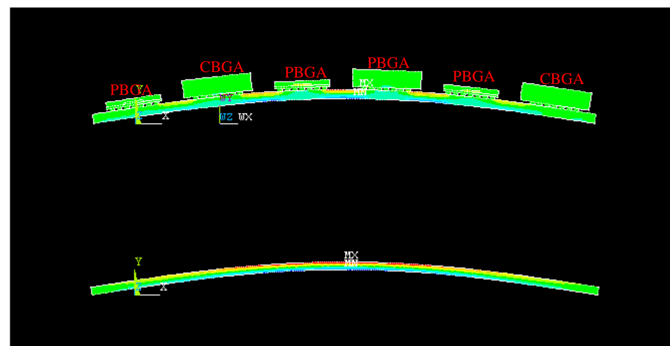

Ref Figure 4.8: Global Model for Mix Components (PBGA and CBGA) Mounted on the PWB Vs. PWB

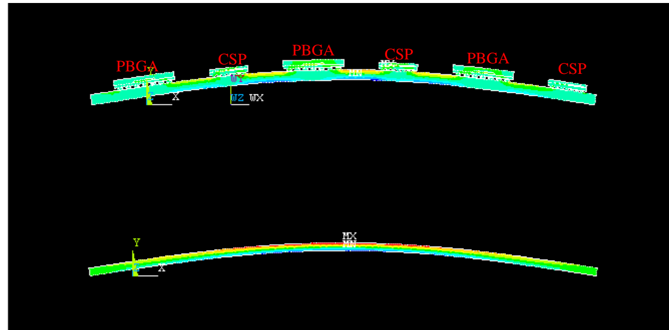

Ref Figure 4.8: Global Model for Mix Components (PBGA and CSP) Mounted on the PWB Vs. PWB

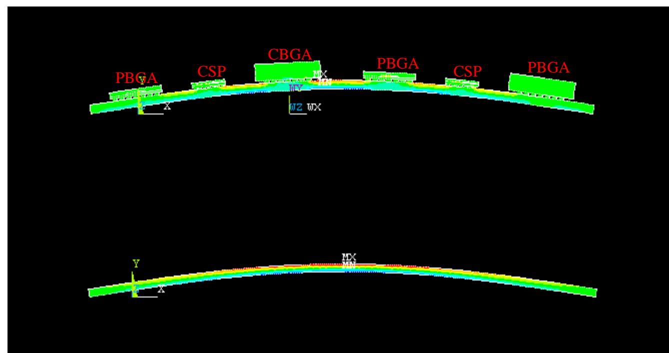

Ref Figure 4.8: Global Model for Mix Components (PBGA, CSP and CBGA) Mounted on the PWB Vs. PWB

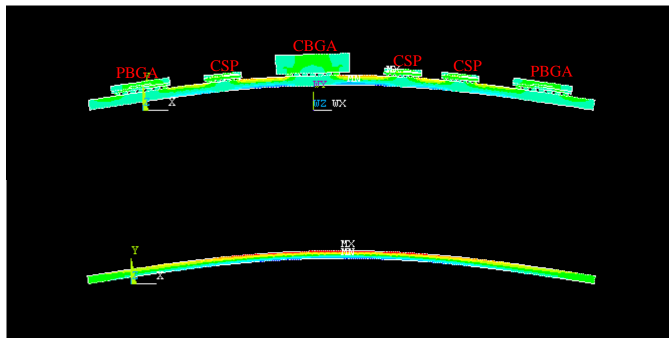

Ref Figure 4.8: Global Model for Mix Components Mounted on the PWB Vs. PWB

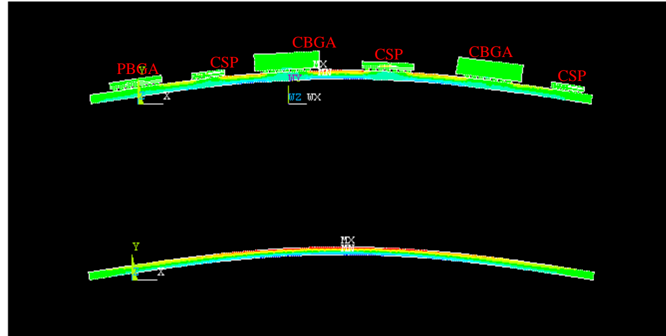

Ref Figure 4.8: Global Model for Mix Components Mounted on the PWB Vs. PWB

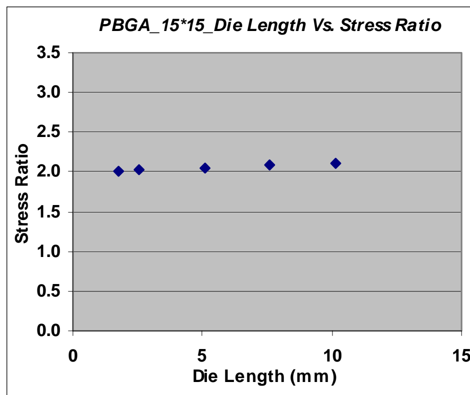

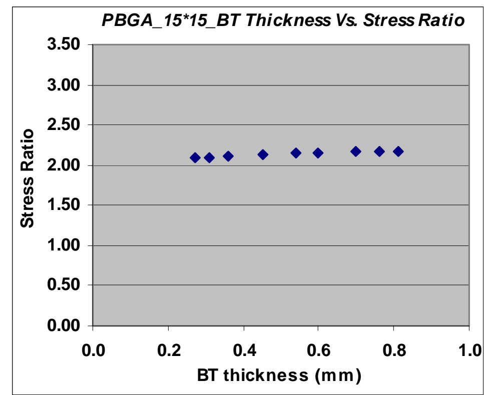

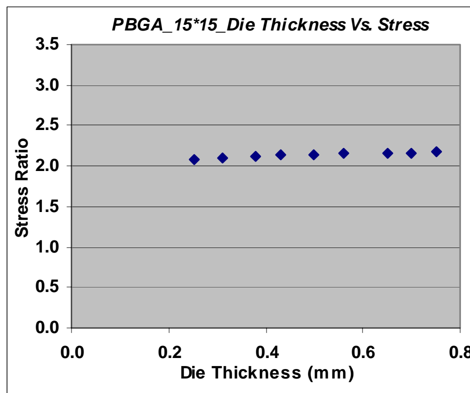

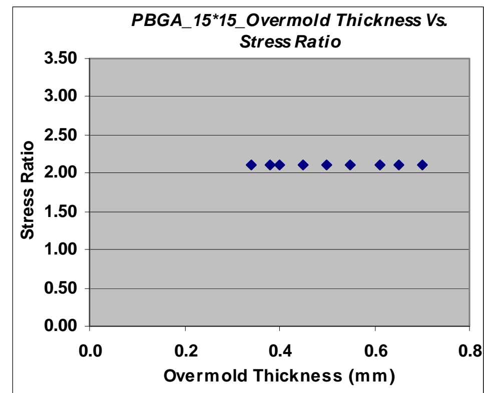

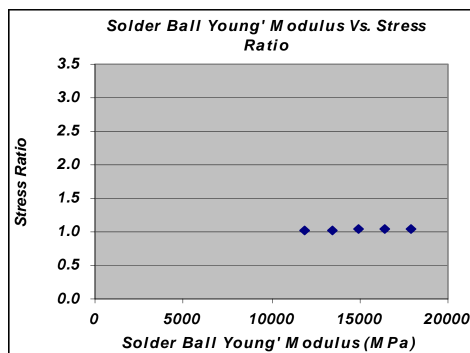

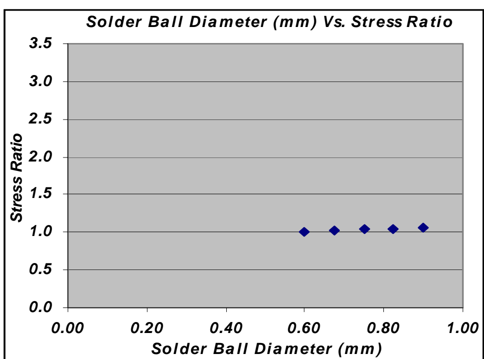

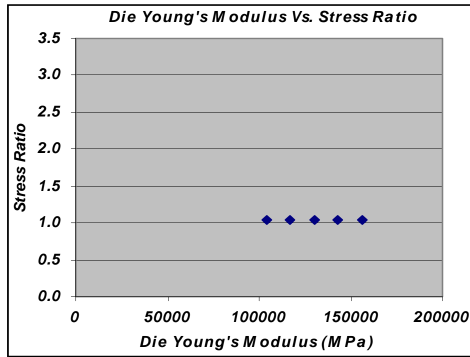

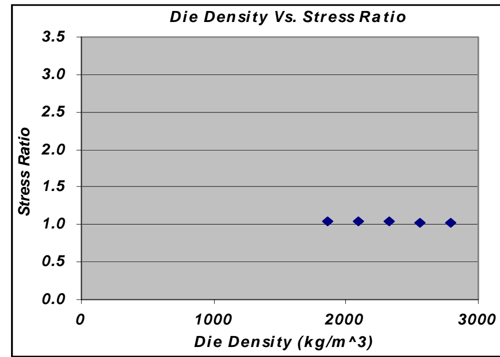

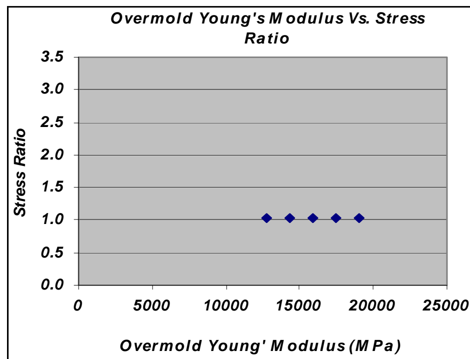

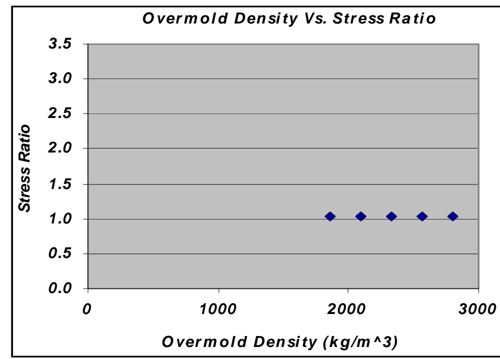

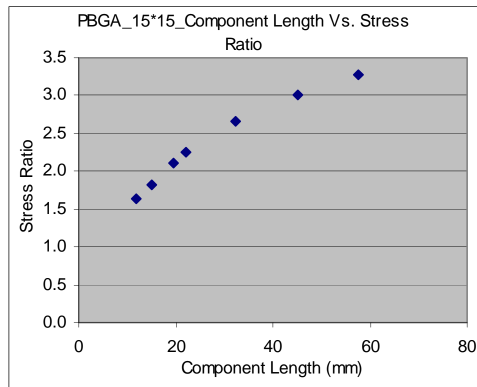

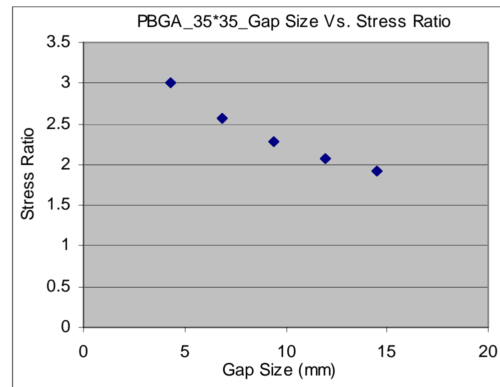

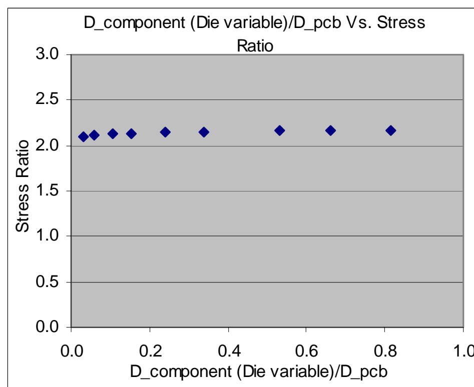

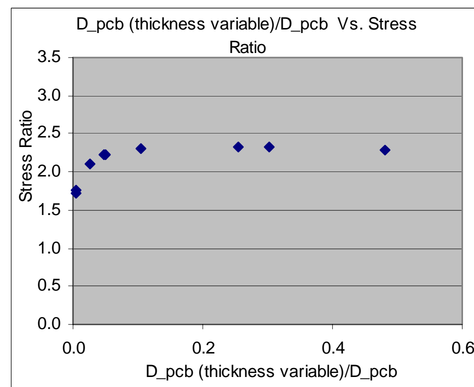

Ref Figure 4.20: Dependent Variable (response variable) and the Independent Variables (factors)

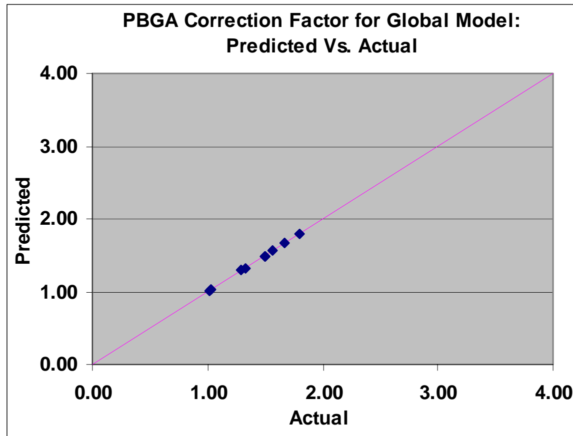

Ref Figure 4.28: PBGA Correct Factor for Global Model: Predicted Vs. Actual

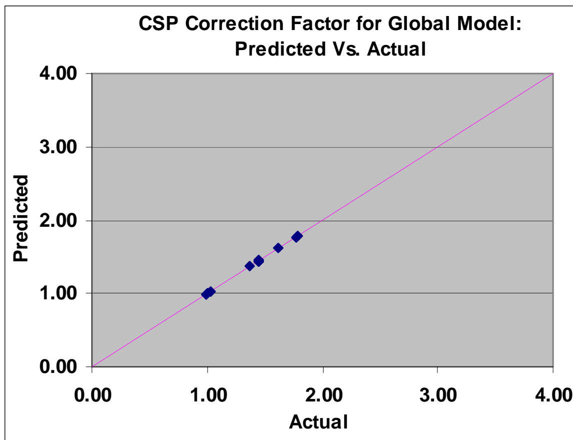

Ref Figure 4.28: CSP Correct Factor for Global Model: Predicted Vs. Actual

Ref Table 4.1: Comparison of 2D and 3D Finite Element Analysis results

PBGA: 15*15 I/O counts	$C = \frac{K_{ANSYS}}{K_{CALCE_PWA}}$
2D Finite Element Result	1.55805
3D Finite Element Result	1.50321
% Difference	3.5191

CSP: 7*7 I/O counts	$C = \frac{K_{ANSYS}}{K_{CALCE_PWA}}$
2D Finite Element Result	1.36721
3D Finite Element Result	1.41739
% Difference	3.5402

Ref Table 4.3: Global Model Comparison Single Component and Mix Components

PBGA_CSP	All PBGA	Mix_PBGA_CSP	All CSP
Frequency ratio	0.928232	0.94471	0.99362
Stress ratio	1.17285	1.18629	1.22935
% Difference stress ratio	1.13347	Standard	-3.62950
Stiffest	PBGA>CSP		

PBGA_CBGA	All PBGA	Mix_PBGA_CBGA	All CBGA
Frequency ratio	0.928232	0.754436	0.63958
Stress ratio	1.17285	1.022531819	0.832586
% Difference stress ratio	-14.70069	Standard	18.57603
Stiffest	PBGA>CBGA		

CBGA_CSP	All CSP	Mix_CBGA_CSP	All CBGA
Frequency ratio	0.99362	0.713602	0.63958
Stress ratio	1.229353	0.945861	0.832586
% Difference stress ratio	-29.9718	Standard	11.97586
Stiffest	CBGA> CSP		

PBGA_CSP_CBGA	All PBGA	PBGA_CSP_CBGA	All CBGA	All CSP
Frequency ratio	0.928232	0.948486	0.63958	0.99362
Stress ratio	1.17285	0.991219	0.832586	1.229353
% Difference stress ratio	-18.32400	Standard	16.00383	-24.02436
Stiffest	CBGA>PBGA>CSP			

PBGA_CSP_CBGA_ CSP_CSP_PBGA	All PBGA	All CBGA	PBGA_CSP_CBGA_ CSP_CSP_PBGA	All CSP
Frequency ratio	0.928232	0.63958	0.785352	0.99362
Stress ratio	1.17285	0.832586	0.994781	1.229353
% Difference stress ratio	-17.90032	16.30459	Standard	-23.58027
Stiffest	CBGA>PBGA>CSP			

PBGA_CSP_CBGA_ PBGA_CBGA_CSP	All PBGA	PBGA_CSP_CBGA_ PBGA_CBGA_CSP	All CBGA	All CSP
Frequency ratio	0.928232	0.756821	0.63958	0.99362
Stress ratio	1.17285	0.946842	0.832586	1.229353
% Difference stress ratio	-23.86966	Standard	12.06706	-29.83719
Stiffest	CBGA>PBGA>CSP			

Ref Table 4.21: Global Model Uncertainties: *CALCE_PWA* Material Properties and Geometry

Error %	PCB_thickness (mm)	K_rms (1/mm)	% Different
-20	1.26	0.0001015	-4.78
-10	1.41	0.0001072	0.56
0	1.57	0.0001066	0.00
10	1.73	0.0001038	-2.63
20	1.88	0.0001001	-6.10

Error %	Pitch Size (mm)	K_rms (1/mm)	% Different
-20	1.20	0.0000950	3.09
-10	1.35	0.0000940	2.00
0	1.5	0.0000922	0.00
10	1.65	0.0000896	-2.77
20	1.80	0.0000878	-4.71

Error %	PCB_Density (kg/m^3)	K_rms (1/mm)	% Different
-20	1550	0.0000863	-6.38
-10	1744.2	0.0000877	-4.83
0	1938	0.0000922	0.00
10	2132	0.0000920	-0.14
20	2326	0.0000969	5.15

Error %	Ball_E (MPa)	K_rms (1/mm)	% Different
-20	11920	0.0000922	0.00
-10	13410	0.0000922	0.00
0	14900	0.0000922	0.00
10	16390	0.0000922	0.00
20	17880	0.0000922	0.00

Error %	Ball height(mm)	K_rms (1/mm)	% Different
-20	0.40	0.0000922	0.00
-10	0.45	0.0000922	0.00
0	0.50	0.0000922	0.00
10	0.55	0.0000922	0.00
20	0.60	0.0000922	0.00

Error %	BT_Density (kg/m^3)	K_rms (1/mm)	% Different
-20	1518	0.0000922	0.00
-10	1708	0.0000922	0.00
0	1898	0.0000922	0.00
10	2088	0.0000922	0.00
20	2278	0.0000922	0.00

Error %	BT_thickness (mm)	K_rms (1/mm)	% Different
-20	1.320	0.0000958	3.98
-10	1.485	0.0000942	2.17
0	1.650	0.0000922	0.00
10	1.815	0.0000898	-2.59
20	1.980	0.0000870	-5.56

Error %	BT_E (MPa)	K_rms (1/mm)	% Different
-20	12160	0.0000922	0.00
-10	13680	0.0000922	0.00
0	15200	0.0000922	0.00
10	16720	0.0000922	0.00
20	18240	0.0000922	0.00

Error %	Die_E (MPa)	K_rms (1/mm)	% Different
-20	104000	0.0000922	0.00
-10	117000	0.0000922	0.00
0	130000	0.0000922	0.00
10	143000	0.0000922	0.00
20	156000	0.0000922	0.00

Error %	Die_thickness (mm)	K_rms (1/mm)	% Different
-20	0.48	0.0000922	0.00
-10	0.54	0.0000922	0.00
0	0.60	0.0000922	0.00
10	0.66	0.0000922	0.00
20	0.72	0.0000922	0.00

Error %	Overmold_ thickness(mm)	K_rms (1/mm)	% Different
-20	0.80	0.0000922	0.00
-10	0.90	0.0000922	0.00
0	1.00	10.000092	0.00
10	1.10	0.0000922	0.00
20	1.20	0.0000922	0.00

Error %	Overmold_Density (kg/m^3)	K_rms (1/mm)	% Different
-20	1864	0.0000922	0.00
-10	2097	0.0000922	0.00
0	2330	0.0000922	0.00
10	2563	0.0000922	0.00
20	2796	0.0000922	0.00

Ref Table 4.25: Global Model Uncertainties: *ANSYS* Material Properties and Geometry

Error %	PCB_thickness (mm)	Stress Ratio	% Different
-20	1.26	0.99912	-3.39
-10	1.41	1.01898	-1.47
0	1.57	1.03422	0.00
10	1.73	1.04572	1.11
20	1.88	1.05436	1.95

Error %	Pitch Size (mm)	Stress Ratio	% Different
-20	1.20	0.99712	-3.59
-10	1.35	1.01753	-1.61
0	1.5	1.03422	0.00
10	1.65	1.04805	1.34
20	1.80	1.05986	2.48

Error %	Ball Diameter (mm)	Stress Ratio	% Different
-20	0.60	1.00954	-2.39
-10	0.68	1.02191	-1.19
0	0.75	1.03422	0.00
10	0.83	1.04653	1.19
20	0.90	1.05901	2.40

Error %	Ball_E (MPa)	Stress Ratio	% Different
-20	11920	1.02739	-0.66
-10	13410	1.03106	-0.31
0	14900	1.03422	0.00
10	16390	1.03693	0.26
20	17880	1.03930	0.49

Error %	Ball height (mm)	Stress Ratio	% Different
-20	0.40	1.05370	1.88
-10	0.45	1.04388	0.93
0	0.50	1.03422	0.00
10	0.55	1.02473	-0.92
20	0.60	1.01553	-1.81

Error %	BT_Density (kg/m^3)	Stress Ratio	% Different
-20	1518	1.05946	2.44
-10	1708	1.04659	1.20
0	1898	1.03422	0.00
10	2088	1.02225	-1.16
20	2278	1.01067	-2.28

Error %	BT_thickness (mm)	Stress Ratio	% Different
-20	1.320	1.05884	2.38
-10	1.485	1.04630	1.17
0	1.650	1.03422	0.00
10	1.815	1.02247	-1.14
20	1.980	1.01107	-2.24

Error %	BT_E (MPa)	Stress Ratio	% Different
-20	12160	1.02999	-0.41
-10	13680	1.03229	-0.19
0	15200	1.03422	0.00
10	16720	1.03581	0.15
20	18240	1.03721	0.29

Error %	Overmold_E (MPa)	Stress Ratio	% Different
-20	12720	1.03394	-0.03
-10	14310	1.03405	-0.02
0	15900	1.03422	0.00
10	17490	1.03433	0.01
20	19080	1.03445	0.02

Error %	Die_Density (kg/m^3)	Stress Ratio	% Different
-20	1864	1.04529	1.07
-10	2097	1.03969	0.53
0	2330	1.03422	0.00
10	2563	1.02879	-0.53
20	2796	1.02343	-2.28

Error %	Overmold_E (MPa)	Stress Ratio	% Different
-20	0.80	1.04342	0.89
-10	0.90	1.03879	0.44
0	1.00	1.03422	0.00
10	1.10	1.02970	-0.44
20	1.20	1.02518	-0.87

Error %	Die_Density (kg/m^3)	Stress Ratio	% Different
-20	1864	1.04376	0.92
-10	2097	1.03896	0.46
0	2330	1.03422	0.00
10	2563	1.02953	-0.45
20	2796	1.02490	-0.90

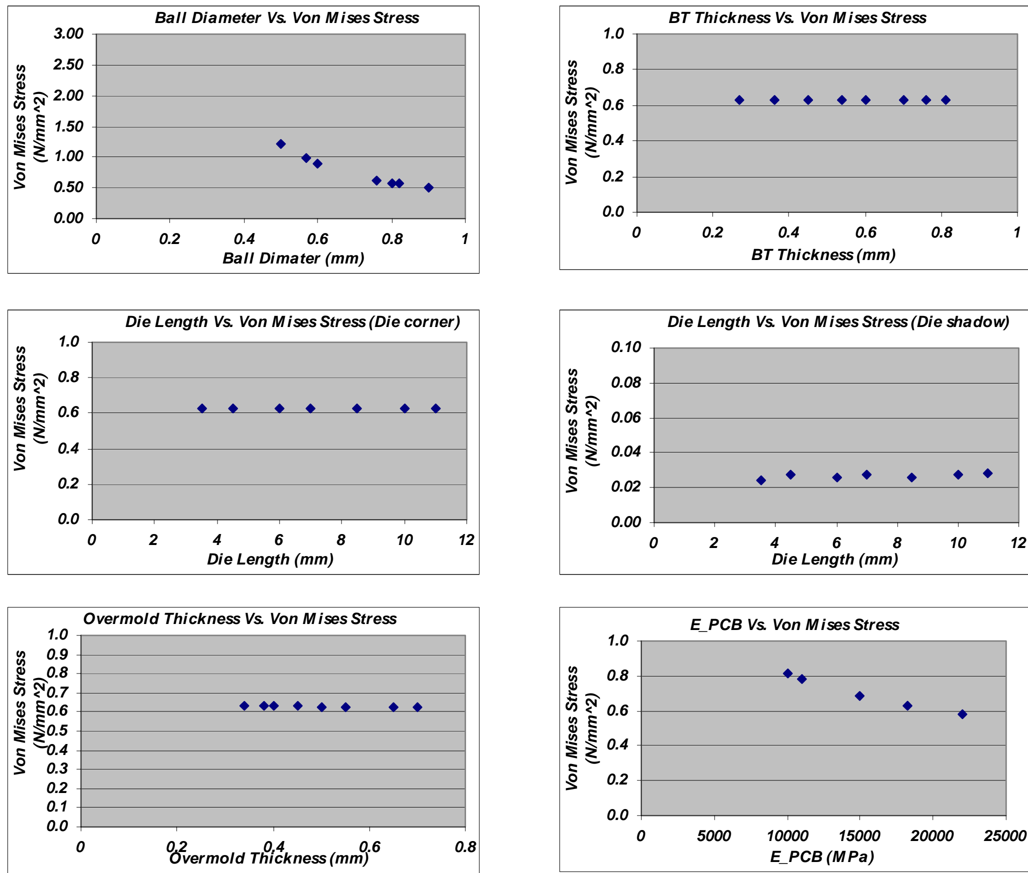

Ref Figure 5.10: Dependent Variable (response variable) and the Independent Variables (factors)

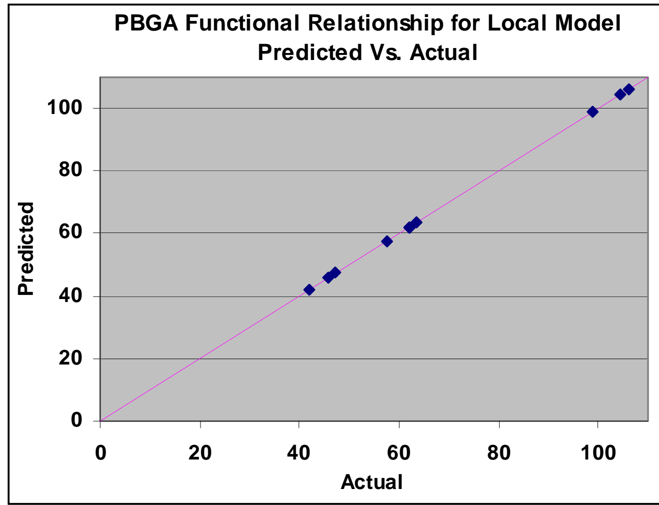

Ref Figure 5.16: PBGA Functional Relationship Factor for Local Model: Predicted Vs. Actual

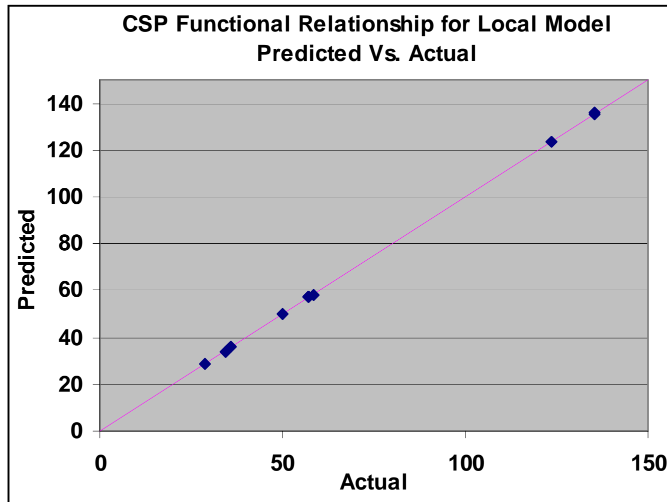

Ref Figure 5.16: CSP Functional Relationship Factor for Local Model: Predicted Vs. Actual

Ref Table 5.13: Local Model Uncertainties: *CALCE_FEA* Material Properties and Geometry

Error %	PCB_thickness (mm)	σ_{rms}
-20	1.26	1.739
-10	1.41	0.23
0	1.57	1.740
10	1.73	0.29
20	1.88	1.735

Error %	Ball_E (MPa)	σ_{rms}
-20	11920	1.673
-10	13410	-3.57
0	14900	1.705
10	16390	-1.73
20	17880	1.735

Error %	BT_thickness (mm)	σ_{rms}
-20	0.416	1.320
-10	0.468	1.744
0	0.52	0.52
10	1.485	1.485
20	1.739	1.739

Error %	BT_E (MPa)	σ_{rms}
-20	12160	1.698
-10	13680	1.718
0	15200	1.735
10	16720	1.749
20	18240	1.762

Error %	Die_E (MPa)	σ_{rms}
-20	104000	1.735
-10	117000	1.735
0	130000	1.735
10	143000	1.735
20	156000	1.735

Error %	Die_thickness (mm)	σ_{rms}
-20	0.32	0.48
-10	0.36	1.742
0	0.40	0.40
10	0.	0.54
20	1.738	1.738

Error %	Overmold_E (MPa)	σ_{rms}
-20	12720	1.738
-10	14310	1.736
0	15900	1.735
10	17490	1.733
20	19080	1.732

Error %	Overmold_thickness (mm)	σ_{rms}
-20	1.2	0.80
-10	1.35	1.735
0	1.50	0.00
10	1.65	0.90
20	1.8	1.735

Ref Table 7.23: Critical Solder Joint Stress for PBGA in *CALCE_FEA* in different vibration levels

JGPP: Vibration Level_2 (12 Grms)	Moment (N*mm)	Rapid Assessment Method
Component	M	C: (Von Mises Stress)
U2	3.087	1.307
U4	4.336	1.836
U5	3.927	1.662
U6	3.501	1.482
U18	2.900	1.228
U21	2.862	1.212
U43	3.203	1.356
U44	4.060	1.719
U55	1.026	0.434
U56	1.182	0.500

JGPP: Vibration Level_3 (14 Grms)	Moment (N*mm)	Rapid Assessment Method
Component	M	C: (Von Mises Stress)
U2	3.602	1.525
U4	5.060	2.142
U5	4.582	1.940
U6	4.085	1.729
U18	3.385	1.433
U21	3.341	1.415
U43	3.739	1.583
U44	4.736	2.005
U55	1.198	0.507
U56	1.379	0.584

JGPP: Vibration Level_4 (16 Grms)	Moment (N*mm)	Rapid Assessment Method
Component	M	C: (Von Mises Stress)
U2	4.115	1.742
U4	5.782	2.448
U5	5.235	2.217
U6	4.669	1.977
U18	3.867	1.637
U21	3.817	1.616
U43	4.272	1.809
U44	5.413	2.292
U55	1.369	0.579
U56	1.576	0.667

JGPP: Vibration Level_5 (18 Grms)	Moment (N*mm)	Rapid Assessment Method
Component	M	C: (Von Mises Stress)
U2	4.630	1.960
U4	6.506	2.755
U5	5.891	2.494
U6	5.253	2.224
U18	4.352	1.842
U21	4.296	1.819
U43	4.808	2.036
U44	6.094	2.580
U55	1.540	0.652
U56	1.774	0.751

JGPP: Vibration Level_6 (20 Grms)	Moment (N*mm)	Rapid Assessment Method
Component	M	C: (Von Mises Stress)
U2	5.145	2.178
U4	7.231	3.061
U5	6.544	2.771
U6	5.837	2.471
U18	4.834	2.046
U21	4.775	2.022
U43	5.341	2.261
U44	6.770	2.866
U55	1.711	0.724
U56	1.970	0.834

JGPP: Vibration Level_7 (28 Grms)	Moment (N*mm)	Rapid Assessment Method
Component	M	C' : (Von Mises Stress)
U2	7.201	3.049
U4	10.120	4.285
U5	9.162	3.879
U6	8.170	3.459
U18	6.767	2.865
U21	6.682	2.829
U43	7.477	3.166
U44	9.477	4.012
U55	2.395	1.014
U56	2.757	1.167

Ref Table 7.25: Damage Ratio for Time to Failure in JGPP in different vibration levels

U5						
SnPb/SnPb	Von Mises Stress (N/mm^2)	Constant	N (number of cycles)	t (min)	Miners Rule	Damage Ratio
Vibration Level_1 (9.9 Grms)	1.680	977,171,616	7,549,559	60	0.7526128	1.009439874
Vibration Level_2 (12 Grms)	2.037	977,171,616	2,212,342	6	0.256827074	
Vibration Level_3 (14 Grms)	2.376	977,171,616	822,558		0	
Vibration Level_4 (16 Grms)	2.715	977,171,616	349,867			
Vibration Level_5 (18 Grms)	3.054	977,171,616	164,603			
Vibration Level_6 (20 Grms)	3.394	977,171,616	83,977			
Vibration Level_7 (28 Grms)	4.751	977,171,616	9,751			
Total time to failure				66		

U6						
SnPb/SnPb	Von Mises Stress (N/mm^2)	Constant	N (number of cycles)	t (min)	Miners Rule	Damage Ratio
Vibration Level_1 (9.9 Grms)	1.680	977,171,616	15,746,510	60	0.360835162	1.001216738
Vibration Level_2 (12 Grms)	2.037	977,171,616	4,613,788	31	0.640381576	
Vibration Level_3 (14 Grms)	2.376	977,171,616	1,719,595			
Vibration Level_4 (16 Grms)	2.715	977,171,616	728,356			
Vibration Level_5 (18 Grms)	3.054	977,171,616	342,822			
Vibration Level_6 (20 Grms)	3.394	977,171,616	174,703			
Vibration Level_7 (28 Grms)	4.751	977,171,616	20,314			
Total time to failure				91		

U18						
SnPb/SnPb	Von Mises Stress (N/mm^2)	Constant	N (number of cycles)	t (min)	Miners Rule	Damage Ratio
Vibration Level_1 (9.9 Grms)	1.680	977,171,616	52,520,060	60	0.108185224	1.008986194
Vibration Level_2 (12 Grms)	2.037	977,171,616	15,330,011	60	0.370638636	
Vibration Level_3 (14 Grms)	2.376	977,171,616	5,715,879	32	0.530162335	
Vibration Level_4 (16 Grms)	2.715	977,171,616	2,437,945		0	
Vibration Level_5 (18 Grms)	3.054	977,171,616	1,144,349			
Vibration Level_6 (20 Grms)	3.394	977,171,616	585,401			
Vibration Level_7 (28 Grms)	4.751	977,171,616	67,782			
Total time to failure				152		

U21						
SnPb/SnPb	Von Mises Stress (N/mm^2)	Constant	N (number of cycles)	t (min)	Miners Rule	Damage Ratio
Vibration Level_1 (9.9 Grms)	1.680	977,171,616	57,218,852	60	0.09930109	1.005469964
Vibration Level_2 (12 Grms)	2.037	977,171,616	16,675,786	60	0.34072723 2	
Vibration Level_3 (14 Grms)	2.376	977,171,616	6,196,634	37	0.56544164 2	
Vibration Level_4 (16 Grms)	2.715	977,171,616	2,649,807			
Vibration Level_5 (18 Grms)	3.054	977,171,616	1,240,598			
Vibration Level_6 (20 Grms)	3.394	977,171,616	630,814			
Vibration Level_7 (28 Grms)	4.751	977,171,616	73,591			
Total time to failure				157		

Appendices C: Matlab Global Model Failure Analysis Codes

```
% Global Model for PBGA

Clear all
% Global parameter means
Ball=0.76;
Length=17.78;
E_c=15200;
t_c=0.81;
nu_c=0.2;
E_pwb=18200;
t_pwb=1.57;
nu_pwb=0.2;
gap=10;
Ratio=0.001d0;

% Global parameter standard deviations

Ball_sigma=Ball*Ratio;
Length_sigma=Length*Ratio;
%E_c_sigma=E_c*Ratio;
E_c_sigma=300;
t_c_sigma=t_c*Ratio;
nu_c_sigma=nu_c*Ratio;
%E_pwb_sigma=E_pwb*Ratio;
E_pwb_sigma=300;
t_pwb_sigma=t_pwb*Ratio;
nu_pwb_sigma=nu_pwb*Ratio;
gap_sigma=gap*Ratio;

% Additional parameter for Global Model and table 4.11 formula

%check local model
%   A=Ball/Length
%   D_c=E_c*t_c^3/(12*(1-nu_c^2));
%   D_pwb=E_pwb*t_pwb^3/(12*(1-nu_pwb^2));
%   D=D_c/D_pwb
%   c=(1/(-0.017483805+29.70607565*A+0.082097493*D-45.61270524*A*D...
%       -1104.825999*A^2-
0.036898518*D^2+765.3569837*A^2*D+134.7674615*A*D^2))^2

count=22000;
B=zeros(count,1); % length/gap
D=zeros(count,1);
C=zeros(count,1);
```

```
O=zeros(count,1); % length
P=zeros(count,1); % gap
Q=zeros(count,1); % t_pwb
T=zeros(count,1); % t_c

for n=1:count

   B=normrnd(Length,Length_sigma)/normrnd(gap,gap_sigma);

   %O=normrnd(Length,Length_sigma);
   %P=normrnd(gap,gap_sigma);
   %Q=normrnd(t_pwb,t_pwb_sigma);
   %T=normrnd(t_c,t_c_sigma);

   D=(normrnd(E_c,E_c_sigma)*normrnd(t_c,t_c_sigma)^3/(12*(1-
normrnd(nu_c,nu_c_sigma)^2)))/...
      (normrnd(E_pwb,E_pwb_sigma)*normrnd(t_pwb,t_pwb_sigma)^3/(12*(1-
normrnd(nu_pwb,nu_c_sigma)^2)));

% global table 4.11

   C(n,1)=(1.075216292+0.052452684*B-0.671710596*D+2.483034054*B*D...
      -0.002373847*B^2-23.34399238*D^2-0.043092713*B^2*D-
19.32806298*B*D^2)^2;

end

%results
B_nom=Length/gap;
D_c=E_c*t_c^3/(12*(1-nu_c^2));
D_pwb=E_pwb*t_pwb^3/(12*(1-nu_pwb^2));
D_nom=D_c/D_pwb;

C_nom=(1.075216292+0.052452684*B_nom-
0.671710596*D_nom+2.483034054*B_nom*D_nom...
      -0.002373847*B_nom^2-23.34399238*D_nom^2-0.043092713*B_nom^2*D_nom-
19.32806298*B_nom*D_nom^2)^2;

C_mean=mean(C);
C_sort=sort(C);
% clip tails
confidence=[.8,.85,.9,.95];
half_tail_area=(1-confidence)./2;
fprintf('\n\n\n')
for nn=1:4
```

```
   %begin=uint32(count*half_tail_area(nn));
   begin=round(count*half_tail_area(nn));
   %last=uint32(count*(1-half_tail_area(nn)));
   last=round(count*(1-half_tail_area(nn)));
   C_new=[C_sort(begin:last,1)];
   C_new_mean=mean(C_new);
   fprintf('C_nom=%12.3f    C_mean=%12.3f    C_new_mean%12.3f\n',C_nom, C_mean,
C_new_mean);
   new_size=size(C_new);
   fprintf('confidence=%3.2f     Range %6.3f to %6.3f \n', confidence(1,nn),
C_new(1,1),C_new(new_size(1),1));
   figure(nn)
   hist(C_new,100)
end
```

Appendices D: Matlab Local Model Failure Analysis Codes

```
% Local Model for PGBA

clear all
% Local parameter means
Ball=.76;
Length=17.78;
E_c=15200;
t_c=0.81;
nu_c=0.2;
E_pwb=18200;
t_pwb=1.57;
nu_pwb=0.2;
gap=10;
Ratio=0.001d0;

% Local parameter standard deviations

Ball_sigma=Ball*Ratio;
Length_sigma=Length*Ratio;
%E_c_sigma=E_c*Ratio;
E_c_sigma=300;
t_c_sigma=t_c*Ratio;
nu_c_sigma=nu_c*Ratio;
%E_pwb_sigma=E_pwb*Ratio;
E_pwb_sigma=300;
t_pwb_sigma=t_pwb*Ratio;
nu_pwb_sigma=nu_pwb*Ratio;
gap_sigma=gap*Ratio;

%check
%   A=Ball/Length
%   D_c=E_c*t_c^3/(12*(1-nu_c^2));
%   D_pwb=E_pwb*t_pwb^3/(12*(1-nu_pwb^2));
%   D=D_c/D_pwb
%   c=(1/(-0.017483805+29.70607565*A+0.082097493*D-45.61270524*A*D...
%       -1104.825999*A^2-
0.036898518*D^2+765.3569837*A^2*D+134.7674615*A*D^2))^2

count=50000;
A=zeros(count,1);
D=zeros(count,1);
C=zeros(count,1);
for n=1:count
   A=normrnd(Ball,Ball_sigma)/normrnd(Length,Length_sigma);
```

```
   D=(normrnd(E_c,E_c_sigma)*normrnd(t_c,t_c_sigma)^3/(12*(1-
normrnd(nu_c,nu_c_sigma)^2)))/...
      (normrnd(E_pwb,E_pwb_sigma)*normrnd(t_pwb,t_pwb_sigma)^3/(12*(1-
normrnd(nu_pwb,nu_c_sigma)^2)));
   C(n,1)=(1/(-0.017483805+29.70607565*A+0.082097493*D-45.61270524*A*D...
      -1104.825999*A^2-
0.036898518*D^2+765.3569837*A^2*D+134.7674615*A*D^2))^2;
end
% results
A_nom=Ball/Length;
D_c=E_c*t_c^3/(12*(1-nu_c^2));
D_pwb=E_pwb*t_pwb^3/(12*(1-nu_pwb^2));
D_nom=D_c/D_pwb;
C_nom=(1/(-0.017483805+29.70607565*A_nom+0.082097493*D_nom-
45.61270524*A_nom*D_nom...
      -1104.825999*A_nom^2-
0.036898518*D_nom^2+765.3569837*A_nom^2*D_nom+134.7674615*A_nom*D_no
m^2))^2;
C_mean=mean(C);
C_sort=sort(C);
% clip tails
confidence=[.8,.85,.9,.95];
half_tail_area=(1-confidence)./2;
fprintf('\n\n\n')
for nn=1:4
   %begin=uint32(count*half_tail_area(nn));
   begin=round(count*half_tail_area(nn));
   %last=uint32(count*(1-half_tail_area(nn)));
   last=round(count*(1-half_tail_area(nn)));
   C_new=[C_sort(begin:last,1)];
   C_new_mean=mean(C_new);
   fprintf('C_nom=%12.3f    C_mean=%12.3f    C_new_mean%12.3f\n',C_nom, C_mean,
C_new_mean);
   new_size=size(C_new);
   fprintf('confidence=%3.2f     Range %6.3f to %6.3f \n', confidence(1,nn),
C_new(1,1),C_new(new_size(1),1));
   figure(nn)
   hist(C_new,100)
end
```

Appendices E: Matlab Global-Local Model Failure Analysis Codes

```
% Global-Local Model for PGBA
% monte carlo simulation of errors

Clear all;
% parameter means
Ball=.76;
Length=17.78;
E_c=15200;
t_c=0.81;
nu_c=0.2;
E_pwb=18200;
t_pwb=1.57;
nu_pwb=0.2;
% Local parameter standard deviations (expressed as fraction of mean)
Ball_sigma=.001*Ball;
Length_sigma=.001*Length;
E_c_sigma=.001*E_c;
t_c_sigma=0.002*t_c;
nu_c_sigma=0.008*nu_c;
E_pwb_sigma=.001*E_pwb;
t_pwb_sigma=.002*t_pwb;
nu_pwb_sigma=0.008*nu_pwb;
% Additional parameter for Global Model and table 4.11 formula
gap=10.16;
gap_sigma=.001*gap;

% %check
%    A=Ball/Length
%    B=Length/gap
%    D_c=E_c*t_c^3/(12*(1-nu_c^2));
%    D_pwb=E_pwb*t_pwb^3/(12*(1-nu_pwb^2));
%    D=D_c/D_pwb
%    s=(1/(-0.017483805+29.70607565*A+0.082097493*D-45.61270524*A*D...
%        -1104.825999*A^2-
0.036898518*D^2+765.3569837*A^2*D+134.7674615*A*D^2))^2
% % global table 4.11
%    c=(1.075216292+0.052452684*B-0.671710596*D+2.483034054*B*D...
%        -0.002373847*B^2-23.34399238*D^2-0.043092713*B^2*D-
19.32806298*B*D^2)^2
% pause
count=50000;
fprintf('\n\n\nMonte Carlo Simulation, count=%d\n\n',count)
A=zeros(count,1); % ball/length
B=zeros(count,1); % length/gap
```

```
D=zeros(count,1);
C=zeros(count,1);
S=zeros(count,1);
R=zeros(count,1);
for n=1:count
   A=normrnd(Ball,Ball_sigma)/normrnd(Length,Length_sigma);
   B=normrnd(Length,Length_sigma)/normrnd(gap,gap_sigma);
   D=(normrnd(E_c,E_c_sigma)*normrnd(t_c,t_c_sigma)^3/(12*(1-
normrnd(nu_c,nu_c_sigma)^2)))/...
      (normrnd(E_pwb,E_pwb_sigma)*normrnd(t_pwb,t_pwb_sigma)^3/(12*(1-
normrnd(nu_pwb,nu_c_sigma)^2)));
% global table 4.11
   C(n,1)=(1.075216292+0.052452684*B-0.671710596*D+2.483034054*B*D...
      -0.002373847*B^2-23.34399238*D^2-0.043092713*B^2*D-
19.32806298*B*D^2)^2;
% local
   S(n,1)=(1/(-0.017483805+29.70607565*A+0.082097493*D-45.61270524*A*D...
      -1104.825999*A^2-
0.036898518*D^2+765.3569837*A^2*D+134.7674615*A*D^2))^2;
end
R=S.*C; % joint
% results
A_nom=Ball/Length;
B_nom=Length/gap;
D_c=E_c*t_c^3/(12*(1-nu_c^2));
D_pwb=E_pwb*t_pwb^3/(12*(1-nu_pwb^2));
D_nom=D_c/D_pwb;
S_nom=(1/(-0.017483805+29.70607565*A_nom+0.082097493*D_nom-
45.61270524*A_nom*D_nom...
     -1104.825999*A_nom^2-
0.036898518*D_nom^2+765.3569837*A_nom^2*D_nom+134.7674615*A_nom*D_no
m^2))^2;
C_nom=(1.075216292+0.052452684*B_nom-
0.671710596*D_nom+2.483034054*B_nom*D_nom...
      -0.002373847*B_nom^2-23.34399238*D_nom^2-0.043092713*B_nom^2*D_nom-
19.32806298*B_nom*D_nom^2)^2;
R_nom=S_nom*C_nom;
S_mean=mean(S);
S_sort=sort(S);
C_mean=mean(C);
C_sort=sort(C);
R_mean=mean(R);
R_sort=sort(R);
% clip tails
confidence=[.8,.85,.9,.95];
half_tail_area=(1-confidence)./2;
```

```
%fprintf('\n\n\n')
for nn=1:4
   begin=uint32(count*half_tail_area(nn));
   last=uint32(count*(1-half_tail_area(nn)));
   C_new=[C_sort(begin:last,1)];
   C_clip_mean=mean(C_new);
   S_new=[S_sort(begin:last,1)];
   S_clip_mean=mean(S_new);
   R_new=[R_sort(begin:last,1)];
   R_clip_mean=mean(R_new);
   fprintf('C_nom=%12.3f    C_mean=%12.3f    C_clip_mean%12.3f\n',C_nom, C_mean,
C_clip_mean);
   new_size=size(C_new);
   fprintf('confidence=%3.2f    C Range %6.3f to %6.3f (percent: %6.3f to %6.3f)\n',
confidence(1,nn), C_new(1,1),C_new(new_size(1),1),(C_new(1,1)-
C_nom)/C_nom*100,(C_new(new_size(1),1)-C_nom)/C_nom*100);
   figure (nn)
   hist(C_new, 100)
   fprintf('S_nom=%12.3f    S_mean=%12.3f    S_clip_mean%12.3f\n',S_nom, S_mean,
S_clip_mean);
   new_size=size(S_new);
   fprintf('confidence=%3.2f    S Range %6.3f to %6.3f (percent: %6.3f to %6.3f)\n',
confidence(1,nn), S_new(1,1),S_new(new_size(1),1),(S_new(1,1)-
S_nom)/S_nom*100,(S_new(new_size(1),1)-S_nom)/S_nom*100);
   fprintf('R_nom=%12.3f    R_mean=%12.3f    R_clip_mean%12.3f\n',R_nom, R_mean,
R_clip_mean);
   figure (nn+4)
   hist(S_new, 100)
   new_size=size(R_new);
   fprintf('confidence=%3.2f    R Range %6.3f to %6.3f (percent: %6.3f to %6.3f)\n\n',
confidence(1,nn), R_new(1,1),R_new(new_size(1),1),(R_new(1,1)-
R_nom)/R_nom*100,(R_new(new_size(1),1)-R_nom)/R_nom*100);
   figure (nn+8)
   hist(R_new, 100)
end
```

Bibliography

Barker, Donald B., Abhijit Dasgupta, Michael G. Pecht, "PWB Soder Joint Fatigue Life Calculations Under Thermal and Vibration Loading," Journal of the IES, Vol.35, no. 1, pp17-25, January 1992

Barker, Donald B., Chen, Y.S., and Dasgupta, A., "Estimating the Vibration Fatigue Life of Quad Leaded Surface Mount Components," Journal of Electronic Packaging, Vol. 115, pp. 195-200, 1993

Basaran, C., Alexander, C., Yang Z. and Dishongs, T., "Reliability of BGA Under Vibrations," Proceeding Of the Surface Mount Technology International Conference September 30 – October 4, 2001

Basaran, C. and R. Chandaroy, "Thermomechanical Analysis of Solder Joints Under Thermal and Vibration Loading," EEP-Vol. 26-1, Advances in Electronic Packaging, ed. by Agonafer et al., pp. 419-426, 1999

Bret A. Zahn, "solder Joint fatigue life model Methodology for 63Sn37Pb and 95.4Sn4Ag0.5Cu Materials", Electronic Components and Technology Conference, , pp.83-94, 2003

Bradley, E., and Banerji, K., "Effect of PCB Finish on the Reliability and Wettability of Ball Grid Array Packages," Proceeding IEEE ECTC, pp. 1028-1038, 1995

Box, George E. P., and Norman R. Draper, Empirical Model-Building and Response Surfaces, John Wiley and Sons, New York, 1987

Bryan, Dodson, *Weibull Analysis: with software*. ASQC Quality Press, Milwaukee, Wisconsin, 1994

CALCE_PWA, Version 4.1, User Manual, University of Maryland-College

CALCE_FEN, Version 4, User Manual, University of Maryland-College

Chang, T.S., and Magrab, E.B., "An Improved Procedure for the Determination of the Elastic Constants of Component-Lead-Board Assemblies," ASME Journal Electronic Packaging, Vol.113, pp. 427-430, 1991

Chiu, Cheng, et, al. " Effect of Thermal Aging on Board Level Drop Reliability for Ph-Free BGA Packages", Lead-Free Area Array Webcast sponsored by Universal Instruments, September 16, 2004

Corbin, J.S., "Finite Element Analysis for Solder Ball Connect (SBC) Structural Design Optimization" IBM J. Res. Develop, Vol.37, pp. 583-596, 1993

Daniel, C., "Use of half-Normal Plots in Interpreting Factorial Two Level Experiments," Technometrics, Vol. 1, pp.311-342, 1959

Dasgupta A., Pecht M.G., "Design-of-Experiment Methods for Computational Parametric Studies in Electronic Packaging," Finite Elements in Analysis and Design, Vol. 30, pp. 125-146, 1998

Darbha, K., Ling, S., and Dasgupta, A., "Stress Analysis of surface Mount Interconnects Due to Vibration Loading," Proceedings of the 1996 ASME international Mechanical Engineering Congress and Exhibition, EEP 1-14, 1996

Darveaux, R., Syed, A., "Reliability of Area Array Solder Joints in Bending," SMTA International, September 2000

Darveaux, R., Heckman J., and Mawer A., "Effect of Test Board Design on the 2nd Level Reliability of a Fine Pitch BGA Package," Proceeding SMI, pp.105-111, 1998

Elishakoffm I., "Probabilistic methods in the Theory of structures," John Wiley & Sons, 1983

Ejim, T., Holliday A., Bader, F.E., and Gahr, S., "Designed Experiment to Determine Attachment Reliability Drivers for PBGA Packages," Proceeding SMI, pp. 385-392, 1995

Engel, P. A. 1993, "Structural Analysis Printed Circuit Board Systems," Spring Verlag, New York

Engel, P. A., Caletka, D. V., and Palmer, M. R., "Stiffness and Fatigue for Surface Mounted Module/Lead/Card Systems,'' ASME J. Electron. Package, **113**, pp. 129–137, 1991

Engel, P.A. "Structural Analysis for Circuit Card Systems Subject to Bending," ASME journal of Electronic Packaging, Vol. 112, Mar., pp.2-10, 1990

Engel, P.A., and Lim, C. k., " Finding the Stresses with Finite Elements," Mechanical Engineering, Vol. 108, No. 10, Oct., pp. 46-50, 1986

Ferdie, Ron, Shah, Milan, "EMMA Component Analysis Evaluation for Vibration and Shock", RMSC-Tucson, March, 2000

Green T.J. and Launsby R.G., "Using DOE to Reduce Costs and Improve the Quality of the Microelectronics manufacturing Process," International J. of Microcircuits and Electronic Packaging, No.3, 1995

Gupta, V.K., and Baker, D.B., "Modeling Solder Joint Fatigue Life for Gullwing Leaded Packages: Part I-Elastic Plastic Stress model" ASME Journal of Electronic Packaging, Vol. 117, Number 2, pp. 123-129, June, 1995

Hillman David, Waskow Jennifer, England Luke, and Pietersom Jim Van, "Assembly Level Text Vehicle Manufacturing Report for the EMMA project" WP01-2006, Rockwell Collins, Inc., 2001

Jih, Edward and Jung, Wayne, "Vibration Fatigue of Surface Mount Solder Joints," Proceedings of Inter Society Conference on Thermal Phenomena, pp. 246-250, 1998

Kivilahti L. and Ekere N, "Parameter Interaction in Stencil Printing of Solder Paste," J. of Electronics manufacturing, No.4, 1996

Khuri, Andre I., and John A. Cornell, Response Surfaces: Designs and Analyses, Marcel Dekker, Inc.,New York, 1987

Kumar Upadhyayula*, and Abhijit Dasgupta, "Physics-of-failure guidelines for accelerated qualification of electronic systems," CALCE Electronic Products and Systems Consortium, University of Maryland, College Park, MD 20742, USA

J-01-EM-026-P1, "Draft Joint Test protocol for Validation of Alternatives to Eutectic Tin-Lead Solders used in Manufacturing and Rework of Printed Wiring Assemblies", Joint Group on Pollution Prevention (JGPP), February 14, 2003

Lau, J., et al., "Solder Joint Reliability of Surface Mount Connectors," Journal of Electronic Packaging, Vol. 115, pp180-188, 1993

Lau, J., Gratalo, K., Schneider, E., Marcotte T., and Baker T., "Solder Joint Reliability of Large Plastic Ball Grid Array Assemblies under Bending, Twisting, and vibration Conditions", Circuit World, Vol. 22 No.1, 1995

Lau, J., Schneider, E., and Baker, T., "Shock and Vibration of Solder Bumped Flip Chip on Organic Coated Copper Boards," Journal of Electronic Packaging, Vol. 118, pp. 101-104, 1996

Lau, J.H. and Y.H. Pao, "Solder Joint Reliability of BGA, CSP, Flip Chip and Fine Pitch SMT assemblies," McGraw-Hill, Inc., 1997

Lee, J. and Rassaian, M., "Effective local Flexural Stiffness of Ball Grid Array Assemblies," Transactions of the ASME, Vol. 124, Sept. 2002

Lee, S.B., and Ham, S.J., "Experimental Study for Reliability of Electronic Packaging under Vibration" Experimental Mechanics, Vol. 36, No.4, pp.339-344, 1996

Li Ron S., "A Methodology for Fatigue Prediction of Electronic Components under Random Vibration Load," Transactions of the ASME, Vol. 123, Dec. 2001

Liguore, S., and Followell, D., "Vibration Fatigue of Surface Mount Technology Solder Joints," Proceedings of Annual Reliability and maintainability Symposium, pp. 18-26, 1995

Lipson Charles, Sheth narendra, "Statistical Design and Analysis of Engineering Experiments", McGraw-Hill, Inc., 1973

Lin, Y.K., "Probabilistic Theory of Structural Dynamics," McGraw-Hill, 1973

Marinis, T. F., Reinert, R. C., Sherry, W., Impact of external lead design on the fracture of HIC-PWB assemblies subjected to bending, Proc. Of the 34th ECC, May 14-16, 1984, New Orleans, Louisiana.

Mawer, A., Cho, D., and Darveaux, R., "The Effect of PBGA Solder Pad Geometry on Solder Joint Reliability," proceeding SMI, pp.127-135, 1996

Markstein, H. W., "Designing Electronics for High Vibration and Shock,"Electronic Packaging & Production, pp.40-43, April 1987

Mercado, L., Sarihan, V., Guo, Y., and mawer, A., "Impact of solder Pad Size on Solder Joint Reliability in Flip Chip PBGA Packages," Proceeding IEEE ECTC, pp.255-259, 1999

Mathieu, B., Dasgupta, A., Pecht, M.G., and Evans, J., "Design-of –Experiment Methods for Computational Parametric Studies in Electronic Packaging", Accepted for Publication Journal of Computational Mechanics, 1995

Methieu, B., "Stress Analysis of Gloass Lead Seals Under General Mechanical Loading," M.S. Thesis, University of Maryland, College Park, MD, 1993

Meirovitch, L., " Analytical methods in Vibration," The Macmillan Company, Collier-Macmillan Limited, London, 1967

Markstein, H.W., "Designing Electronics for High Vibration and Shock," Electronic Packaging & Production, pp.40-43, 1987

Myers R.H., and D.C. Montgomery, "Response Surface Methodology: process and product optimization using designed experiments," John Wiley and Sons Inc. USA, 1995

MIL-STD 810F, Section 514.5B-3, paragraph 2.2, Annex B

Nigam, N.C. "Introduction to Random Vibrations" Cambridge, MA: The MIT Press. 1983

NCMS Report 0096RE01, "Lead-Free, High-Temperature Fatigue-Resistant Solder, Final Report", national Center for manufacturing Sciences, August, 2001

Perkins, S. Sitaraman, “Vibration-Induced Solder Joint Fatigue Failure of a Ceramic Column Grid Array (CCGA) Package”, 2004 Electronic Components and Technology Conference Proceedings, Las Vegas, June 2-4, 2004

Pitarresi, J.M., Celetka, D., Coldwel, R. and Smith, D., “The Smeared Properties Approach to FE Vibration Modeling of Printed Circuit Cards,” ASME Journal of Electronic Packaging, Vol. 113, September, pp. 250-257, 1991

Pitarresi, J.M. and Primavera, A., “Comparison of Vibration Modeling Techniques for Printed Circuit Cards,” ASME Winter Conference, Atlanta, Ga., December 1-6, paper no. 91-WA-EEP-34, 1991

Pitarresi, J.M. and Akanda, A., “Random Vibration Response of a Surface Mounted Lead/Solder Joint,” proc. ASME International Electronics packaging Conference, Vol. 1, Binghamton, MY, Sept, pp.207-217, 1993

Pitarresi, J.M., Sethuraman S., Nandagopal B., “Reliability Modeling of Chip Scale packages,” IEEE/CPMT Inter. Electronics manufacturing Technology Symposium, 2000

Roberts, J.C., and Stillo, D.M., “Random Vibration Analysis of a Printed Wiring Board with Electronic Components,” Journal of IES, January/February, pp. 25-31, 1991

Ross R. J., Taguchi Techniques for Quality Engineering, McGraw-Hill, New York, 1996

Sidharth S., Barker, D.B., “Life Prediction Models in Electronic Packaging Using Finite Element Analysis and Design of Experiments”, Experimental/Numerical Mechanics in Electronic Packaging, Society for Experimental Mechanics, Vol. 1, pp. 126-135, 1997

Sidharth, D.B., and Barker, Donald B., “Vibration Induced Fatigue Life Estimation of Corner Leads of Peripheral Leaded Components,” Journal of Electronic Packaging, Vol. 118, pp.244-249, 1996

Singal, R.K., Gorman, D.J., “A General Analytical Solution for Free Vibration of Rectangular Plates on Fixed Supports and with Attached masses,” ASME Journal of Electronic Packaging, Vol. 114, pp.239-425, 1992

Steinberg, D.S., Vibration Analysis for Electronic Equipment, 3rd Ed., John Wiley and Sons, New York, NY, 1988

Steinberg, D.S., Preventing Thermal Cycling and Vibration Failures in Electronic Equipment, Wiley, New York, NY, 2001

Suhir, E., “Is the Maximum Acceleration an Adequate Criterion of the Dynamic Strength of a Structural Element in an Electronic Product?” IEEE Transactions on Component, Packaging, and Manufacturing Technology, Part A, Vol. 20, No.4, pp. 513-517, 1997

Suhir, E., “Could Compliant External Leads Reduce the Strength of a Surface Mounted Device?” proceedings of the 38th Electronic Components Conference, pp. 1-6, 1988

Sloan, Joel, Design and Packaging of Electronic Equipment, Van Nostrand Reinhold Company, NY, 1985

Tu, P. L., Chan, Y. C., Hung, K. C., and J. K., Lai, L., “Comparative study of micro-BGA reliability under bending stress,” IEEE Trans. Adv. Packaging, vol. 23, pp. 750-756, Nov. 2000.

Wong, T.E., B.A. Reed, H.M. Cohen and D.W. Chu, “Development of BGA Solder joint Vibration Fatigue Life Prediction Model,” 49th Electronic Components & Technology Conference, San Diego, CA, pp. 149-154, June 1999

Wong, T.E., F.W. Palmieri, Kachatorian L.A., “Experimentally Validated Vibration Fatigue Life Prediction Model for Ball Grid Array Solder Joint,” ASME, Packaging of Electronic and Photonic Devices, Vol. 28, pp.113-118, 2000

Wapole, Meyers, Meyers, & Ye “Probability and Statistics for Engineers & Scientists”, 7th edition, Prentice Hall, 2002

Wong, T.E., Palmieri, F.W., B.A. Reed, H.S. Fenger, H.M. Cohen, and K.T. Teshiba, “Durability/Reliability of BGA Solder Joints under Vibration Environment,” to be published in 50th Electronic Components & Technology Conference, Las Vegas, NV, 21-24, May 2000

Wong, T.E., Palmieri, F.W., Fenger, H.S., “Under-Filled BGA Solder Joint Vibration Fatigue Damage,” IEEE, Internal Society Conference on Thermal Phenomina, pp. 961-966, 2002

Woodrow, Tom “The Effect of Trace Amounts of Lead on the Reliability of Six Lead-Free Solders”, Proceedings of the 3rd International Conference on Lead-Free Components and Assemblies, San Jose, CA, April 23-24, 2003

Wayne, Nelson "Weibull Analysis of Reliability Data with Few or No Failures," *Journal of Quality Technology*, Vol. 17, No. 3, 1985

Yang, Q.J., Lim, G.H., Lin, R.M., Yap, F.F., H.L.J., Wang, Z.P., “Experimental Modal Analysis of PBGA Printed Circuit Board Assemblies,” IEEE, Electronic Packaging Technology Conference, 1997

Yang Q.J., Lim G.H., Wang Z.P., and Pang H.L., “Characterization of PBGA Assemblies’ Dynamic Properties and Vibration Fatigue Failures”, ASME International Mechanical Engineering Congress and Exposition, Anaheim, CA, USA, 1998

Yang, Q.J., Wang, Z.P., Lim, G.H., Pang, F, Lin, R.M., "Reliability of PBGA Assemblies under out-of-plane Vibration Excitations", IEEE Transactions on Components and Packaging Technologies, Vol. 25, No.2, pp 293-300, June, 2002

Yang, Q.J., Pang, H.L.J., Wang, Z.P., Lim, G.H., Yap, F.F., and Lin, R.M., 2000, "Reliability of PBGA Assemblies Under Out-Of-Plane Excitaiotns,' IEEE Transactions of Components and packaging Technologies, Vol. 25, No.2, pp. 293-300, June 2002

Zienkiewicz, O.C., and Taylor, R.L., The Finite Element Method. New Yourk: McGraw-Hill, 1989